WATER TUNNEL INVESTIGATION OF THE VORTEX DYNAMICS OF PERIODICALLY PITCHED WINGS

THESIS

Michael David
Captain, USAF

AFIT/GAE/AA/88D-06

DEPARTMENT OF THE AIR FORCE
AIR UNIVERSITY
AIR FORCE INSTITUTE OF TECHNOLOGY
Wright-Patterson Air Force Base, Ohio

AFIT/GAE/AA/88D-06

WATER TUNNEL INVESTIGATION OF THE VORTEX DYNAMICS OF PERIODICALLY PITCHED WINGS

THESIS

Michael David
Captain, USAF

AFIT/GAE/AA/88D-06

Approved for public release, distribution unlimited

AFIT/GAE/AA/88D-06

WATER TUNNEL INVESTIGATION OF THE VORTEX DYNAMICS OF PERIODICALLY PITCHED WINGS

THESIS

Presented to the Faculty of the School of Engineering
of the Air Force Institute of Technology
Air University
In Partial Fulfillment of the
Requirements for the Degree of
Master of Science in Aeronautical Engineering

Michael David, B.S.
Captain, USAF

December 1988

Acknowledgements

Completion of this thesis was possible only with the help of several individuals. I'd like to start by thanking my thesis advisor, Major Lanson Hudson, for his guidance and especially for his motivation over the course of this project. I would also like to thank the other members of my committee, Lt Col Paul King and Prof Hal Larsen for their inputs to the experiment and for their critique of the written work. For technical support I owe much to Mr Jay Anderson for his help with programming the motion control system and with the data reduction link between the cameras and computer. The models were the work of Mr Dave Driscole--definitely a highly skilled craftsman. A special thanks to Lt Francis J. Geiser III and Mr Karl Shoffstall for the long hours spent running the tunnel and camera systems and also for their advice on flow visualization and model modifications. Other members of the Flight Dynamics Lab who were always willing to listen were Lt Scott LeMay and Mr Larry Rogers. Finally I'd like to thank my wife, Berni, for her support and understanding during the entire AFIT experience.

Table of Contents

List of Figures

Figure Page

List of Tables

List of Symbols

c	Root chord length
C_L	Coefficient of lift
$C_{L_{Max\ Dyn}}$	Maximum dynamic coefficient of lift
$C_{L_{Max\ St}}$	Maximum static coefficient of lift
f	Pitching frequency
k	Reduced frequency, $2\pi fc/u$
Re	Reynolds number, uc/υ
s	Local semi-span
t	time (seconds)
u,U	Freestream velocity
x	Distance from apex parallel to wing chord
y	Distance from root chord parallel to trailing edge
α	Angle of attack (degrees)
$\dot{\alpha}$	Pitch rate (degrees/sec)
$\dot{\alpha}_{ND}$	Nondimensional pitch rate, $c\dot{\alpha}/u$
$\alpha_{Dyn\ Stall}$	Angle at which dynamic stall occurs
α_{Sep}	Angle at which quarter chord separation occurs
β	Vortex core inclination angle
ρ	Density of water
υ	Kinematic viscosity of water
ϕ	Vortex swirl angle

Abstract

The vortex structure above semi-span wings was investigated in the Flight Dynamics Lab's 24-inch water tunnel to determine the effects of periodic pitching using a saw-tooth motion. Each of the six wings was pitched about the mid-chord at nondimensional upstroke rates ($c\dot{\alpha}/U$) ranging from 0.05 to 0.30 and downstroke rates from 0.025 to 0.600 at tunnel flow rates of 0.6 to 3.6 in/sec. Visualization of the vortices obtained through dye injection from the models was recorded using both high speed and three-quarter-inch standard speed video systems. Digitized data from the high speed system provided trend data which showed the saw-tooth motion caused a hysteresis effect on the vortex breakdown location for the swept wings where during the upstroke the vortex would burst further aft than during the downstroke. In addition, comparison of two 65 degree sweep wings with different cross sections (flat plate and NACA 0012-34) showed a smaller hysteresis effect for the thicker wing. For the rectangular wing, increasing downstroke rates resulted in higher dynamic stall vortex convection rates. Information was also gathered on the oscillation of static breakdown location and the effects on vortex breakdown of tunnel flow velocity.

WATER TUNNEL INVESTIGATION OF THE VORTEX DYNAMICS OF PERIODICALLY PITCHED WINGS

I. Introduction

Perspective

Since the early days of flight, researchers have studied steady flow over wings and airfoils to predict aerodynamic characteristics. In the case of an unswept wing at low angles of attack the flow is attached on both the upper and lower surfaces while the lift produced is a function of the circulation. As the angle of attack is increased lift also increases, essentially in a linear manner; however at some point the flow on the upper surface starts to separate near the trailing edge. Further increases in angle of attack cause the separation point to move toward the leading edge eventually resulting in stall.

In comparison, the lift producing mechanism of a typical delta wing is similar at low angles of attack; however, at moderate to high angles of attack the flow separates from the leading edge and produces counter-rotating, leading edge vortices as shown in Figure 1. The flow is drawn over these vortices and accelerated downward causing the flow to reattach which results in additional lift commonly called vortex lift. As with the unswept wing, lift increases with angle of attack; but unlike the unswept wing

the increase is not necessarily linear and flow separation is not the cause of stall. Instead, loss of lift is due to a breakdown of the leading edge vortices.

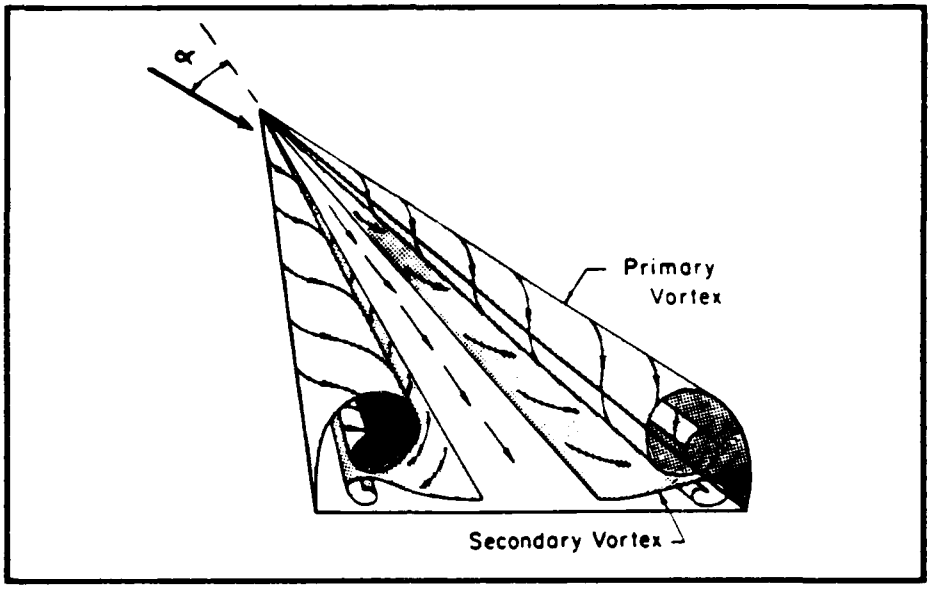

Figure 1. Vortical Flow Over a Delta Wing [1]

This breakdown or bursting, as it is commonly called, refers to the sudden structural change which usually results in the turbulent dissipation of the vortex. Vortex bursting is characterized by a sudden deceleration of the axial flow in the vortex core, the formation of a small recirculatory flow region, a decrease in the circumferential velocity, and an increase in the size of the vortex [1]. Other observed physical features of vortex core breakdown include a divergence of the stream tubes in the core just upstream of the breakdown, an external pressure gradient in the axial direction, and swirl angles (ϕ) generally in excess of 40 degrees [2]. Although re-

searchers have identified several different types of bursting, the two most common are the bubble and the spiral types--shown in Figure 2, reproduced from reference 1.

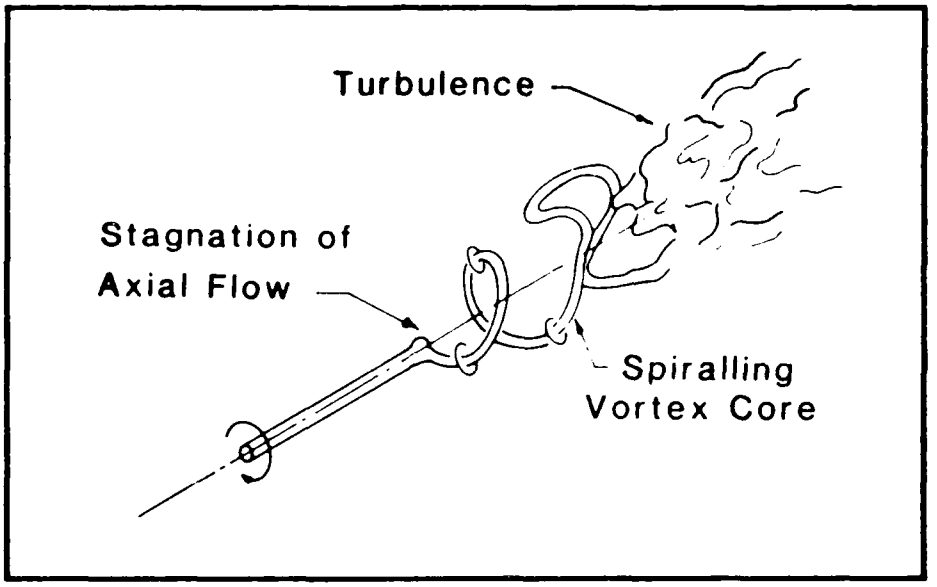

a. Spiral-Type Breakdown

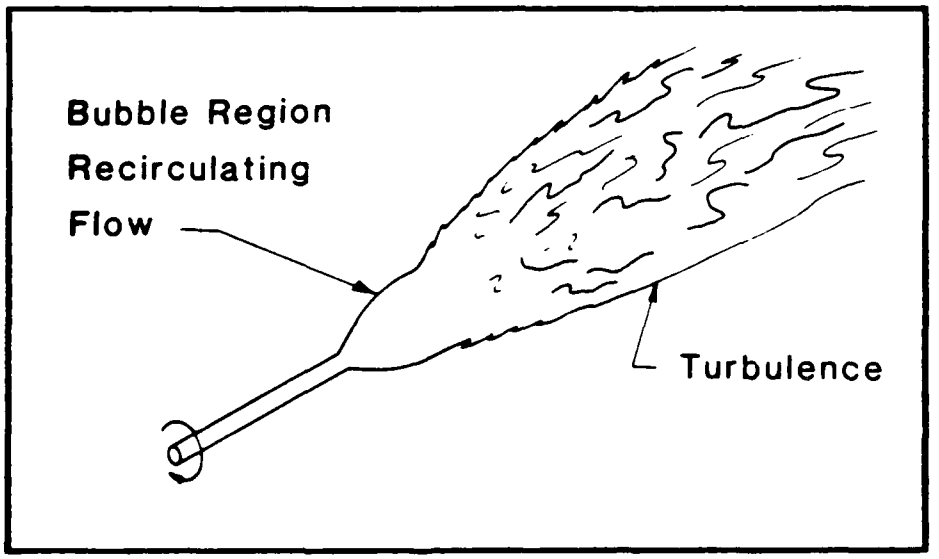

b. Bubble-Type Breakdown

Figure 2. Typical Vortex Breakdowns [1]

Regardless of the type of bursting that occurs, the result is the same--loss of lift as the point of vortex breakdown moves forward over the wing's upper surface towards the apex. Just where this breakdown occurs is influenced by several factors, one of which is obviously angle of attack; another is side slip angle; while a third, the focus of this effort, is unsteady flow over the wing.

There are several reasons for an empirical study of the effects of a pitching or oscillating wing. One reason is that an aircraft spends much of its time in an unsteady environment; takeoffs, landings and maneuvering all represent unsteady events. Another reason is that research shows that the unsteady motion of a wing significantly alters the lift curve characteristic possibly serving as a lift augmentation device. Yet another reason is that future fighters might have to operate at very high angles of attack in what has become known as the post-stall region [2]. Time dependent flow will surely play an important role for this next generation, super maneuverable aircraft.

Background

One of the earliest studies recognizing the connection between lift and unsteady flow was completed by Kramer in 1932 [4]. In the years to follow other researchers reached similar conclusions using different experiments; however, there was still a lack of understanding of the mechanism behind the increased lift. It was the late sixties when

engineers, unable to predict the performance of high speed helicopters using conventional aerodynamics, went looking for other answers. This led to several studies that indicated a vortex dominated flow field was probably responsible. Interest in what was dubbed "dynamic stall" spread when the phenomenon was associated with electric power generating wind turbines, jet engine compressors, and rapidly maneuvering aircraft. These early studies, almost all two-dimensional, provided a large base of information on the effects of variables like pitch rate, pitch axis location, and airfoil type. To complement these studies researchers began looking at three dimensional effects--a necessary step to fully understand the impact on maneuvering aircraft and to access possible ways of exploiting the phenomenon in the future. The remainder of this section gives a brief history, summarizing some of the major works in the field and serves as a backdrop for this study.

Early Studies

The study by Kramer completed in 1932 [4] was motivated by pilot reports of unexplained high lift while flying through turbulent air. To simulate this environment his experiment consisted of a fixed airfoil mounted in a wind tunnel with the unsteady flow provided by moving guide vanes in front of the airfoil. His results showed a direct relationship between the flow's angular rotation rate and the

maximum lift coefficient. By using a nondimensional angular rate parameter $c\dot{\alpha}/U$, Kramer derived the relationship shown below.

$$C_{L_{MAX\ Dyn}} = C_{L_{MAX\ ST}} + 0.36\ c\dot{\alpha}/U \qquad (1)$$

Another early study published by Harper and Flanigan in 1950 took a different approach. They pitched a model of a P-47 in a wind tunnel at non-dimensional rates from 0.002 to 0.02, at speeds up to 0.8 Mach number. They also found higher possible values of $C_{L_{MAX}}$, but noted that the effects decreased with increasing Mach number [5].

Helicopters

Although these early studies concluded that higher lift coefficients were possible, the mechanism behind the increase was yet to be explored. Motivation to go further came when helicopter design engineers were unable to predict the performance of high speed helicopters using conventional aerodynamics [6].

The phenomenon of dynamic stall, commonly referred to as retreating blade stall in helicopters, occurs due to the flow velocity difference between the advancing and retreating blades. In forward flight the slower relative speed of the retreating blade means that it must have a higher angle of attack to maintain balanced lift. In high performance heli-

copters this could put the blade above the steady -state stall angle for as much as half the revolution.

In 1968 Harris and Pruyn [7] and Ham and Garelick [8] recognized that the higher than expected lift values of the retreating blade were associated with a vortex formed on the airfoil during the increase in angle of attack. Later that same year Ham [9] used interferograms to show that the mechanism of dynamic stall included the shedding of a large leading edge vortex. As the vortex passed over the airfoil it created a large negative moment which he used to explain the torsional oscillations during retreating blade stall.

Two Dimensional Studies

The studies by Ham and others generated interest that extended beyond the field of helicopters. Several two dimensional studies followed that seeked to improve the understanding of dynamic stall. Although only a few will be mentioned here, an excellent source of references on the progress in analysis and prediction of dynamic stall was written in 1985 by Dr L. W. Carr of the NASA Fluid Dynamics Branch [6].

In 1978 McAlister and Carr performed a flow visualization experiment on a NACA 0012 airfoil with $k=0.25$, $Re=21000$, and $\alpha=10^{\circ}+10^{\circ}\sin\omega t$. They found the onset of dynamic stall began with a rapid movement of flow reversal toward the leading edge of the airfoil.

Between this region and the inviscid stream an unstable free shear layer formed which eventually transformed into several discrete clockwise vortices. As the reversed flow approached the leading edge a vortex appeared over the first 6 percent of the surface and eventually grew into the classic "dynamic-stall vortex" [9].

That same year, Deekens and Kuebler reported on an investigation of dynamic stall which evaluated the effects of constant airfoil pitch rate. They were able to show a direct relation between stall angle and angular rate as shown below [11].

$$\alpha_{Dyn\ Stall} = \alpha_{St\ Stall} + 143.2\ \dot{\alpha}_{ND} \qquad (2)$$

The effect of pitch location on dynamic stall was was investigated by Dimmick in 1985 [12]. As part of his investigation he transformed the above equation into a form comparable with that of Kramer's (Eq 1).

$$C_{LMax\ Dyn} = C_{LMax\ St} + 4.8c\dot{\alpha}/U \qquad (3)$$

Dimmick attributed the significant difference between the equations to the different experimental procedures used. Kramer's airfoil was fixed as previously mentioned yet for Deekens' and Kuebler's the flow was steady and the airfoil was pitched--a non-accelerating

versus an accelerating reference system. In each case Dimmick was able to show independent confirmation of both experiments. He also found that for a given pitch rate moving the pitch location aft of the leading edge would increase the dynamic stall angle of attack.

In 1987 Siuri, Walker, and Chou [13] conducted a study to further explore the effects of nondimensional pitch rate. They used pitch rates as high as 1380 degrees/second ($\dot{\alpha}_{ND}$= 0.6) and found the percent change in lift associated with dynamic stall was greater for the lower values of $\dot{\alpha}_{ND}$ (less than 0.2). They also found that the increase in the time averaged lift was nowhere as great as the change in the maximum lift. However, they did conclude that pitching the airfoil completely through the dynamic stall angle of attack was not necessary to realize an increase in lift.

Along those lines, a study by Stephen in 1987 attempted to take advantage of gaining higher lift values by stopping short of the dynamic stall angle. He used a periodic saw-tooth motion that consisted of different increasing and decreasing pitch rates. The best combination of rates for his experiment proved to be a nondimensional pitch rate up of 0.0145 from 10 to 20 degrees with a pitch down rate of 0.025. This profile provided a 10 percent increase over the static maximum coefficient of lift [14].

Further analysis of Stephen's results by Jumper [15] gave more insight into the effects of the periodic pitching. Jumper concluded that the cases which gave the highest average lift values were for pitch rate and angle combinations where the pitching was reversed before flow separation reached the quarter chord. He also felt that higher values of averaged lift might be realized by increasing the lower angle of attack limit.

Three Dimensional Studies

One study that compared two-dimensional and three-dimensional results was done by Robinson and Wissler using a pitching rectangular wing. They found that at distances greater than 1.4c from the wing tip the separated flow had the same characteristics as in previous two-dimensional studies. However, between 0.4c and 1.4c the dynamic stall vortex convection was restrained by the influence of the wing tip vortex. Furthermore, inside of 0.4c little downstream convection was observed--the leading edge vortex appeared to be pinned in place. These flow characteristics were used to explain two originally unexpected aspects of the pressure profiles. First, the magnitude of the pressure minimum peak did not vary along the span, and second, the duration of the vortex-wing interaction actually increased at span locations near the wing

tip. They concluded that previous two-dimensional studies could provide a good indication of three-dimensional rectangular wing performance [16].

Another topic that has received much attention in recent years is the effect of pitching a swept or delta wing; wings which are more representative of those used on modern aircraft. A study by Gad-el-Hak and Ho used a water channel to investigate the effects of pitching delta wings with sweep angles of 45 and 60 degrees. The 45 degree wing had an NACA 0012 profile and the 60 degree wing was a flat plate with sharp edges. For both wings they used a sinusoidal motion with an angle of attack range of 0 to 30 degrees. They found that

> During the upstroke, the separation first started across the whole trailing edge at α = 2 deg. As the angle of attack increased, the separation vorticies started to develop at the two corners of the trailing. The unsteady separation process looked as if a vortex sheet first peeled off from the corner of the wing and then rolled up into the separation vortex. The separation propagated from the corner to the apex. The upstream propagation speed along the leading edge was approximately equal to the freestream speed. During the downstroke, . . . As the angle of attack dereased from 30 deg, the flow near the whole leading edge (from the apex to the corners) became reattached [16:1662].

They also noticed that the leading-edge separation vortex went through a growth-decay cycle with a hysteresis during the pitching period [17].

The leading edge vortex of a pitching 70 degree

flat plate delta wing was the topic of an investigation by LeMay in 1988 [18]. He showed that for sinusoidal pitching the hysteresis in the vortex breakdown location increased with increased reduced frequency ($2\pi fc/u$).

Objectives

Most past research on pitching wings has involved the use of sinusoidal oscillations or constant ramp motions to a fixed angle of attack; however, very little has been done using a saw-tooth motion. In that light, the objectives of this experiment were

1. To design and build a motion system that would produce a saw-tooth motion for use in the Flight Dynamics Lab's 24-inch water tunnel. Also, design and build a variety of semi-span model wings for use in a parametric study.

2. Using the above system, explore the effects of saw-tooth motions which included combining different upstroke and downstroke rates on the vortex dynamics of each model wing.

3. Obtain trend data on the vortex development by digitizing select frames of the high speed video used to record the experiment.

II. Theory

Role of the Water Tunnel

A common concern when testing under other than full scale conditions is how well the test data will correlate with the real world. Accurate results require both geometric as well as dynamic similarity. Geometric similarity is a function of scale, whereas dynamic similarity normally requires the matching of certain dimensionless parameters which reflect the relative importance of viscous, inertial, and other forces. For fluid flow the dimensionless form of the Navier-Stokes equations as used by Erickson [2:51] is

$$(\bar{q}\ \nabla)\bar{q} = -(p_\infty/\rho U_\infty^2)\nabla p + Re\ \nabla^2\bar{q} \qquad (4)$$

which shows one of the key requirements for dynamic similarity is matching of the Reynolds number.

In his study of vortex flow correlation he showed the importance of Reynolds number matching. However, as he pointed out, the density of water is approximately 800 times higher, the kinematic viscosity 60 times higher, and the dynamic viscosity 0.08 that of air. As a result, a given Reynolds number for a water tunnel test can be obtained with a model one-third the size at only one-fourth of the free stream velocity. In any case, water tunnels are normally run at speeds of 0.15 to 0.25 feet/second for

flow visualization purposes resulting in Reynolds numbers two to three orders of magnitude below those for wind tunnel tests. Erickson concluded that for the water tunnel to truly represent the real situation, the fluid motion under consideration must be the kind which is insensitive to changes in Reynolds number [2].

An example of this type of flow is that characterized by the free vortex sheets emerging from the sharp leading edge of a delta wing. The vortices essentially become embedded in the inviscid fluid away from the boundary layer. "The fact that computational methods ignoring viscous effects are capable of predicting the aerodynamics of vortical flows with reasonable accuracy is one indication of the Reynolds number insensitivity of such flows [2:52]." A sharp leading edge is important because it forces the leading edge to be the separation point. "Since the vortex sheet originates at the leading edge, its structure is essentially independent of Reynolds number and consequently, one expects the water tunnel to be capable of simulating the position of the vortex core as well as the lift [2:59]."

The above does not hold true when dealing with a blunt-nosed wing, since without the sharp leading edge the separation point is very much a function of Reynolds number. As Erickson pointed out, results reveal earlier vortex formation and greater vortex induced lift. "In the

case of blunt-nosed wing, however, once the condition for which separation occurs everywhere along the leading edge is reached, it is considered that the fundamental character of the flow will be quite similar to that observed at high Reynolds number [2:181]."

One condition that will help insure that the leading edge is the separation point is high angle of attack. As the angle increases, vortex strength increases and the vortex shifts up and away from the boundary layer. "For example, at angles of attack at which vortex breakdown of the vortex occurs forward of the trailing edge reasonably good correlation at all wing sweep angles can be made [2:181]."

There are several studies that have compared results obtained from a water tunnel with either wind tunnel or computational data. A study by Davies compared the characteristics of the flow field around a generic missile gained from a water tunnel with subsonic and supersonic wind tunnel data. He found ". . . the flow field characteristics derived from the water tunnel can be representative of those at subsonic speeds. Isolated body vortex locations however have been found to agree more closely with those measured in the wind tunnel at supersonic speeds [19]."

There have also been some comparisons of dynamic angle of attack change studies. Using a 60 degree sweep, flat-plate delta wing, Wolffelt showed a good comparison of wind and water tunnel data for a pitching wing as shown in Figure 3 [20]. In addition, Erickson [2:278] cites several studies, one of which by Werle where the trajectories of air bubbles over an airfoil undergoing pitch oscillations in ONERA water tunnel experiments were in qualitative agreement with streamlines computed from the Navier-Stokes equations.

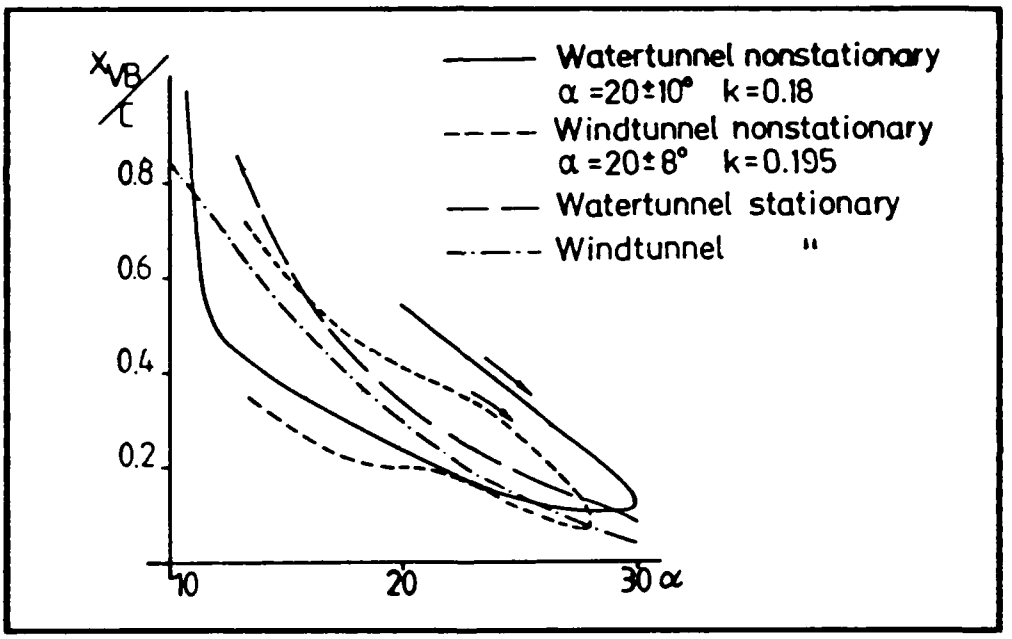

Figure 3. Comparison of Water Tunnel and Wind Tunnel Results for Static and Dynamic Vortex Burst Positions [20]

Flow Visualization

There are many different techniques in use today to visualize flow in a water tunnel. Some of these, as summarized by Werle [21], include the use of gaseous, liquid, or solid tracers. Gaseous tracers are normally bubbles, small in size to avoid buoyancy effects, generated through electrolysis. Common liquid tracers like dye, condensed milk, and food coloring can be injected either from a point upstream or from small ports on the model. Finally, one example of a solid tracer would be small polystyrene beads with a density very close to that of water.

For this experiment use of the liquid tracer was considered most practical since the facility had an in-place dye injection system and most of the expertise of the lab's personnel was in this area. However, no previous dynamic experiments had been performed in the tunnel, so much of the early part of the experiment involved trial-and-error tests to determine the best location, orientation and size of the dye ports.

Appendix D covers many of the lessons learned as a result of the early flow visualization trials. In short, the best results came from having dye ports on the model verses using a dye rake upstream. Also, when trying to track vortex development and breakdown, ports (or tubes) located just below and perpendicular to the leading edge

while being oriented parallel to the chord line worked well. Upper surface ports probably would have helped follow flow separation, although they were not used. The best size for the ports proved to be about 0.05 to 0.06 inches--slightly larger than the 0.02 to 0.03 inches used on previous static experiments. Also, running a single dye port from one dye reservoir (versus two or more ports per reservoir) proved helpful when trying to fine tune the flow picture.

III. Experimental Apparatus

Hydrodynamic Test Facility

The Hydrodynamic Test Facility operated by the Flight Dynamics Laboratory is a closed circuit vertical water tunnel designed to study the behavior of vortical flow about airframes and airframe components. There are five basic parts to the facility: the reservoir, the test section, the holding tanks, the flow control system, and the dye injection system.

The constant head reservoir measures 8 feet by 8 feet and is 16 feet high; it holds approximately 7000 gallons of water. A converging inlet from the reservoir to the test section has a contraction ratio of 16:1 over an 8 foot length.

The test section measures 24 inches by 24 inches and is 48 inches long. Currently it has 2-inch plexiglas on 2 sides with short range plans calling for the addition of a third window. The remaining side serves as a quick access door and slides out on tracks. This door also houses a motorized sting which allows angle of attack changes to be made from outside the tunnel. For this experiment the sting was replaced with the motion system described later in this section.

After the water passes the test section it drains into a series of four 6500 gallon storage tanks located in the basement of the facility. Water is returned to the reservoir by a parallel system of 250 gallon/minute pumps. Presently the system can operate at maximum continuous flow rate of 0.85 feet/second. Alternatively, the tunnel can operate in a gravity feed mode where a full reservoir will, for example, give a 15 minute run at 0.35 feet/second. Original plans called for a maximum gravity feed flow rate of 35 feet/second but valve and plumbing restrictions now limit this to 0.85 feet/second.

The dye injection system has 12 quart-size, independently controlled, pressurized reservoirs to permit fine tuning of the flow picture. The pressure is required to overcome the head pressure in the test section.

The most recent calibration of the facility was done in early 1988 using a hot film probe. Shortly thereafter measurements were also taken using laser velocimetry. Results from the tests were similar and showed turbulence levels of approximately three to four percent and a velocity profile with slightly slower flow rates down the center of the test section. The turbulence levels were considered good, on the other hand, improvement was still sought for the velocity profile. One possible explanation for the uneven rate was the honeycomb/foam combination in use as a flow straightener. This was replaced with a foam/screen combination, unfortunately a complete recalibration

of the tunnel was not possible before the start of this experiment. However, a rough calibration was done by moving a dye rake around the test section and visually checking the quality of the streamlines; velocity was checked by timing dye elements in the flow. The procedure and results are covered in Section IV and Appendix C. Figure 4 shows a schematic of the tunnel.

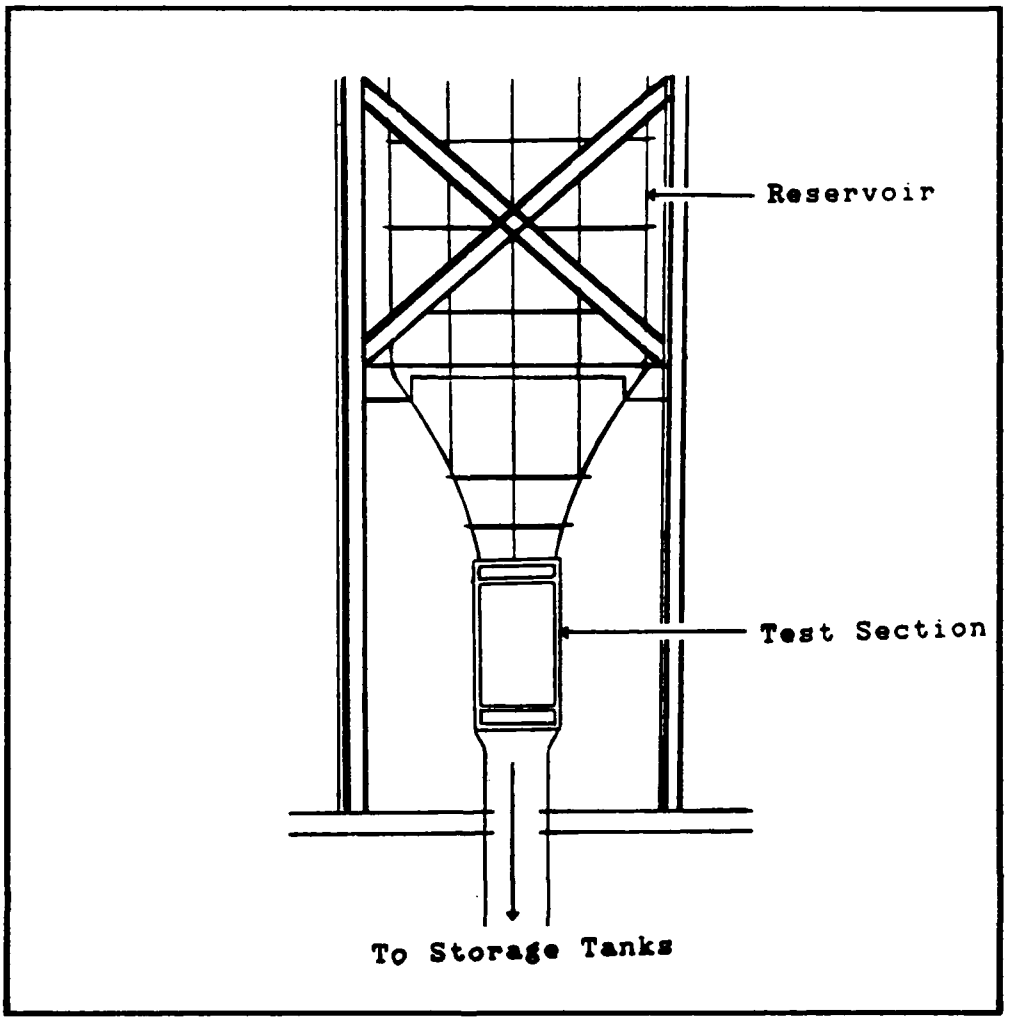

Figure 4. Water Tunnel Schematic

Models

The models used for this experiment consisted of interchangeable semi-span wings mounted on a splitter plate. Six wings total, three with an NACA 0012-34 profile (0.12c thick at 0.4c) and sweep angles of 0, 45, and 65 degree; and three flat plates with sweep angles of 25, 45, and 65 degrees were studied. Small stainless steel tubes (0.05 inches inner diameter) were cast inside the aluminum/ epoxy composite wings (NACA 0012-34) to serve as internal reservoirs near the leading edge. The reservoirs in turn could be tapped at various locations by drilling holes near the leading edge to provide the best flow picture. The flat plate wings were constructed from 0.09-inch-thick stainless steel with a 20 degree double bevel used to form a sharp leading and trailing edge. Dye tubes attached to the lower surface were used to place dye near the leading edge.

The wings were mounted on the splitter plate so that they were free to rotate about mid-chord. There was insufficient space to run the dye tubes through the mounting shafts; instead the tubes were routed into the wings at the 0.4 chord location. However, this meant that a slot had to be cut in the splitter plate to allow the wings to rotate. To seal this hole, each wing was mounted on a 2-inch diameter disk which fit into a matching recess milled into the plate. The wings were painted white, and the splitter plate light grey, to provide contrast with the dye. In

addition, each wing was marked with a 1 inch black grid pattern to help in data reduction. Dimensions for each wing are shown in Figure 5.

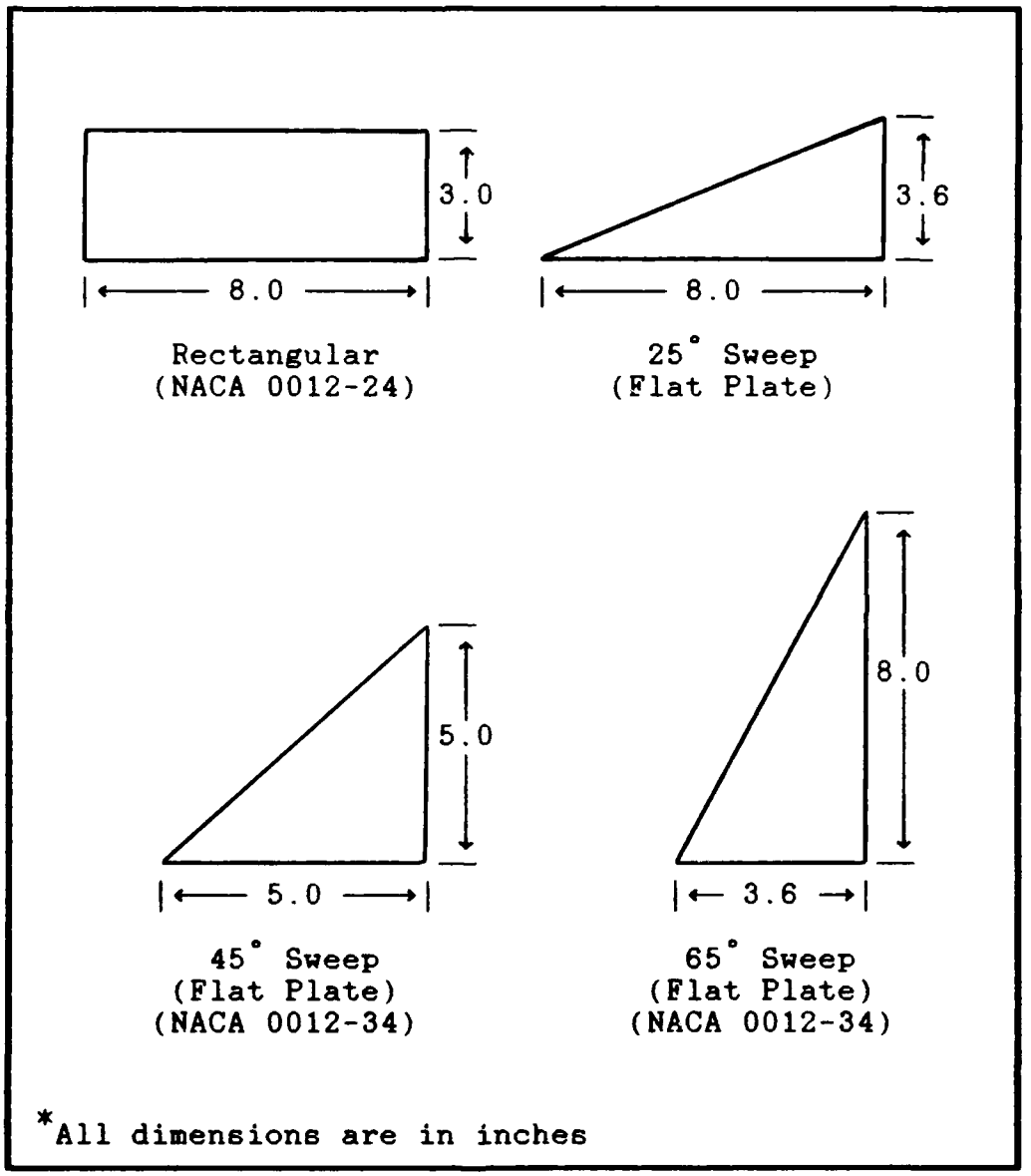

Figure 5. Illustration of Models

Motion System

The system was designed to provide a constant pitch rate motion including the capability to program a periodic saw-tooth motion with different increasing and decreasing rates. The major components included a DC servo motor, a Zenith Z100 personal computer, a motion control card, and a DC amplifier.

The motor used to pitch the wings was an EG&G Torque Systems MTE-3528 DC servo motor whose shaft output power was 245 watts (approximately one-third horse power) with a peak torque rating of 1500 ounce inches. The high torque translated to quick acceleration--constant speed was reached in close to 1/100 of a second. A 10:1 worm gear reducer connected the motor to the tunnel input shaft. This was necessary to smooth out rough motion at slow speeds caused by a 500 encoder-point count per 360 degree revolution.

Control for the system was centered around the Z100 PC. Using the BASIC program MOTOR (found in Appendix A), commands could be sent through an RS232 interface to a Delta Tau Data Systems MC^2 Mini Motion Control Card. The MC^2 has a full range of commands to control the position, velocity, and acceleration of the motor's output shaft through a Westamp A721 series DC amplifier. The system also includes a digital readout of shaft position.

Video and Photographic Equipment

This aspect was critical because all records pertaining to the experiment were photographic in nature. Data was recorded using high speed black and white video, three-quarter inch color video, and black and white still photography. The high speed camera provided a means of obtaining trend data while the color video provided the best qualitative record. On the other hand, the purpose of the still photographs was to serve as an example of the video records.

The system used to collect the high speed data was an SP2000 Motion Analysis System made by the Spin Physics Division of Eastman Kodak. This system offered several useful features for this experiment. First, the video display removed the uncertainty from the lighting requirements--what showed on the screen is what ended up on tape. Second, the system has dual camera capability, allowing for a full choice of imaging from both cameras on the same screen. This made it possible to consider three dimemsional aspects from a simultaneous side and top view of a wing. Finally, the system has a built-in reticle control which displays x and y coordinates of a selected point. By using software obtained from Kodak, the coordinate values could be transferred across an IEEE 488 interface, in this case to a Zenith 248 computer, thereby eliminating the need for a digitizing table.

Two other types of cameras used were the Panasonic Digital 5000 and the Hasselblad 2-1/4 inch by 2-1/4 inch square negative still camera. The Panasonic had an 8x1:14 TV zoom lens and was used with a Sony VO-5600 video cassette recorder. As with the SP2000, two cameras were used to provide a split-image recording while information concerning the experiment was superimposed on the tape using a VTW-100 video typewriter. For the still photographs, two Hasselblad cameras were used; however, it was not possible to take simultaneous pictures of the side and top views due to equipment limitations.

IV. Experimental Procedure

Water Tunnel Flow Rate Calibration

The flow rate of the tunnel was calibrated by timing small dye elements in the flow using the Digital 5000 video camera. Although a more complete picture of the flow could have been obtained with a hot film anemometer or a laser velocimeter, neither was available for this study. Results showed that the tunnel's flow meter was accurate to about 3.0 percent for the middle to higher speeds used; however, the error increased close to 10 percent at the slowest speed of 0.6 inches/second. A more detailed explanation can be found in Appendix C.

Model Motion Calibration

The pitching motion of the models was calibrated with the SP2000 high speed video system under tunnel flow conditions of 0.2 ft/sec (2.4 in/sec). The predicted time required to accelerate to a constant rate varied with pitch rate with typical values of 2 to 4 milliseconds based on the parameters used in the motion program (Appendix A).

Results showed that acceleration to the desired rate was quick, as predicted, and that the increasing and decreasing ramps of the saw-tooth motion were linear. More

details and plots for rates of 1, 10 , and 20 degrees per. second can be found in Appendix C.

Accuracy of the SP2000 Reticle System

Video data was central to this study and was reduced with the aid of the XY reticle on the SP2000. Knowledge of its accuracy was important before trying to analyze data.

The data area covered by the reticle on the SP2000 was 236 horizontal (X) units by 192 vertical (Y) units. Since these values were fixed, the accuracy of measurements was affected by the size of the image on the screen. Typical values, assuming the reticle could be placed within one unit, ranged from 0.006c to 0.008c.

Another possible source of error was shifting of the video image when it was replayed in the freeze-frame mode. To determine if this was a problem, a small cross which could just be covered by the reticle cross hairs was filmed at rates of 60 and 200 frames per second. For each rate 100 samples of XY coordinates were taken and compared. There were no differences noted, therefore this was eliminated as a possible source of error. Although higher accuracy could have been obtained with high speed film and a digitizing table, the video was more economical and was considered sufficiently accurate for this study.

Data Collection

Data collection consisted of taping or photographing each model with the Kodak SP2000, the Panasonic Digital 5000, and the Hasselblad 2-1/4 inch by 2-1/4 inch square-negative still camera. For the video systems a simultaneous side and top view was split-imaged on a single tape. In each case the side camera was aligned with the pitching axis while the top camera was centered on the intersection of the pitching axis and a line drawn vertically through the mid-span of the trailing edge. The video cameras were located approximately 75 inches from the model; the still cameras approximately 18 inches. Lighting was provided by four intensity-adjustable 1000-watt lights. With a model in place, the tunnel was filled and then allowed to run for 20 to 30 minutes while adjustments were made to the dye and lighting systems. Dye reservoir pressure was adjusted with a master valve to overcome the test section head pressure and then fine tuned with an individual needle valve. To avoid constant changes to these settings the tunnel was run in the continuous flow mode which kept the main reservoir, and as a result the test section pressure, at the same level.

To provide a baseline for comparison with dynamic data, each model was filmed for a range of static angles of attack. The range used for each model is shown in Tables I to VI; in each case a 2 degree increment was used. With the SP2000 approximately 6 seconds of data was taken at 60

frames per second representing about 360 frames while with the Digital 5000, 30 seconds of data was recorded at 30 frames per second. After taking the static data, each model was pitched through 5 cycles using the ranges and rates shown in Tables I to VI and again recorded with both systems using the same frame rates. Additionally, the effect of flow velocity on vortex breakdown for a fixed angle of attack was looked at using the 65 degree sweep flat plate wing at incremental speeds of 0.05 ft/sec from 0.1 to 0.4 ft/sec.

The Hasselblad Cameras provided the other photographic record of the experiment. The still results were not intended to be a source of data, but instead were to serve as an example of the video data for the results section of this report.

TABLE I

Pitch Rate Combination Summary - Rectangular Wing
(Flow Rate 0.6 in/sec)

Angle of Attack (Deg)	$\dot{\alpha}_{ND}$ Up	$\dot{\alpha}$ Up (Deg/Sec)	$\dot{\alpha}_{ND}$ Down	$\dot{\alpha}$ Down (Deg/Sec)
(Static)				
Center Span				
0 to 20	0	0	0	0
Tip				
6 to 26	0	0	0	0
(Dynamic)				
5 to 25	0.100	1.15	0.050	0.57
	0.100	1.15	0.075	0.86
	0.100	1.15	0.100	1.15
	0.100	1.15	0.150	1.72
	0.100	1.15	0.200	2.29
5 to 25	0.200	2.29	0.100	1.15
	0.200	2.29	0.150	1.72
	0.200	2.29	0.200	2.29
	0.200	2.29	0.300	3.44
	0.200	2.29	0.400	4.58
5 to 25	0.300	3.44	0.150	1.72
	0.300	3.44	0.225	2.58
	0.300	3.44	0.300	3.44
	0.300	3.44	0.450	5.16
	0.300	3.44	0.600	6.88

TABLE II

Pitch Rate Combination Summary - Rectangular Wing
(Flow Rate 1.8 in/sec)

Angle of Attack (Deg)	$\dot{\alpha}_{ND}$ Up	$\dot{\alpha}$ Up (Deg/Sec)	$\dot{\alpha}_{ND}$ Down	$\dot{\alpha}$ Down (Deg/Sec)
(Static)				
Center Span				
0 to 20	0	0	0	0
Tip				
6 to 26	0	0	0	0
(Dynamic)				
0 to 20	0.100	3.44	0.050	1.72
	0.100	3.44	0.075	2.58
	0.100	3.44	0.100	3.44
	0.100	3.44	0.150	5.16
	0.100	3.44	0.200	6.88
0 to 20	0.200	6.88	0.100	3.44
	0.200	6.88	0.150	5.16
	0.200	6.88	0.200	6.88
	0.200	6.88	0.300	10.31
	0.200	6.88	0.400	13.75
0 to 20	0.300	10.31	0.150	5.16
	0.300	10.31	0.225	7.73
	0.300	10.31	0.300	10.31
	0.300	10.31	0.450	15.47
	0.300	10.31	0.600	20.63

TABLE III

Pitch Rate Combination Summary - 25 Degree Sweep
(Flow Rate 1.8 in/sec)

Angle of Attack (Deg)	$\dot{\alpha}_{ND}$ Up	$\dot{\alpha}$ Up (Deg/Sec)	$\dot{\alpha}_{ND}$ Down	$\dot{\alpha}$ Down (Deg/Sec)
(Static)				
4 to 26	0	0	0	0
(Dynamic)				
4 to 32	0.100	2.86	0.050	1.43
	0.100	2.86	0.075	2.15
	0.100	2.86	0.100	2.86
	0.100	2.86	0.150	4.30
	0.100	2.86	0.200	5.73
4 to 32	0.200	5.73	0.100	2.86
	0.200	5.73	0.150	4.30
	0.200	5.73	0.200	5.73
	0.200	5.73	0.300	8.59
	0.200	5.73	0.400	11.46
4 to 32	0.300	8.59	0.150	4.30
	0.300	8.59	0.225	6.45
	0.300	8.59	0.300	8.59
	0.300	8.59	0.450	12.89
	0.300	8.59	0.600	17.19

TABLE IV

Pitch Rate Combination Summary - 45 Degree Sweep
(Flow Rate 1.8 in/sec)

Angle of Attack (Deg)	$\dot{\alpha}_{ND}$ Up	$\dot{\alpha}$ Up (Deg/Sec)	$\dot{\alpha}_{ND}$ Down	$\dot{\alpha}$ Down (Deg/Sec)
(Static)				
6 to 32	0	0	0	0
(Dynamic)				
8 to 32	0.100	2.06	0.050	1.03
	0.100	2.06	0.075	1.55
	0.100	2.06	0.100	2.06
	0.100	2.06	0.150	3.09
	0.100	2.06	0.200	4.13
8 to 32	0.200	4.13	0.100	2.06
	0.200	4.13	0.150	3.09
	0.200	4.13	0.200	4.13
	0.200	4.13	0.300	6.19
	0.200	4.13	0.400	8.25
8 to 32	0.300	6.19	0.150	3.09
	0.300	6.19	0.225	4.64
	0.300	6.19	0.300	6.19
	0.300	6.19	0.450	9.23
	0.300	6.19	0.600	12.38

TABLE V

Pitch Rate Combination Summary - 45 Degree Sweep
(Flow Rate 3.0 in/sec)

Angle of Attack (Deg)	$\dot{\alpha}_{ND}$ Up	$\dot{\alpha}$ Up (Deg/Sec)	$\dot{\alpha}_{ND}$ Down	$\dot{\alpha}$ Down (Deg/Sec)
(Static)				
6 to 32	0	0	0	0
(Dynamic)				
8 to 32	0.100	3.44	0.050	1.72
	0.100	3.44	0.075	2.58
	0.100	3.44	0.100	3.44
	0.100	3.44	0.150	5.16
	0.100	3.44	0.200	6.88
8 to 32	0.200	6.88	0.100	3.44
	0.200	6.88	0.150	5.16
	0.200	6.88	0.200	6.88
	0.200	6.88	0.300	10.31
	0.200	6.88	0.400	13.75
8 to 32	0.300	10.31	0.150	5.16
	0.300	10.31	0.225	7.73
	0.300	10.31	0.300	10.31
	0.300	10.31	0.450	15.47
	0.300	10.31	0.600	20.63

TABLE VI

Pitch Rate Combination Summary - 65 Degree Sweep
(Flow Rate 3.6 in/sec)

Angle of Attack (Deg)	$\dot{\alpha}_{ND}$ Up	$\dot{\alpha}$ Up (Deg/Sec)	$\dot{\alpha}_{ND}$ Down	$\dot{\alpha}$ Down (Deg/Sec)
(Static)				
18 to 36	0	0	0	0
(Dynamic)				
18 to 38	0.050	1.29	0.025	0.65
	0.050	1.29	0.037	0.97
	0.050	1.29	0.050	1.29
	0.050	1.29	0.075	1.93
	0.050	1.29	0.100	2.58
18 to 38	0.100	2.58	0.050	1.29
	0.100	2.58	0.075	1.93
	0.100	2.58	0.100	2.58
	0.100	2.58	0.150	3.87
	0.100	2.58	0.200	5.16
18 to 38	0.200	5.16	0.100	2.58
	0.200	5.16	0.150	3.87
	0.200	5.16	0.200	5.16
	0.200	5.16	0.300	7.73
	0.200	5.16	0.400	10.31

Data Reduction Technique

To analyze trends from the videotaped data, selected frames of the SP2000 records were digitized using the system's xy reticle. The digitized data was transferred across an IEEE 488 interface to a Zenith 248 microcomputer by using the Data Acquisition Software Program (DASP) provided by Kodak. DASP produced arrays equal to the number of points digitized per frame where each array contained values for x, y, and frame number. This information was used as input for the program REDUCE found in Appendix A.

Figure 6 represents a typical digitized frame of video information for the 65 degree sweep wing where the points A to I were used to define angle of attack (α), vortex inclination angle (β), chordwise vortex breakdown location (x/c), and spanwise breakdown location (y/s) [Note: In the photograph the top view contains a shadow]. Following the technique used by LeMay [18], $\overline{AB}$ defined a vector perpendicular to the 0 degree α reference line and $\overline{CD}$ defined the chord line--using the dot product of the two vectors:

$$\alpha = \frac{\pi}{2} - \cos^{-1}\left[\frac{\overline{AB} \cdot \overline{CD}}{|\overline{AB}|\ |\overline{CD}|}\right] \qquad (5)$$

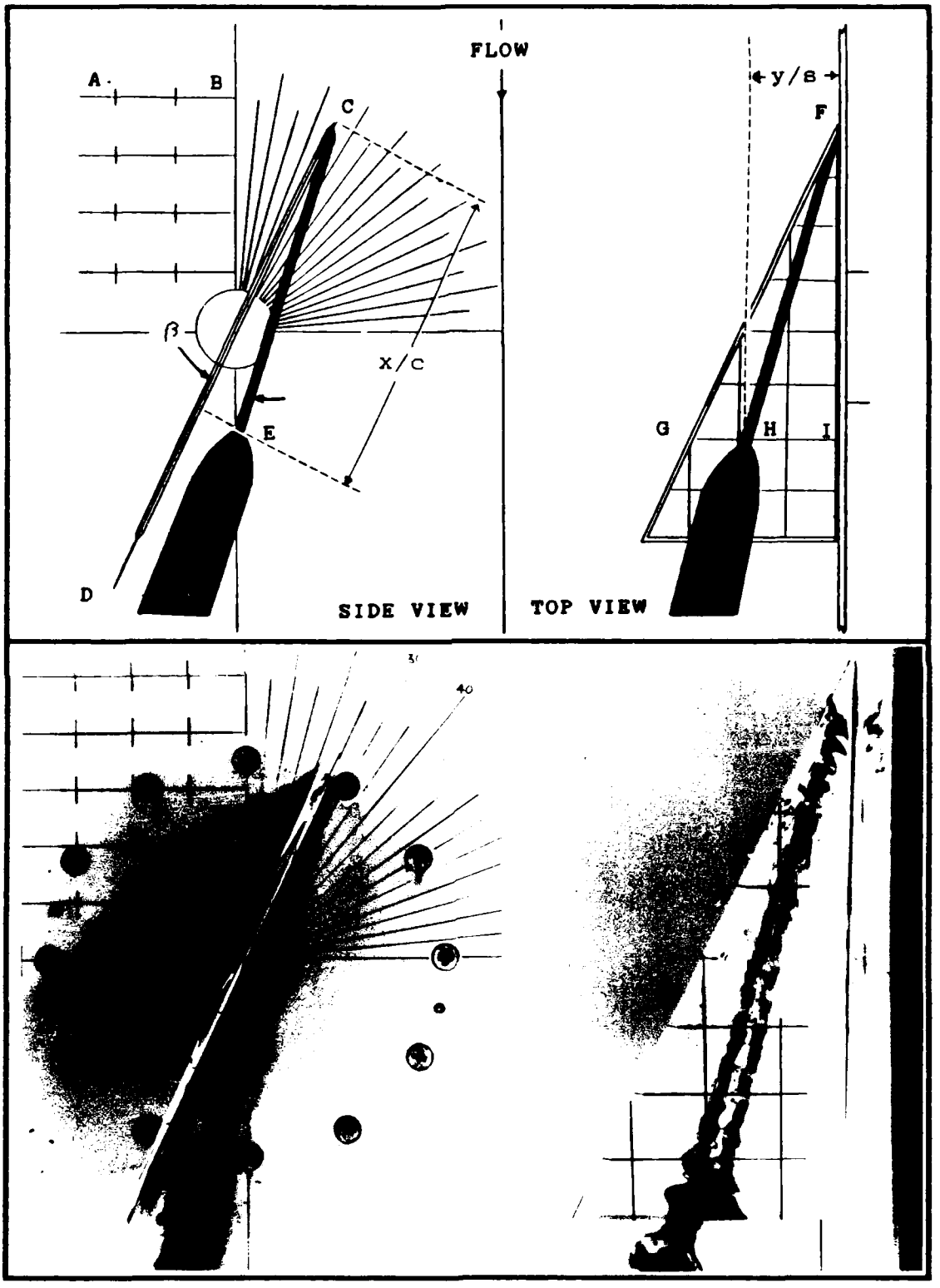

Figure 6. Example Video Frame Illustrating Digitized Points

Similarly, for the vortex inclination angle:

$$\beta = \cos^{-1}\left[\frac{\overline{CD} \cdot \overline{CE}}{|\overline{CD}|\ |\overline{CE}|} \right] \qquad (6)$$

To determine the chordwise location of the vortex breakdown (x/c) the vector $\overline{CE}$ was projected on $\overline{CD}$. The resulting equation, shown below, includes a correction to account for the small trailing edge probe used to better identify the chord line.

$$x/c = \cos(\beta) \left[\frac{|\overline{CE}|}{P\ (|\overline{CD}|)} \right] \qquad (7)$$

Where

$$P = c/(c + \text{probe length})$$

and

$$|\overline{CD}| = c + \text{probe length}$$

Looking at the top view of Figure 6, the points G, H, and I were used to determine the spanwise location of the vortex breakdown using the relation shown below.

$$y/s = \frac{|\overline{HI}|}{|\overline{GI}|} \qquad (8)$$

There was a parallax error to consider for the spanwise breakdown location because the camera angle was perpendicular to the flow and not the model surface. However, with the camera located about 75 inches from the model and typical vortex burst heights on the order of 0.5 inches the parallax correction would be around 3 percent of the spanwise value. Considering the subjectiveness of identifying the burst location this error was considered negligible.

The above procedure was used to reduce the data for both the 45 degree and 65 degree sweep wings while for the rectangular wing only the side view was digitized. In this case, angle of attack was defined in the same manner, however now points E and F were redefined with E used to track the upper surface flow separation point and F used to follow the shed dynamic stall vortex. Unfortunately data for the 25 degree sweep wing was not digitized due to difficulty defining vortex burst on the black and white video. Instead, qualitative comparisons were made based on the clearer color video.

To get the angle and burst information necessary to compare the wings the program REDUCE (Appendix A) was used with the DASP output as the input. Typically four to five frames were averaged to produce a data point. Figure 7, with data taken from the 65 degree sweep flat plate, illustrates how points were averaged for the dynamic data and then fit with a cubic spline approximation to provide

smooth trend data. Static burst data was fit with a linear approximation to serve as a base line for comparison with the dynamic data.

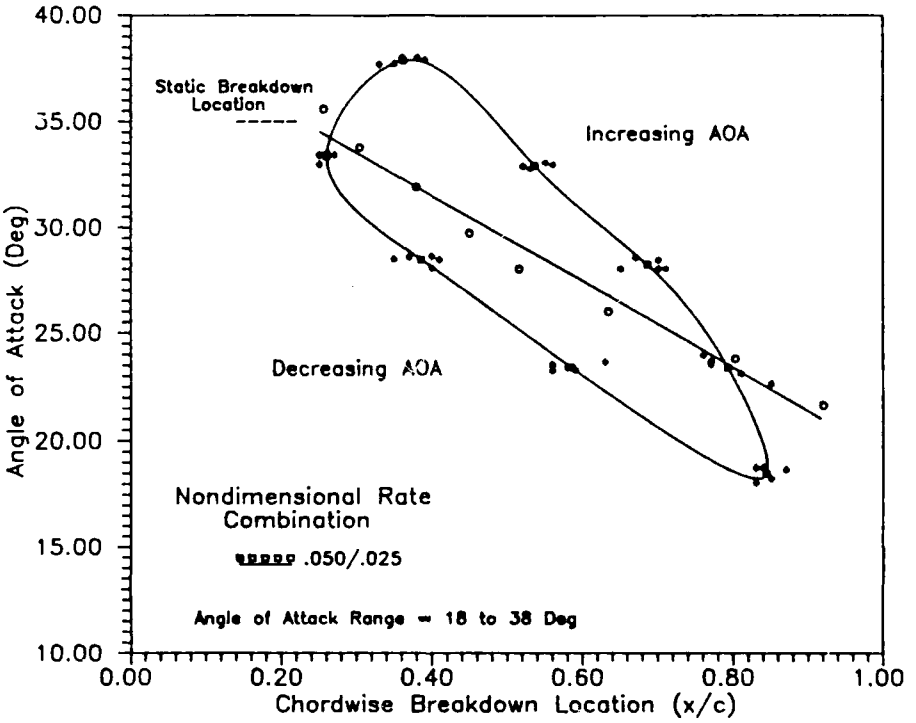

Figure 7. Example Plot Illustrating Data Fit Techniques

V. Discussion of Results

Rectangular Wing

The rectangular wing, pitched with a periodic saw-tooth motion, exhibited many of the characteristics of a sinusoidally pitched wing, including delayed upper surface flow separation during the upstroke and a clearly defined shed vortex commonly called a dynamic stall vortex. The flow separation point, vortex strength, and the vortex convection rate proved to be a function of the various pitch rates. Of the two flow rates used (0.6 and 1.8 in/sec) the slower speed provided a clearer picture of the vortex and was used to determine the trends discussed in the following paragraphs.

Looking first at flow separation, Deekens and Kuebler, and others [11] showed that increasing values of nondimensional pitch rate delayed separation and as a result, stall. Figure 8 shows the chordwise separation location for three different pitch combinations for an angle of attack range of 5 to 25 degrees. Notice that in the case of the lower two rates, quarter-chord separation occurs before reaching the maximum angle of attack. However for the highest nondimensional rate of 0.3, quarter-chord separation essentially occurs only after the wing starts to decelerate just prior to the maximum angle of

attack. This last case is similar to the profile that Jumper and Stephen [15] felt might produce the best time-averaged lift, with the rapid pitch down started before the flow separated at quarter chord. Although in this experiment the nondimensional pitch rates of 0.05 to 3.0 were much higher than their range of 0.01 to 0.038.

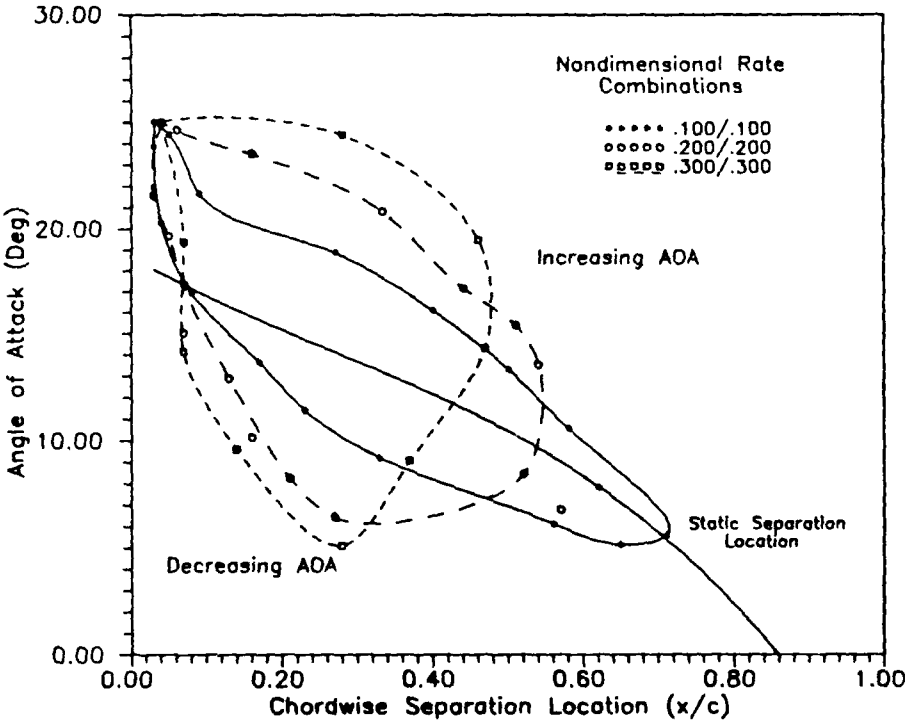

Figure 8. Chordwise Position of Flow Separation, Rectangular Wing, Mid-Span, U = 0.6 in/sec

Jumper appears to believe that the profile where the pitch down is started before quarter-chord prevents the formation of a full-fledged, dynamic-stall vortex as evidenced by the lack of both an appreciable drag rise and a moment spike caused by the vortex convecting over the rear

of the airfoil. For this experiment, in tests not shown, a vortex was shed each time the wing reversed direction after exceeding the static stall angle of attack; however, reversing direction closer to the static stall angle generally produced a smaller vortex.

An alternative explanation for the lack of the spike might be related to the vortex position during the part of the cycle after it is shed. In that light, Figure 9 shows that for a combination of an upstroke rate of 0.3 and a downstroke rate of 0.6 (or a ratio of 0.5) the vortex only reached about 0.3 chord by the time the wing returned to the minimum angle of 5 degrees. And although not shown in

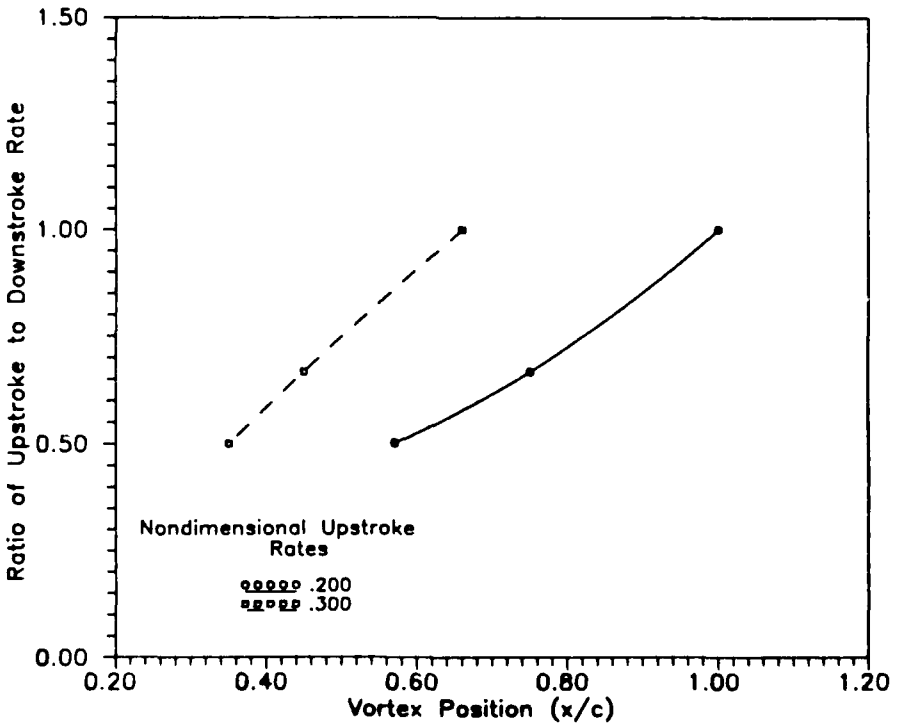

Figure 9. Chordwise Vortex Position at $\alpha = 5^{\circ}$ as a Function of Downstroke Rate, Rectangular Wing, Mid-Span, U = 0.6 in/sec

this case, the vortex does not leave the trailing edge until the wing has almost again reached the maximum angle of 25 degrees.

Another effect of increasing downstroke rate was to increase the vortex convection rate as shown in Figure 10. One possible reason for this is that at the higher pitch rates the vortex spends less time in the wake of the pitched wing. Also, if the vortex is still above the wing as it starts the upstroke, the wing seems to push the vortex along.

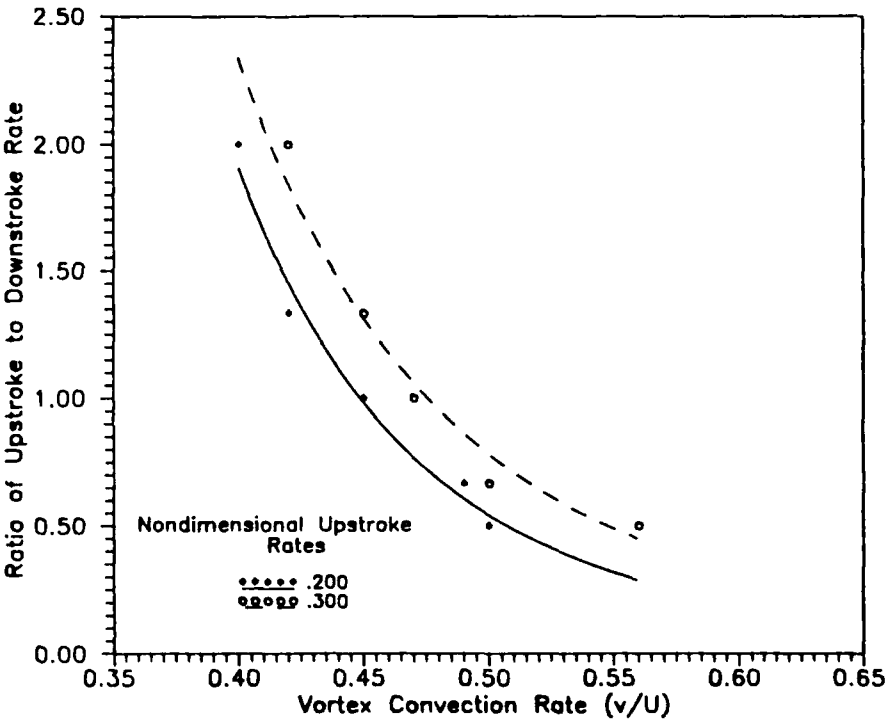

Figure 10. Vortex Convection Rate as a Percentage of Free Stream Velocity, Rectangular Wing, U = 0.6 in/sec

Finally, Figures 11 and 12 provide typical flow visualization examples for the rectangular wing. Figure 11 compares static and dynamic flow separation at 15 degrees angle of attack where in the pitching case the nondimensional rate was 0.1. Additionally, Figure 12 shows the dynamic stall vortex formed by using a nondimensional rate combination of 0.2 up and down.

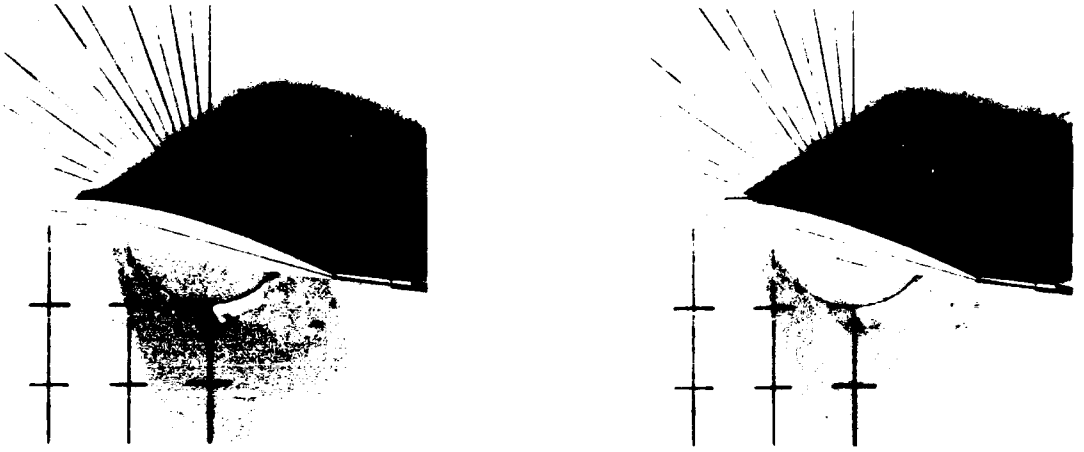

a. Static

b. Pitching

Figure 11. Comparison of Flow Separation on the Rectangular Wing for Static and Pitching Cases, Mid-Span, $\alpha = 15^{\circ}$, $\dot{\alpha}_{ND} = 0.1$, U = 0.6 in/sec

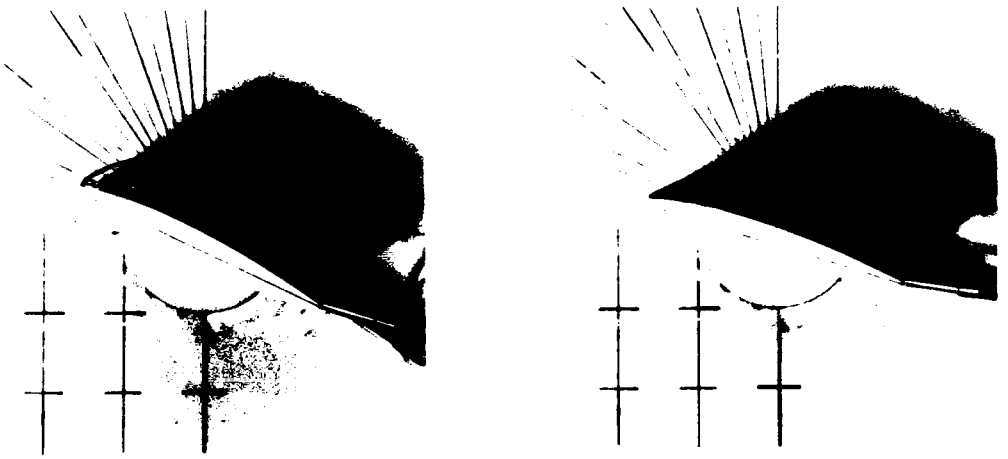

Figure 12. Examples of the Dynamic Stall Vortex Formed by the Rectangular Wing, $\dot{\alpha}_{ND}$ = 0.2 Up and Down, Mid-Span, U = 0.6 in/sec

25 Degree Sweep Wing

The results for the 25 degree sweep wing were similar in terms of flow separation to the rectangular wing for static angles of attack; however, for the pitching cases there was a significant difference. Static angles were varied from 4 to 26 degrees, while for the dynamic cases the range was 4 to 32 degrees. The wing was not tested statically to the dynamic limit because by 26 degrees the

flow had long since separated and there was no vortex activity.

Statically, as angle of attack was increased, there was evidence of span wise flow towards the tip, with substantial separation occurring by 10 degrees and complete separation at about 12 degrees. There was no evidence of any organized leading edge vortex like that commonly found on more highly swept wings, only a weak swirling fluid motion starting about 0.1c behind the apex and extending for about 0.3c. However, the flow changed significantly for the pitching wing.

Pitching the wing affected both the flow separation and the vortex activity above the wing. As with the rectangular wing, pitching delayed separation although not to the same extent. The separation started near the tip and proceeded along the leading edge towards the apex consistent with the findings of Gad-el-Hak [17]. Along with the change in separation, pitching also produced a clear, leading edge vortex.

The vortex generated by pitching resembled the leading edge vortex produced by more highly swept wings including, in some cases, an identifiable breakdown location. Initial vortex activity at mid-span (most outboard dye port) near the leading edge started at about 14 degrees angle of attack for a nondimensional rate of 0.1 and increased by about 2 degrees for each 0.1 increase in pitch rate. This

appears to differ from the findings of Gilliam and others [22] who found no change in the vortex initiation angle with increasing pitch rate for a 30 degree sweep delta. However, their wing was pitched at 0.25c at rates ranging from 0.2 to 1.0 leaving the comparison open to interpretation. For this study, regardless of the pitch rate the vortex would start to roll up parallel to the leading edge and with increasing angle of attack would move to a position approximated by a line drawn from the apex to the mid point of the trailing edge. Figure 13 shows the flow field above wing for the static and dynamic cases illustrating the delayed separation and the leading edge vortex.

Varying the upstroke rate had a significant effect on vortex development, while varying the downstroke rate made no obvious difference. Comparing the wing at 25 degrees angle of attack for different upstroke rates (no figure) showed that for a rate of 0.1 the vortex had reached the orientation mentioned above and was bursting about 0.5c; on the other hand, at a rate of 0.3 the vortex was still predominantly parallel to the leading edge with no identifiable breakdown point. As for the downstroke, with an upstroke rate of 0.1 as soon as the wing reversed direction at 32 degrees, the burst point would move to the apex regardless of the downstroke rate and the vortex would not appear again until the upstroke. In contrast, for an upstroke rate of 0.3 the vortex, appearing weaker and shifted

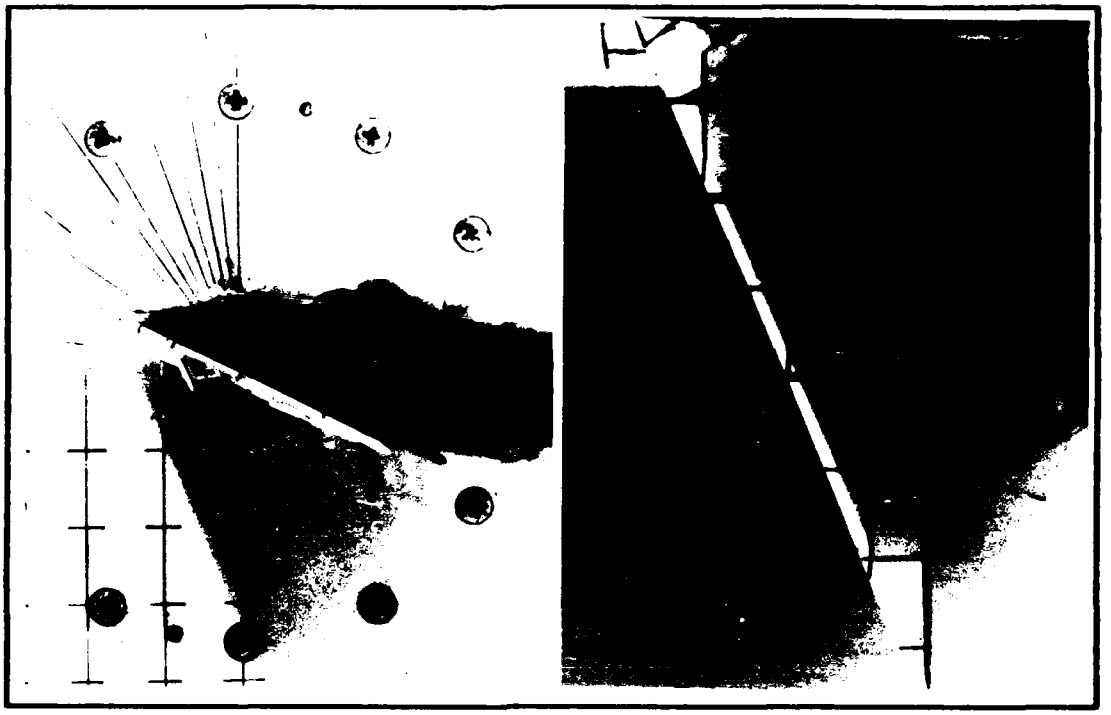

a. Static

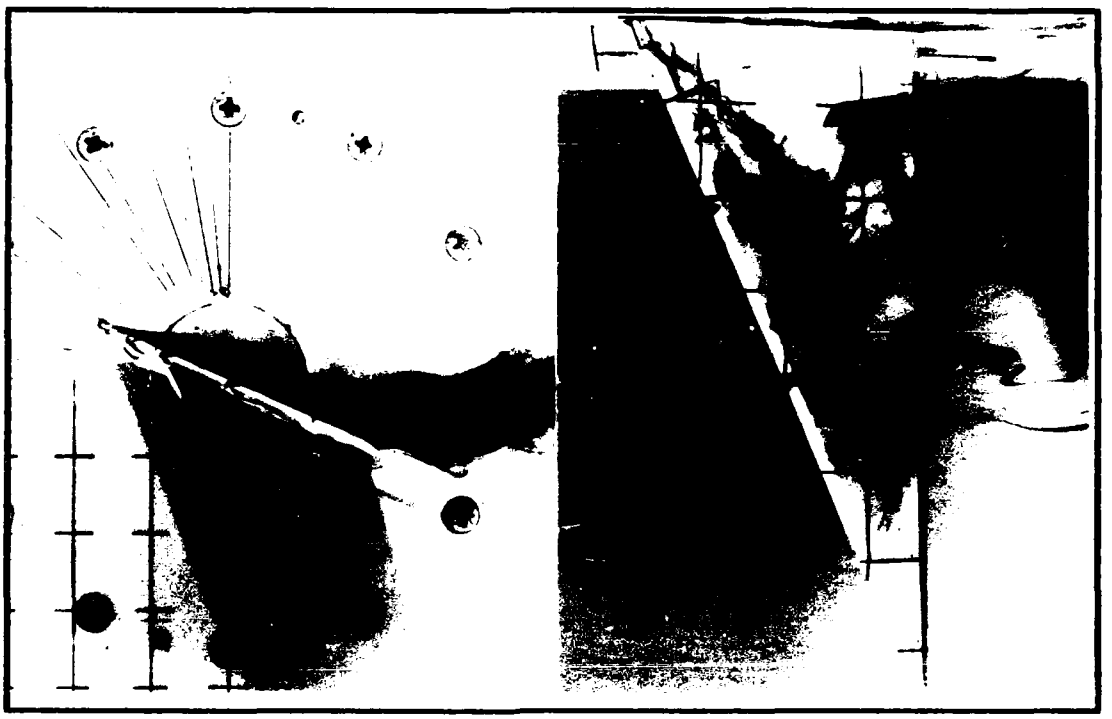

b. Dynamic

Figure 13. Flow Field Comparison above the 25 Degree Sweep Wing, $\alpha = 25^{\circ}$, $\dot{\alpha}_{ND} = 0.2$, U = 1.8 in/sec

slightly inboard, would still be present during the downstroke with a burst point near 0.5c. Perhaps this extended presence of the vortex at the higher rates was due to a stronger vortex created during the upstroke. Again however, regardless of the downstroke rate the flow appeared generally the same.

Unfortunately, individual spanwise locations on the wing were not looked at separately due to the dye distribution necessary to visualize the leading edge vortex. Doing this might have provided more information on vortex convection rates and separation as with the rectangular wing.

45 Degree Sweep Wings

This section includes not only the effect of various pitch rate combinations but also the effect of cross sectional shape by comparing the results for the flat plate and the NACA 0012-34 wings. For these wings there was a clearly definable leading edge vortex using a flow rate of 3.0 in/sec, so the development of this vortex became the primary focus for the static range of 6 to 32 degrees as well as the dynamic range of 8 to 32 degrees.

Statically the vortex produced by each wing was very different. For the flat plate the vortex could be clearly

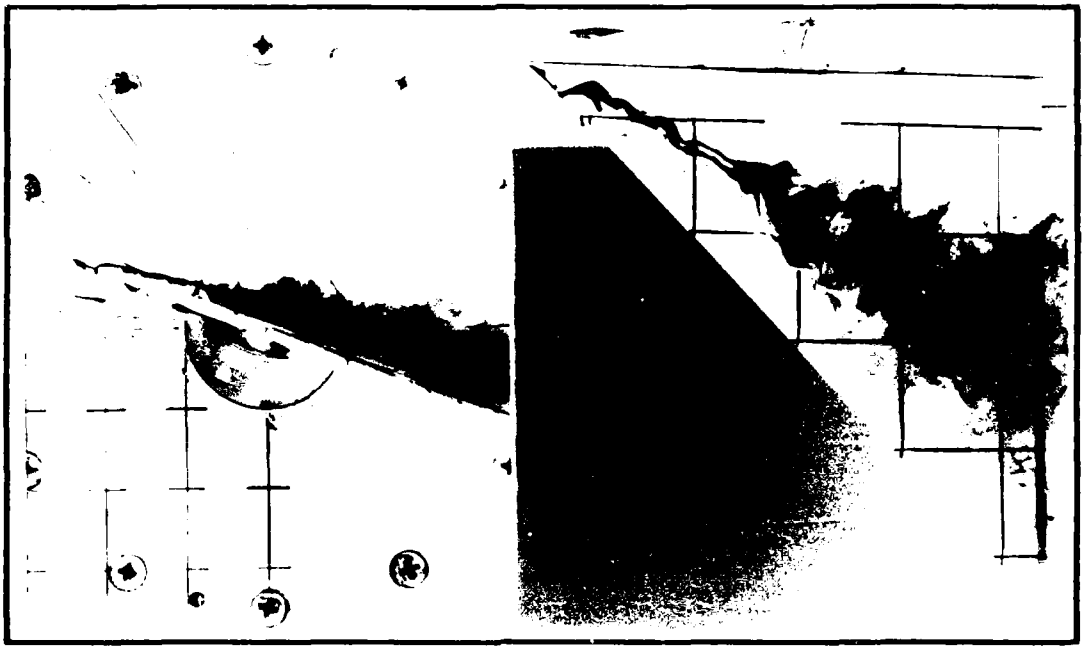

a. Flat Plate

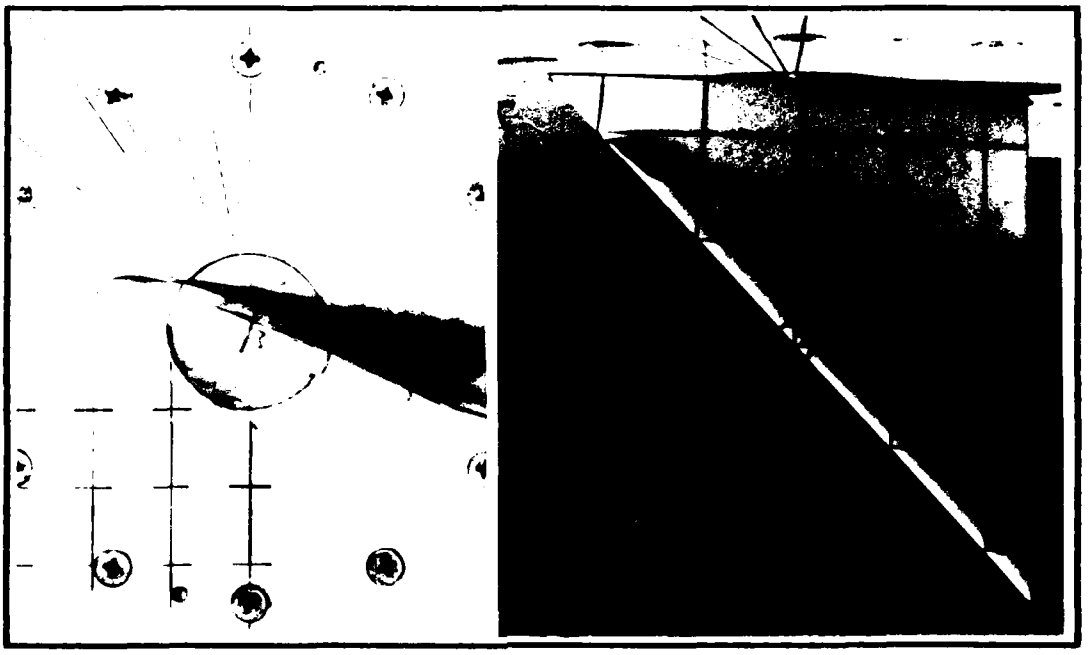

b. NACA 0012-34

Figure 14. Static Comparison of the 45 Degree Sweep Wings at $\alpha = 20^{\circ}$, U = 3.0 in/sec

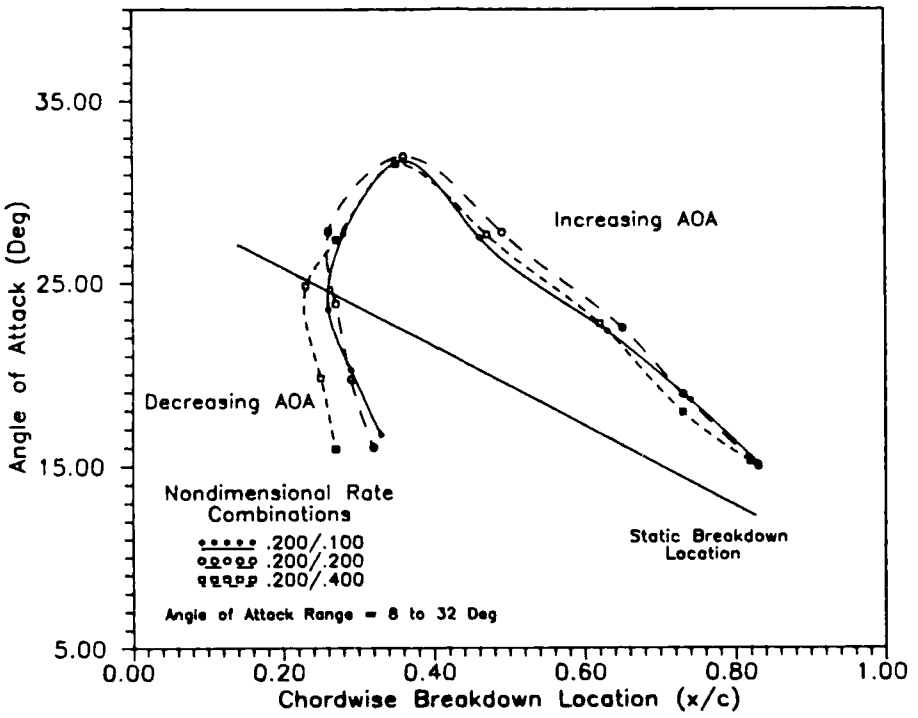

Figure 15. Chordwise Position of Vortex Burst for the 45 Degree Sweep Flat Plate, $\dot{\alpha}_{ND}$Up = 0.2, U = 3.0 in/sec

Also notice that, as with the 25 sweep wing, varying the downstroke rate had no clearly definable effect on the vortex position. Although for the combinations with the lowest nondimensional upstroke rate of 0.1, higher downstroke values did seem to further delay the aft movement of the vortex burst (See Figure 31, Appendix B).

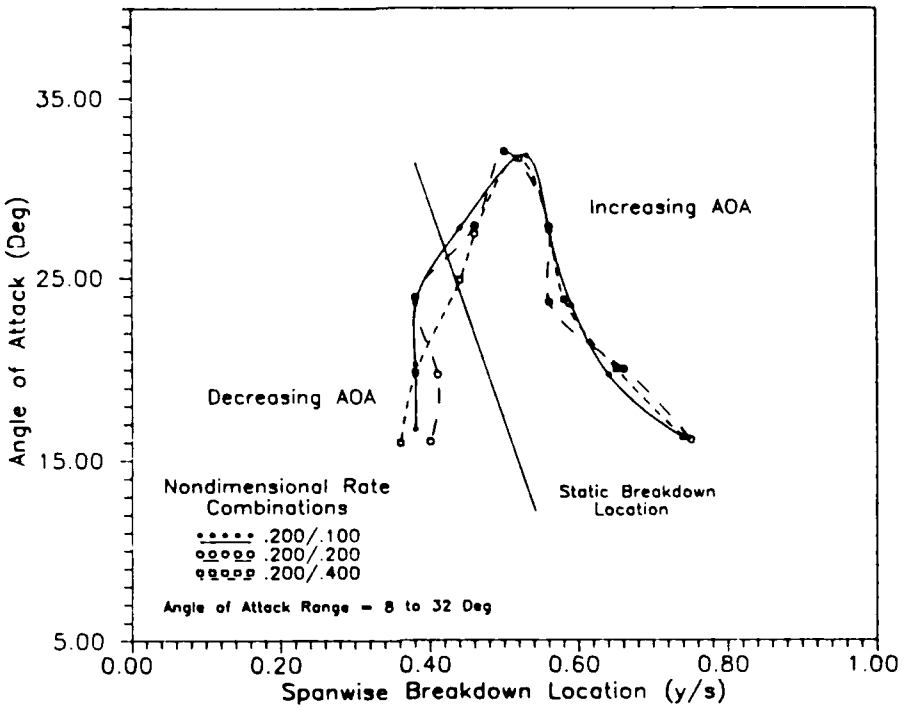

Figure 16. Spanwise Position of Vortex Burst for the 45 Degree Sweep Flat Plate, $\dot{\alpha}_{ND}$ Up = 0.2, U = 3.0 in/sec

A comparison of the two wings during a pitching cycle show similar results for chordwise breakdown location as illustrated in Figure 18. Although, for the NACA 0012-34 wing the vortex breakdown was not visible until around 20 degrees. This was also true at the lower pitch rates for this wing; however at the lower rates the burst point would be further forward. In addition, the vortex during the downstroke for the .12c thick wing appeared weaker and its orientation was much like for the static case. Additional data for the 45 degree sweep wings can be found in Appendix B.

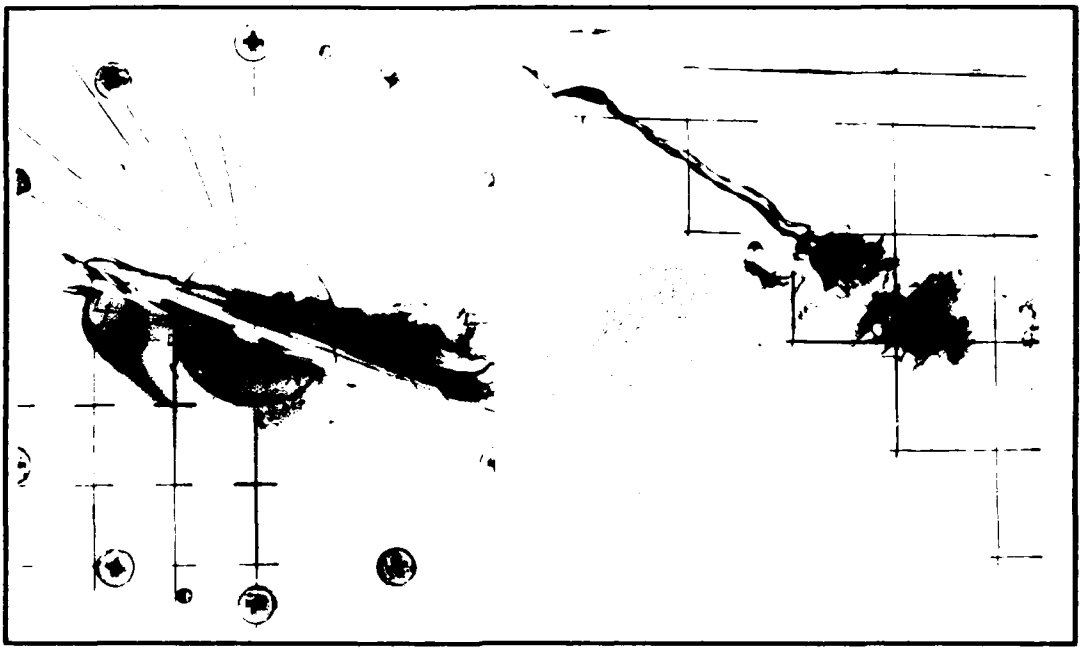

a. Upstroke

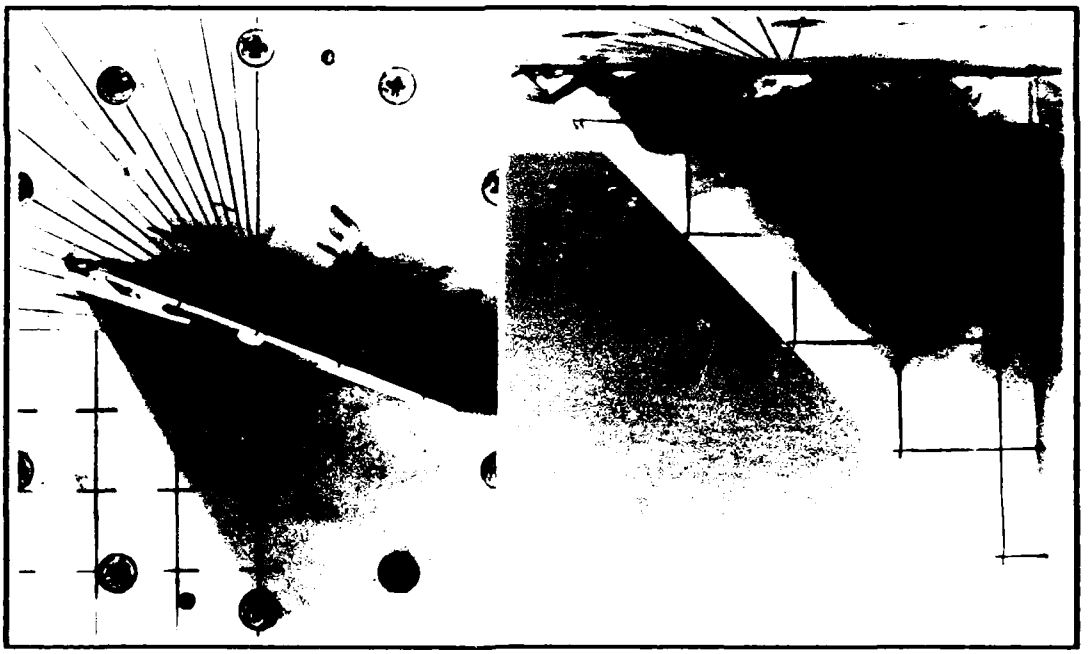

b. Downstroke

Figure 17. Comparison of Vortex Burst During the Upstroke and Downstroke for the 45 Degree Sweep Flat Plate, $\alpha = 20^{\circ}$, $\dot{\alpha}_{ND} = 0.1$, U = 3.0 in/sec

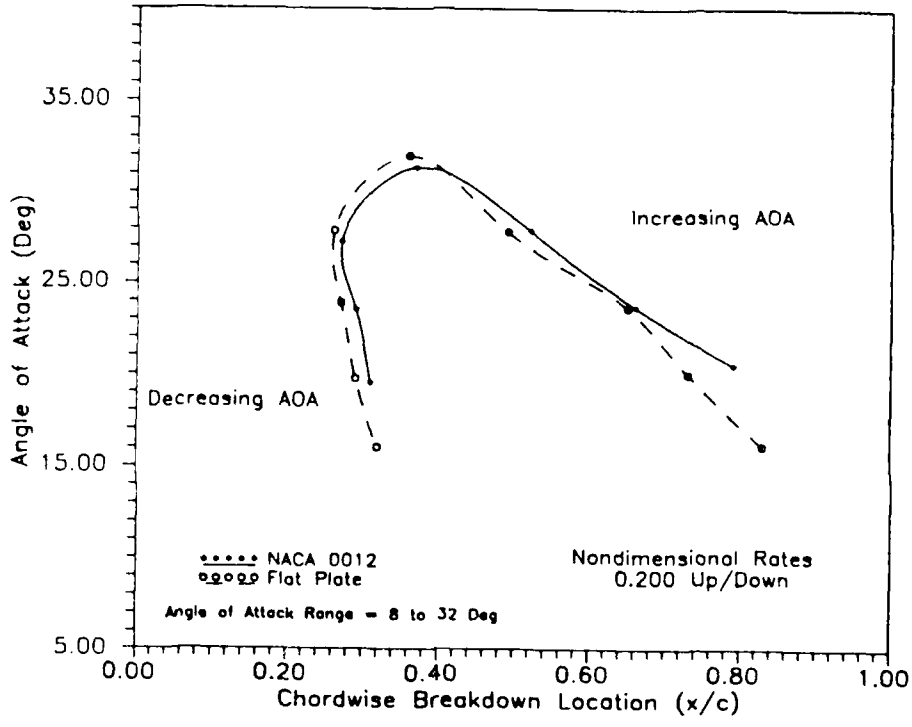

Figure 18. Comparison of Chordwise Vortex Burst Location for the 45 Degree Sweep Wings, $\dot{\alpha}_{N\bar{c}/2U}$ = 0.2, U = 3.0 in/sec

65 Degree Sweep Wings

This category also included a flat plate and an NACA 0012-34 wing tested at static angles and dynamic ranges using the saw-tooth motion. An additional experiment conducted on the flat plate wing involved the effect of tunnel flow rate on the vortex at fixed angles of attack.

Statically both wings produced a well defined leading edge vortex; however, as with the 45 degree sweep wings, the vortex appeared much sooner for the flat plate (8 degrees) than for the NACA 0012-34 wing (12 degrees). Also, the position of the vortex burst at a given angle of attack was different for each wing as shown in Figure 19 and as illustrated for 30 degrees in Figure 20.

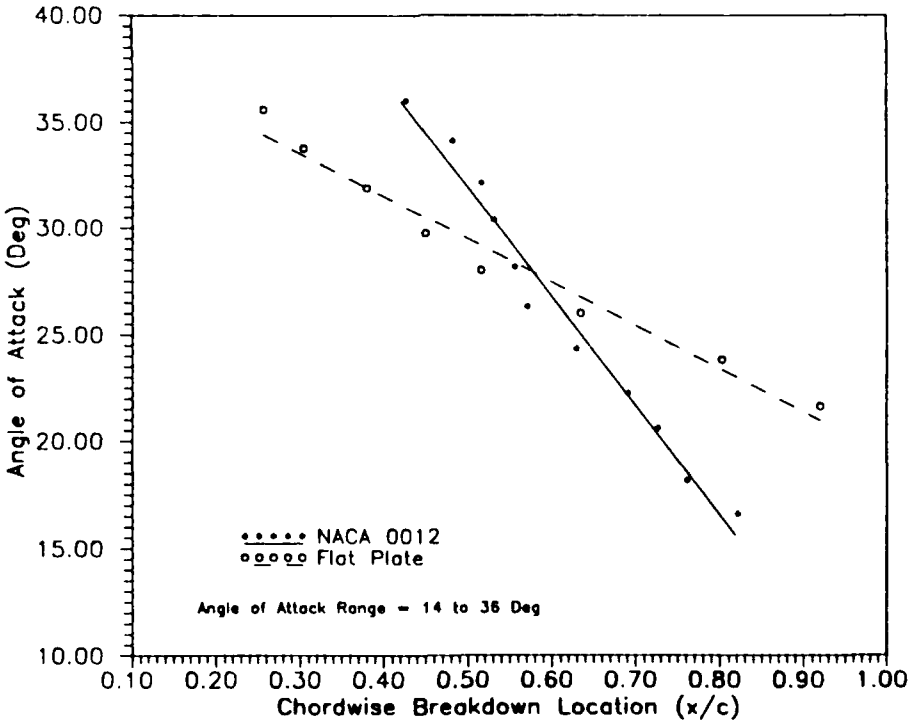

Figure 19. Static Comparison of Vortex Chordwise Burst Location for the 65 Degree Sweep Wings, U = 3.6 in/sec

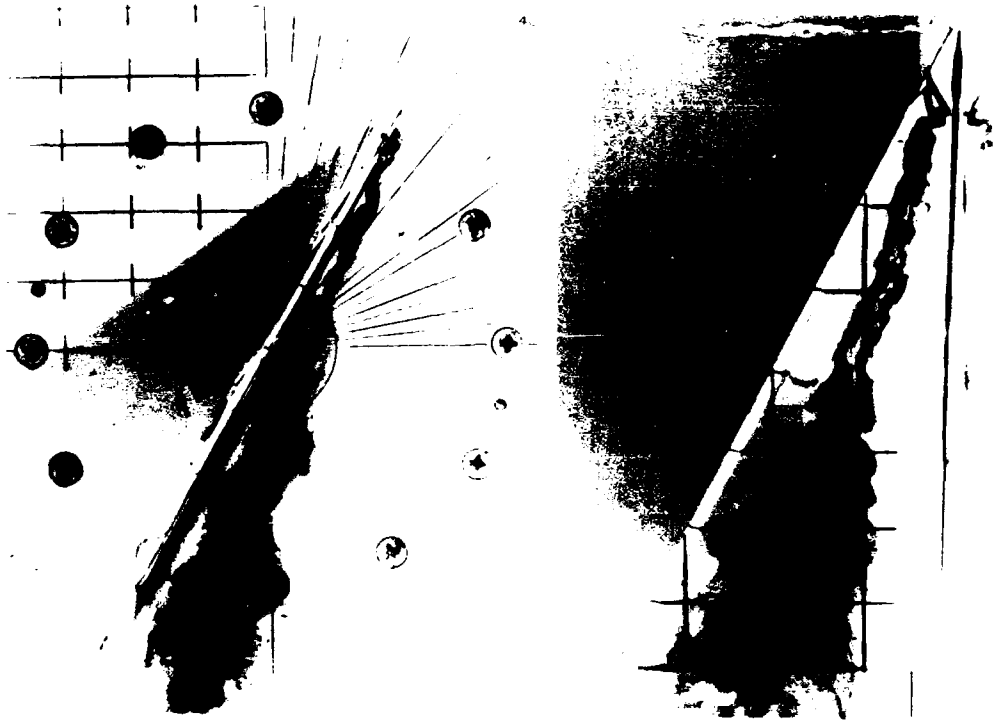

a. Flat Plate

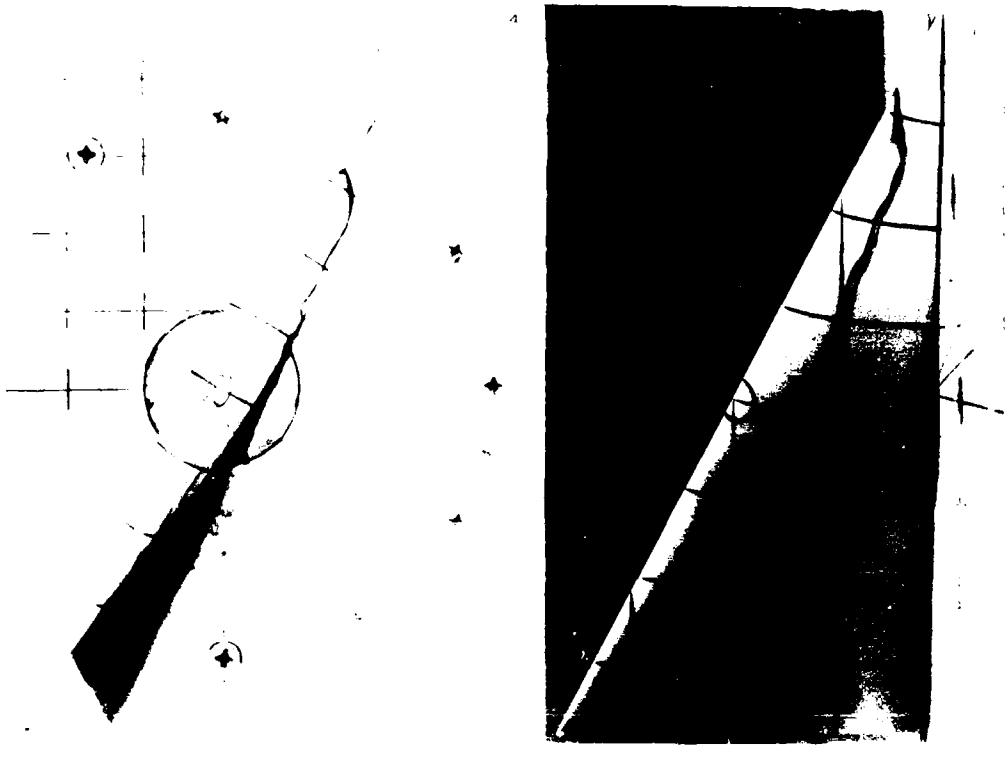

b. NACA 0012-34

Figure 20. Comparison of Chordwise Vortex Burst Location, 65 Degree Sweep Wings, $\alpha = 30^{\circ}$, U = 3.6 in/sec

Another characteristic of leading edge vortex breakdown is that for a fixed angle of attack the burst location oscillates in the axial direction about some mean value. To serve as a comparison the root mean square (RMS) variation of the burst location fluctuation for both wings was determined and plotted in Figure 21. Results showed higher values for the thicker NACA 0012-34 wing while for the flat plate wing the values were similar to those found in LeMay's vortex study of a 70 degree sweep delta wing [18:102]. In all cases there was no identifiable trend found with angle of attack change consistent with the findings of others.

With the static data to serve as a reference both wings were pitched with the saw-tooth motion where in this case, for angle of attack range of 18 to 38 degrees, the burst location could be maintained on the upper surface. Figure 22a and 22b show vortex breakdown location as a function of the saw-tooth motion for the flat plate and the NACA 0012-34 wing respectively. Both wings exhibited a hysteresis effect (this time a closed loop) similar to the 45 degree sweep wings; however for the thicker wing the width of the loop was smaller and more aligned with the line representing the static breakdown location.

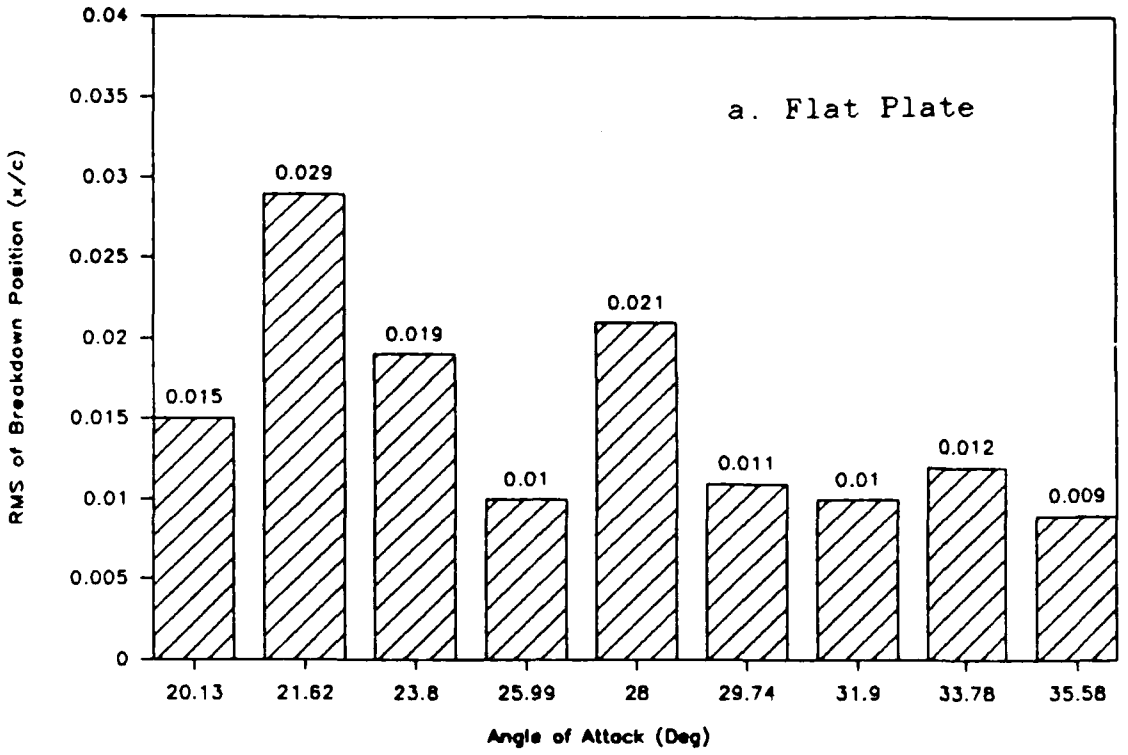

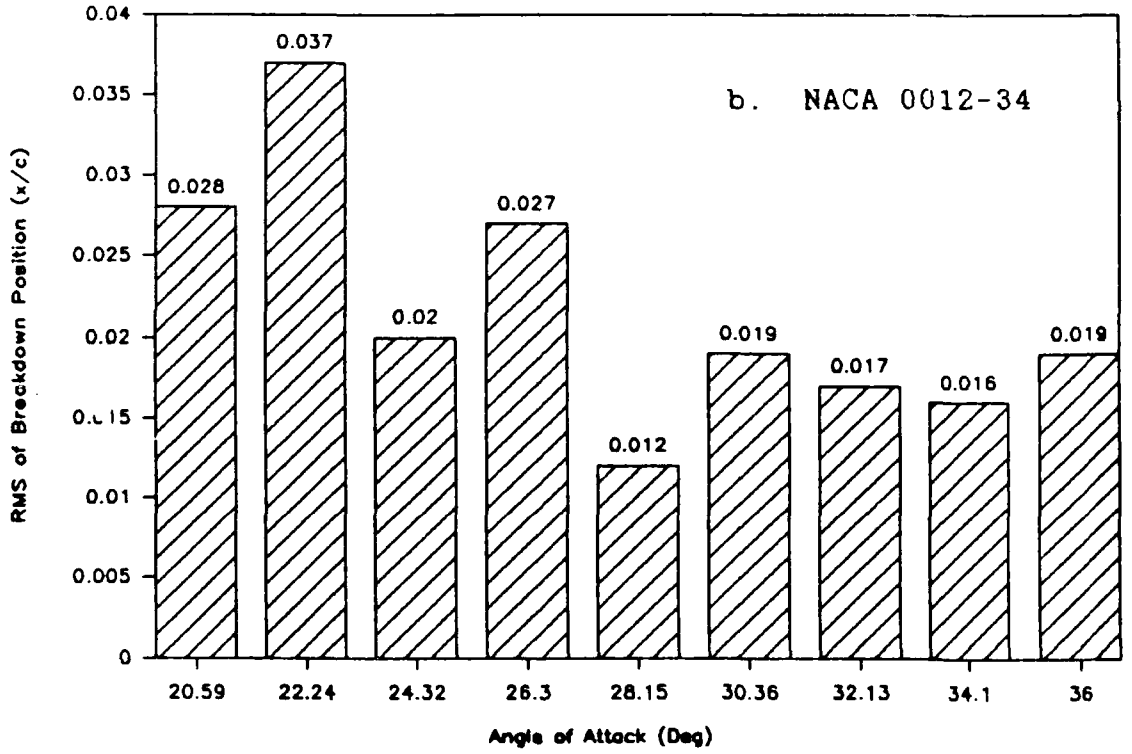

Figure 21. Root Mean Square Variation of the Vortex Burst Fluctuation for Fixed Angles of Attack, 65 Degree Sweep Wings, U = 3.6 in/sec

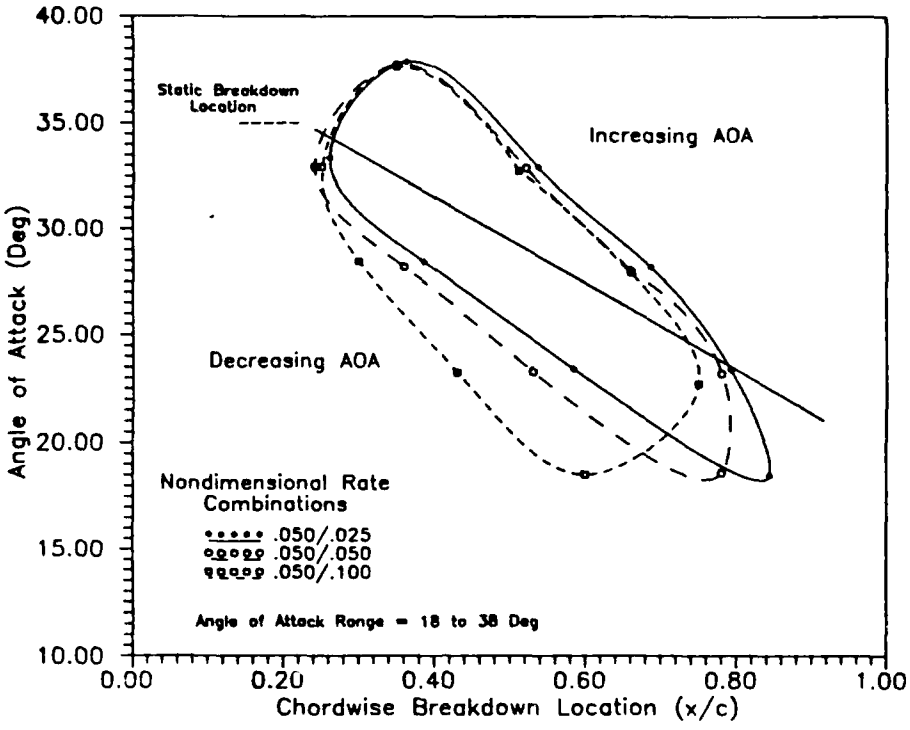

a. Flat Plate

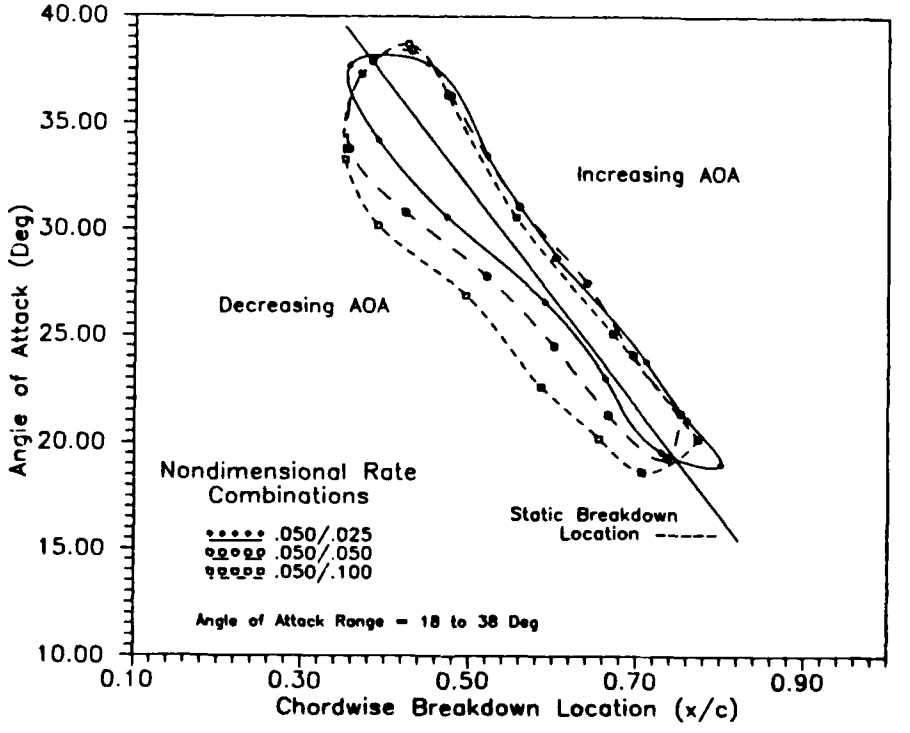

b. NACA 0012

Figure 22. Chordwise Vortex Burst Location for the 65 Degree Sweep Wings, $\dot{\alpha}_{ND}$ Up = 0.05, U = 3.6 in/sec

To help illustrate the hysteresis in the breakdown location, Figures 23a-f and 24a-f show the side and top views of the flat plate during the upstroke and the downstroke for a nondimensional rate combination of 0.2 up and down.

In addition to the chordwise location of the vortex burst the effect of the pitch rate combinations on the spanwise location of the vortex burst was tracked. Here also, there was a hysteresis effect about the static breakdown location as shown in Figure 25. Similar to the 45 degree sweep wings, during the upstroke the breakdown location would shift slightly outboard while for the downstroke it would shift inboard. The effect of increasing the downstroke rate for a given upstroke rate was to widen the loop much like for the chordwise breakdown location.

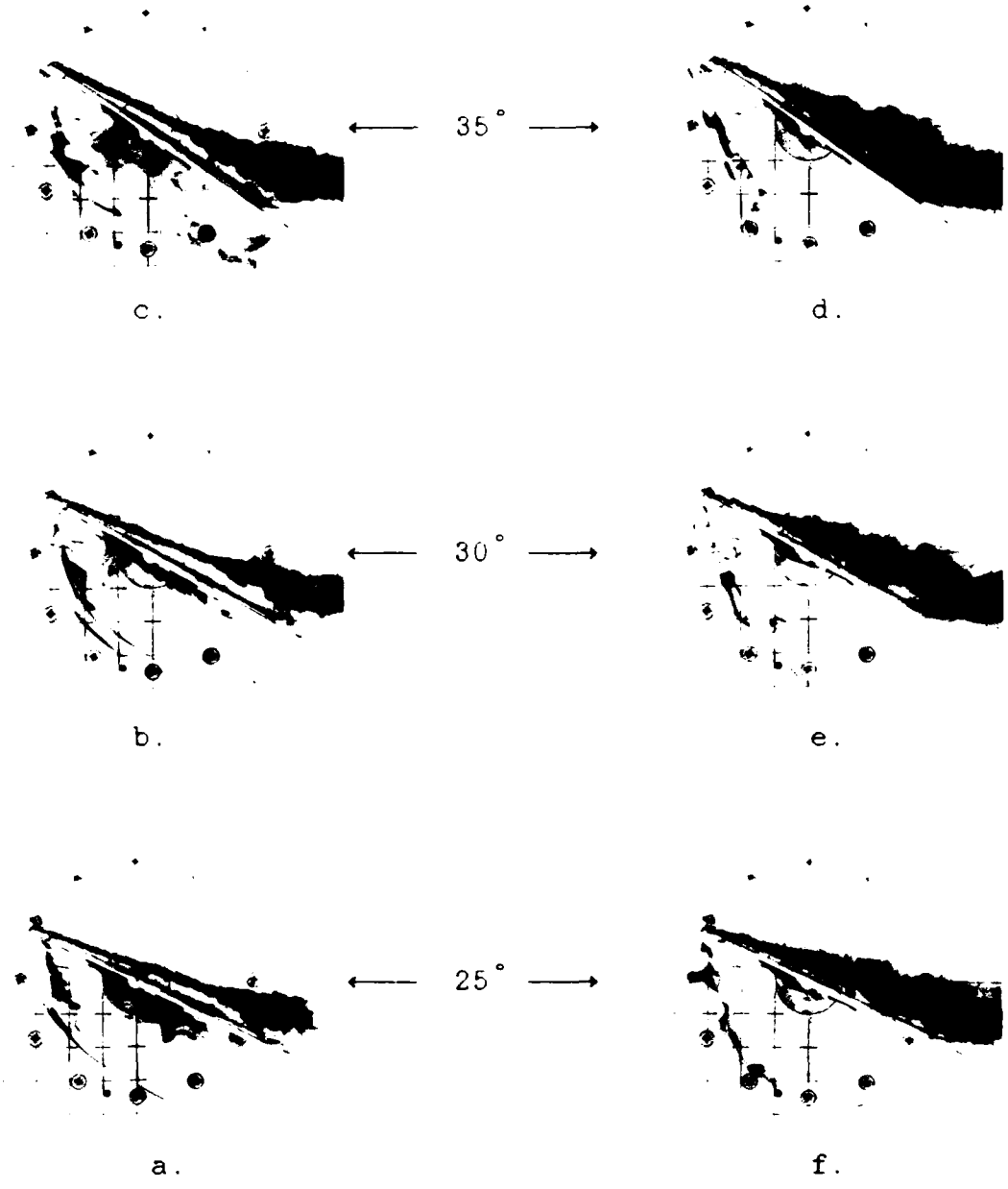

a-c. Upstroke d-f. Downstroke

Figure 23. Sequence of Photographs of the 65 Degree Sweep Flat Plate During a Pitching Cycle, Side View, $\dot{\alpha}_{ND}$ = 0.2, U = 3.6 in/sec

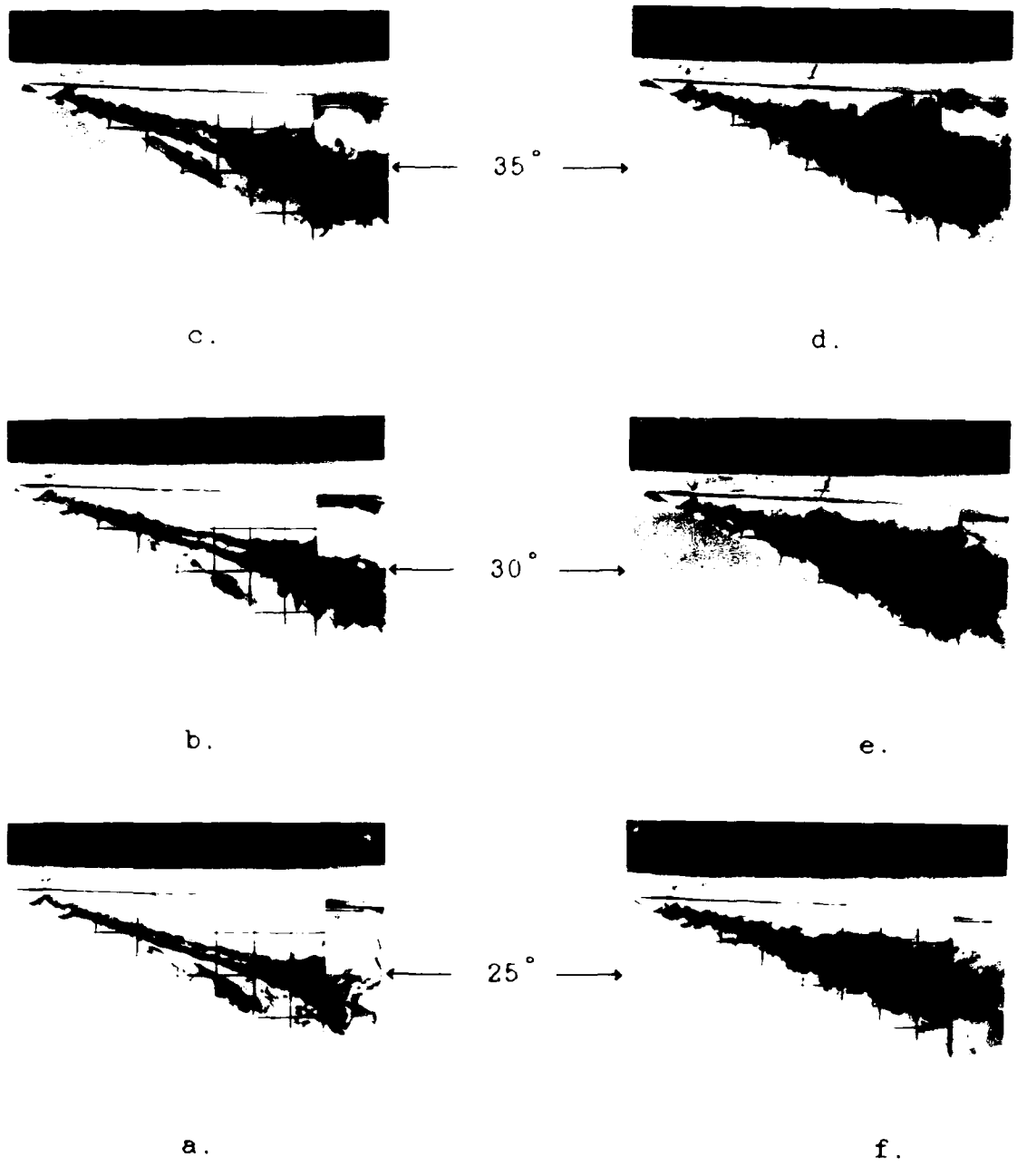

a-c. Upstroke d-f. Downstroke

Figure 24. Sequence of Photographs of the 65 Degree Sweep Flat Plate During a Pitching Cycle, Top View, $\dot{\alpha}_{ND}$ = 0.2, U = 3.6 in/sec

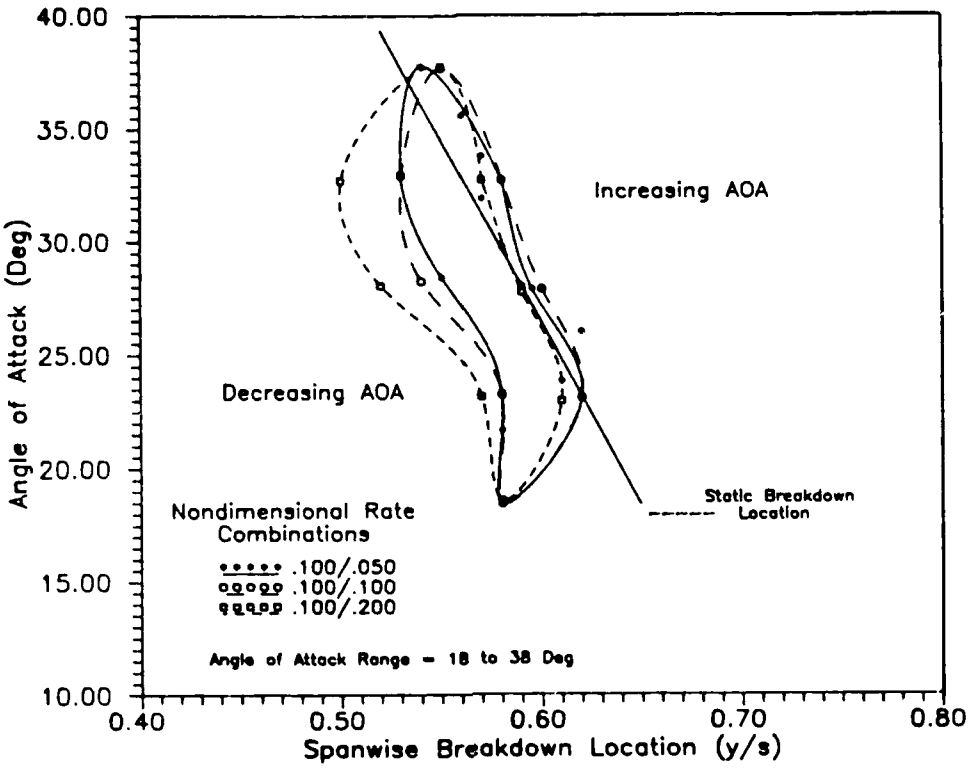

Figure 25. Spanwise Vortex Burst Location for the 65 Degree Flat Plate Wing, U = 3.6 in/sec

The final experiment performed with the flat plate wing was to investigate the effect of the tunnel flow rate on vortex burst location at fixed angles of attack, in this case 25 and 30 degrees. The flow rate was varied from 1.2 to 4.8 in/sec representing a Reynolds number range of 6700 to 27000 based on the root chord of 8 inches. The results, shown in Figure 26, indicate the burst point moves slightly forward with increasing speed; for both angles the change is about the same. No other information concerning vortex burst location as a function of flow rate could found in the literature. However, as mentioned in the introduction, some of the factors that influence vortex burst are the

balance of swirl to axial velocities, the pressure gradient in the axial direction, and core viscous effects. Changes in these factors might have been caused by the higher flow rates.

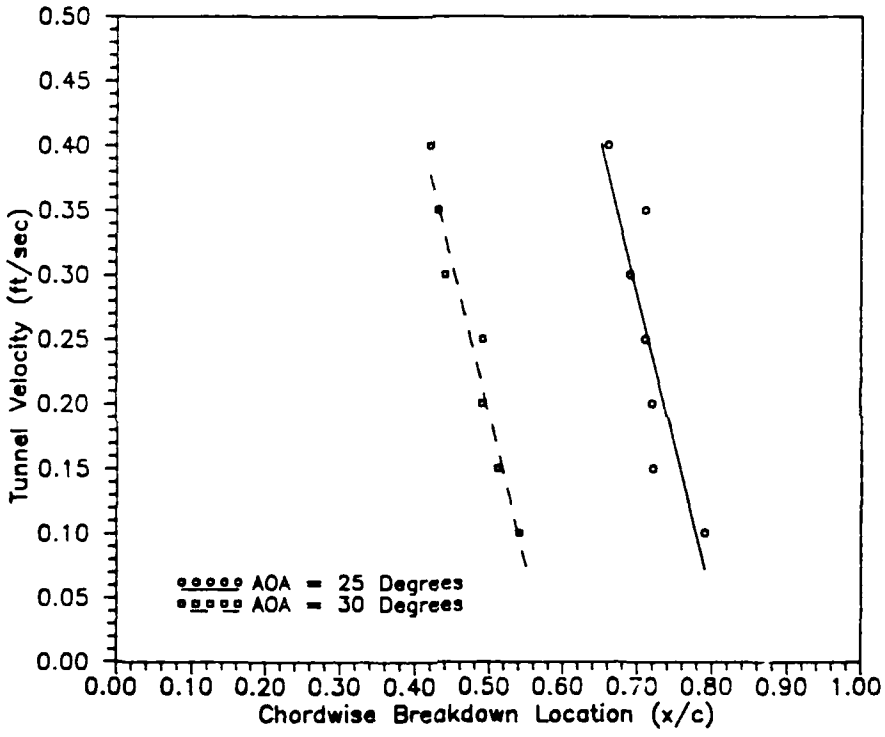

Figure 26. Effect of Tunnel Flow Rate on Vortex Burst Location, 65 Degree Sweep Flat Plate

An attempt was made to compare the results from this study with results for sinusoidal pitching. Although no exact match of parameters between studies could be found, the experiment by LeMay [18] with the 70 degree sweep delta wing was similar in approach and was used to compare with

the closest wing in this study, the 65 degree sweep flat plate.

Figure 27 shows both static and pitching curves for each wing where the 70 degree delta was pitched from 0 to 45 degrees at a reduced frequency (k) of 0.3 and the 65 degree sweep wing was pitched from 18 to 38 degrees at a nondimensional rate of 0.1. The actual pitching frequency of the 70 degree wing was 1.024 Hz which converts to an average nondimensional pitch rate of approximately 0.075.

Comparison of the curves show the same general trends with a hysteresis in breakdown location occurring between the upstroke and the downstroke. On the other hand, a larger percentage of the curve for the saw-tooth motion appears to fall above the static breakdown location. However, the differences in the parameters still leave much room for interpretation and a better match should be considered for future studies.

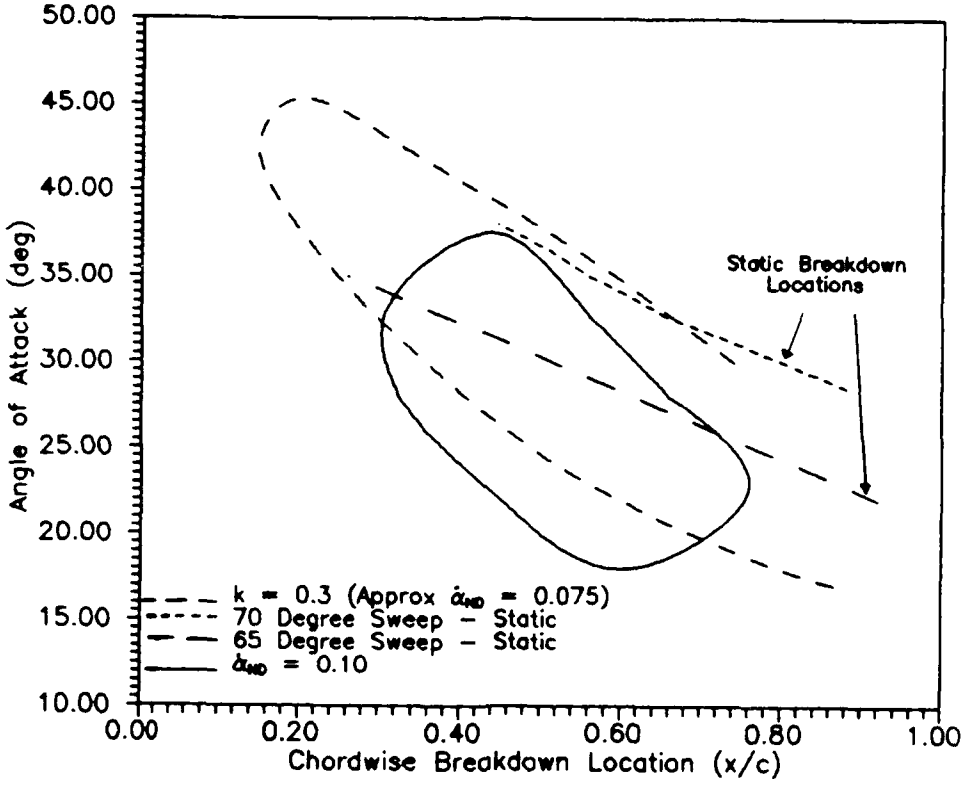

Figure 27. Comparison of Saw-Tooth and Sinusoidal Pitching, 70 Degree Sweep Wing (k =0.3), 65 Degree Sweep Wing ($\dot{\alpha}_{ND}$= 0.1)

VI. Conclusions and Recommendations

Conclusions

The major objectives of this study were to design and build a system capable of pitching a water tunnel model with a variable saw-tooth motion and to to investigate the vortex dynamics of a variety of semi-span wings. NACA 0012-34 wings had sweep angles of 0, 45 and 65 degrees; and flat plate wings had sweep angles of 25, 45 and 65 degrees. The range of nondimensional pitch rates and tunnel flow rates were 0.05 to 0.30 and 0.60 in/sec to 3.6 in/sec respectively.

The motion system worked well--the up and down ramps of the saw-tooth were linear and the programmable feature of the control card allowed great flexibility in varying both angle and rate limits as well as combining different upstroke and downstroke rates. The system should prove valuable for future dynamic studies in the water tunnel.

The results from tests on the rectangular wing showed that for increased values of upstroke rates, separation was delayed to higher angles of attack. For a given upstroke rate, higher values of downstroke rate caused an increase in the convection rate of the shed vortex. Furthermore, in cases where the downstroke was started before the vortex

was shed, the higher downstroke rates allowed the wing to return to the minimum angle of attack and then start the upstroke before losing the influence of the vortex.

The vortex flow above the pitching 25 degree sweep wing proved to be quite different from the rectangular wing. At static angles of attack there was no visible leading edge vortex; however, when the wing was pitched, a vortex formed parallel to the leading edge and with increasing angle of attack, moved to a position approximately in line with the local mid-span. The vortex displayed the bursting characteristic common to more highly swept wings and also appeared to be strengthened by the higher pitch rates. The effects of varying the downstroke of the saw-tooth were not quantified; however, in all cases, reversing direction caused the vortex burst point to move towards the apex. For a given upstroke rate, varying the downstroke rate appeared to make little difference in the vortical flow above the wing.

In contrast to the rectangular and 25 degree sweep wings, the 45 degree sweep wings produced a leading edge vortex at static angles of attack; however, for each wing the vortex produced was quite different. The vortex from the 0.12c thick wing appeared weaker and more aligned with a point outboard of the apex. Pitching the 45 degree sweep wings caused a delay in forward movement of the vortex burst with increasing angle of attack when compared with

the static case. However, increasing the downstroke rate, as with the 25 degree sweep wings, appeared to have little effect on vortex burst except at the lowest nondimensional upstroke rate of 0.1. For this latter case higher downstroke rates delayed the aft movement of the vortex burst

The last set of wings tested, the 65 degree sweep wings, produced the clearest effects of pitching on the leading edge vortex. Comparing the two statically, vortex bursting at the trailing edge occurred later for the flat plate but moved forward quicker for increasing angles of attack with both being equal at about 28 degrees. Dynamically the saw-tooth motion produced a hysteresis in the chordwise breakdown location for both; however the effect was much more pronounced on the flat plate. Here, the effect of higher downstroke rates for a given upstroke rate was a widening of the hysteresis loop. In addition, there was a hysteresis in the spanwise burst location, with the upstroke causing the vortex to shift outboard while the opposite was true for the downstroke. As before, the effect of higher downstroke rates was a widening of the hysteresis loop.

Recommendations

Presented below are recommendations for future research.

1. Much research has been done on the increased lift produced by the pitching two-dimensional wing. In light of the vortex produced by the 25 degree sweep wing, it would be interesting to see, through wind tunnel testing, what effects pitching this wing has on lift. The planform could represent a typical control surface.

2. Early efforts in this experiment included attempts to design a way of obtaining force data from the model. This proved difficult due to the low forces and pressure generated at typical tunnel flow rates. One thought, that was beyond the scope of this work, was to instrument the model surface with the piezoelectric sensors being designed as touch simulators for robots. (Ref AFIT/GE/ENG/88D-41)

3. The motion system should be modified to pitch a sting-mounted model for use with either a full-span wing or an actual scaled model. This would eliminate possible boundary layer effects from the semi-span splitter plate combination used for this experiment and would allow a greater range of testing possibilities.

4. Data reduction by digitizing frames of video proved to be very time consuming. The process could improved by modifying the Data Acquisition Software Program (DASP) or possibly automated by using image processing techniques.

5. Finally, although the Kodak SP2000 had some attractive features for this work, the resolution of the picture was not as good as the color video system and it required special (expensive) tapes. A possible alternative for future work might be the HSV 400. This system uses standard VHS tapes, provides a better quality color picture, and has XY reticle capability. Its limitation is 400 frame per second verses the 2000 frames per second of the SP2000; however with the low speeds used in the water tunnel that is not a problem.

Bibliography

1. Payne, F. M. and Nelson, R. C. "An Experimental Investigation of Vortex Breakdown on a Delta Wing," NASA CP-2416, Vol I, 1985.

2. Erickson, G. E Vortex Flow Correlation AFWAL-TR-80-3143, January 1981.

3. Herbst, W. B. "Supermaneuverability," Workshop on Unsteady Separated Flow, United States Air Force Academy, 1983.

4. Kramer, Von M. "Die Zunahme des Maximalauftriebes von Tragflugeln bei plotzlicher Anstellwinkel-vergro Berung (Boenefekt)," Zeitschrift fur Flugteknik und Motor-luftschiffahrt.7, 14 April 1932.

5. Harper, P. W. and Flanigan, R. E. "The Effect of Change of Angle of Attack on the Maximum Lift of a Small Model," NACA TN-2061, March 1950.

6. Carr, L. W. "Progress in Analysis and Prediction of Dynamic Stall," Journal of Aircraft, Vol. 24, No. 1, January 1988.

7. Harris F. D. and Pruyn, R. R. "Blade Stall-Half Fact, Half Fiction," Journal of the American Helicopter Society," Vol. 13, No. 2, April 1968.

8. Ham, N. D. and Garelick, M. S. "Dynamic Stall Considerations in Helicopter Rotors," Journal of the American Helicopter Society. Vol. 13, No. 2, April 1968.

9. Ham, N. D. "Aerodynamic Loading on a Two-Dimensional Airfoil During Dynamic Stall," AIAA Journal, Vol 6, October 1968.

10. McAlister, K. W. and Carr, L. W. "Water Tunnel Visualization of Dynamic Stall," Journal of Fluids Engineering, Vol 101, September 1979.

11. Deekens, A. C. and Kuebler, W. R. "A Smoke Tunnel Investigation of Dynamic Separation," Air Force Academy Aeronautics Digest, USAFA-TR-79-1, February 1979.

12. Dimick, R. L. Pitch Location Effects on Dynamic Stall. MS Thesis, AFIT/GAE/AA/85D-4, Air Force Institute of Technology (AU), December 1985.

13. Siuru, W. D. Jr., Walker, J. M., and Chou, D. "Aerodynamic Parameters for a Pitching Airfoil," AIAA-87-2352, AIAA 25th Aerospace Sciences Meeting, January 1987.

14. Stephen, E. J. Investigation of Periodic Pitching Through the Static Stall Angle of Attack. MS Thesis, AFIT/GAE/AA/87M-4, Air Force Institute of Technology (AU), March 1987.

15. Jumper, E. J., Dardis, W. J. III and Stephen, E. J. "Toward an Unsteady-Flow Airplane," AIAA-88-0752, AIAA 26th Aerospace Sciences Meeting, January 1988

16. Robinson, M. C. and Wissler, J. B. "Unsteady Pressure Measurements on a Pitching Rectangular Wing," AIAA-88-0328, AIAA 26th Aerospace Science Meeting, January 1988.

17. Gad-el-Hak, M. and Ho, C. "The Pitching Delta Wing," AIAA Journal, Vol. 23, No. 11, November 1985.

18. LeMay, S. P. Leading Edge Vortex Dynamics on a Pitching Delta Wing. MS Thesis, NAG-1-727, University of Notre Dame, April 1988.

19. Davies, A. G. "A Comparative Study of Vortex Flows in Wind and Water Tunnels," AGARD Conference Proceedings No. 413, June 1987.

20. Wolfelt, K. W. "Investigation of the Movement of Vortex Burst Position with Dynamically Changing Angle of Attack for a Schematic Deltawing in a Watertunnel with Correlation to Similar Studies in Windtunnel," AGARD Conference Proceedings No. 413, June 1987.

21. Werle, H. "Hydrodynamic Flow Visualization," Annual Review of Fluid Mechanics, 5: 361-382, 1973.

22. Gilliam, F. and others. "Visualization of Unsteady Separated Flow About a Pitching Delta Wing," AIAA-87-0240, AIAA 25th Aerospace Sciences Meeting, January 1987.

Appendix A

Software Package

This Appendix contains the programs written as part of the experiment. Copies of these as well as the Data Aquisition Software Program are located in Room 145, Building 640, Wright-Patterson AFB.

MOTOR - This program controls the motor pitching parameters. Variables include pitch rates and angle limits. Options include a saw-tooth motion and a continuous jog motion.

REDUCE - This program takes the output from Kodak's Data Aquisition Program (DASP) and returns, for example, angle of attack, vortex inclination angle, and vortex breakdown and separation locations.

PROGRAM - MOTOR

```
10 REM ******************************************************
20 REM * Program to control an EG&G Torque System MTE-3528 *
30 REM * motor using a Delta Tau Mini MC^2 Motion Control  *
40 REM * Card and a Westamp A613 Series linear servo amp   *
50 REM ******************************************************
60     CLS
70  OPEN "COM1:1200,N,8,1" AS #1
80  PRINT#1, "i261"                          'Comm with RS232
90  PRINT#1, "z"                             'Purges Buffer
100 PRINT#1, "Z"                             'Sets Zero Location
110 PRINT#1, "1062000"                       'Rate Multiplier
120 PRINT#1, "i0720"                         'Servo Loop Gain
130 PRINT#1, "i09 20"                        'Sets Jog Rate
140 PRINT#1, "i08 100"                       'Accel Control
150 PRINT#1, "i10 500"
160 PRINT#1, "i11 500"
170 PRINT#1, "i12 100"                       'Decel Control
180 PRINT#1, "i2050000"                      'Sets Max # Points
190 PRINT#1, "i24 500:360"                   'Display Multiplier
200 INPUT "DESIRED MOTION -- SAWTOOTH(S) OR JOG(J)";MOT$
210 IF MOT$="S" THEN 1000 ELSE 2000
220 END
1000 REM ****************************************************
1010 REM * Subroutine to control saw-tooth motion          *
1020 REM * Variables are up/down pitch rate, max AOA, and  *
1030 REM *  # of cycles                                     *
1040 REM ****************************************************
1050 GRATIO = 10          'Gear Ratio of Motor Drive System
1060   CLS
1070 INPUT "ENTER PITCH-UP RATE (DEG/SEC)"; PITCHUP
1080 PITCHUP%=PITCHUP*GRATIO
1090 PRINT ""
1100 INPUT "DESIRED ANGLE OF ATTACK CHANGE (DEG)"; MAXAOA
1110 MAXAOA=MAXAOA*GRATIO
1120 PRINT ""
1130 INPUT "ENTER PITCH-DOWN RATE (DEG/SEC)"; PITCHDOWN
1140 PRINT ""
1150 PITCHDOWN%=PITCHDOWN*GRATIO
1160 INPUT "ENTER NUMBER OF CYCLES"; CYCLES
1170 PRINT ""
1180 INPUT "ARE THE ENTERED VALUES CORRECT? (Y/N)"; CHECK$
1190 PRINT ""
1200 IF CHECK$="N" THEN GOTO 1050
1210 PRINT "PRESS ANY KEY TO CONTINUE!!"
1220 X$=INPUT$(1)
1230 PRINT#1, "z"
1240 PRINT#1, "Z"
1250 PRINT#1, "G70X"+STR$(CYCLES)        'Sets # of Cycles
1260 PRINT#1, "F"+STR$(PITCHUP$)         'Pitch-up Rate Set
```

```
1270 PRINT#1, "X"+STR$(MAXAOA)          'Max AOA Set
1280 PRINT#1, "F"+STR$(PITCHDOWN$)      'Pitch-Down Rate Set
1290 PRINT#1, "X-36000"                 'Return to 0 Deg Comm
1300 PRINT#1, "G71"                     'End Cycles Comm
1310 PRINT#1, "M30"                     'End of Program
1320 PRINT#1, "R"                       'Execute Program
1330 PRINT ""
1340 PRINT "CONTINUE WITH SAW-TOOTH OR JOG (S/J)?"
1350 X$="S" THEN 1000 ELSE 2000
2000 REM ************************************************
2010 REM * Subroutine to provide jog control - i09 Command *
2020 REM * determines rotation (jog) rate                  *
2030 REM ************************************************
2040    CLS
2050 PRINT#1, "z"
2060 INPUT "POSITIVE OR NEGATIVE ROTATION (P/N)"; ROT$
2070 IF ROT$="P" THEN 2200
2080 PRINT#1, "i0920"                   'Sets Jog Rate
2085 REM ***** Negative Rotation Loop ************
2090 PRINT "TYPE P (PROCEED) OR S (STOP)
2100 X$=INPUT$(1)
2110    CLS
2120 PRINT "TYPE P (PROCEED) OR S (STOP)
2130 IF X$="P" THEN PRINT#1, "j"        'Starts Rotation
2140 X$=INPUT$(1)
2150 PRINT ""
2160 IF X$="S" THEN PRINT#1, "Q"        'Stops Rotation
2170 PRINT "CHANGE DIRECTION? (Y/N)"
2180 X$=INPUT$(1)
2190 IF X$="Y" THEN GOTO 2230
2200   CLS
2210 GOTO 2090
2220 REM ****** Positive Rotation Loop ************
2230   CLS
2240 PRINT "TYPE P (PROCEED) OR S (STOP)
2250 PRINT ""
2260 X$=INPUT$(1)
2270 IF X$="P" THEN PRINT#1, "J"        'Starts Rotation
2280 X$=INPUT$(1)
2290 IF X$="S" THEN PRINT#1, "Q"        'Stops Rotation
2300 PRINT "CHANGE DIRECTION ?(Y/N)"
2310 X$=INPUT$(1)
2320 IF X$="Y" THEN GOTO 2040
2330   CLS
2340 GOTO 2190
2350 END
```

PROGRAM - REDUCE

```
c      Program to reduce the output from Kodak's Data
c      Aquisition Software Program (DASP).
c
c      Digitized Points
c
```

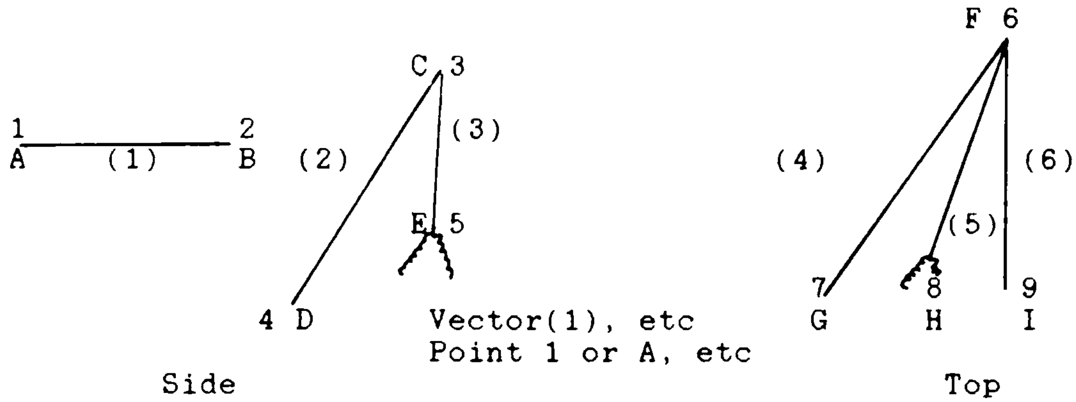

DELTA WINGS

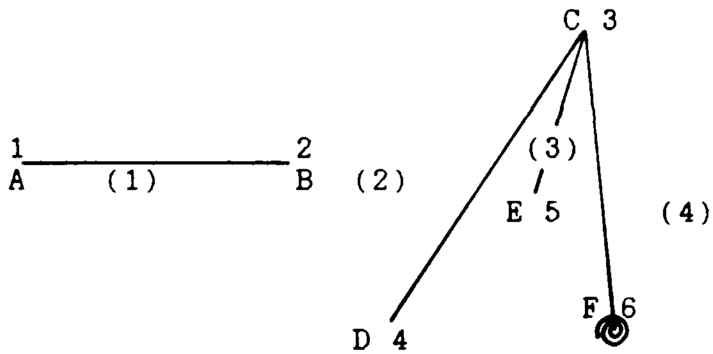

RECTANGULAR WING

```
c
c
c
       Real PPF, FRM, FSKIP, B(80), XC(80), HC(80), AOA(80)
       Real PT(9,2,80), VEC(6,2,80), MAG(6,80), DOT(6,80)
       Real YS(80),AOADEG(80),BVDEG(80)
       Real BDEG(80), TIME(80),BV(80),XCV(80),HCV(80)
       Character*12 name1, name2
c
       PI = ACOS(-1.0)
c      The variable CFRAC is used to convert the length of
c      vector (2),which includes the T.E. extension, to the
c      actual chord length
          CFRAC = 1.0
c
       Write(6,*) 'What file is the data in ?'
            Read(5,10) name1
```

```
      Write(6,*) 'What file should the output be placed in ?'
           Read(5,10) name2
               Open( unit=4, file=name1, status='old')
               Open( unit=7, file=name2, status='new')
   10 Format(a12)
           Rewind(unit=4)
c
c     Definitions
c
c           PPF = points digitized per frame
c           FRM = total number of frames digitized
c           FSKIP = Frames skipped between digitized frames
c
      Read(4,*) PPF, FRM, FSKIP
c
c    Note: DASP output files (*.PRN) must be modified to
c    include these values and to remove some unwanted lines.
c
      Do 100 i=1, PPF
         Do 200 j=1, FRM
            Read(4,*) x,y
                PT(i,1,j) = x
                PT(i,2,j) = y
  200    Continue
  100 Continue
c
c     Form vectors from the points read in above
c
c       Ex. VEC(l,m,n)     l - vector number (ref diagram)
c                          m - 1 indicates x length
c                              2 indicates y length
c                          n - tracks number of "l" vectors
c
      Do 300 j=1, FRM
         VEC(1,1,j) = PT(2,1,j) - PT(1,1,j)
         VEC(1,2,j) = PT(2,2,j) - PT(1,2,j)
         VEC(2,1,j) = PT(3,1,j) - PT(4,1,j)
         VEC(2,2,j) = PT(3,2,j) - PT(4,2,j)
         VEC(3,1,j) = PT(3,1,j) - PT(5,1,j)
         VEC(3,2,j) = PT(3,2,j) - PT(5,2,j)
            If (PPF .eq. 9) then
         VEC(4,1,j) = PT(6,1,j) - PT(7,1,j)
         VEC(4,2,j) = PT(6,2,j) - PT(7,2,j)
            else
  VEC(4,1,j) = PT(3,1,j) - PT(6,1,j)
  VEC(4,2,j) = PT(3,2,j) - PT(6,2,j)
            Endif
c     Rectangular Wing uses a 6 point input
 If (PPF .eq. 6) then
            goto 300
 Endif
  VEC(5,1,j) = PT(6,1,j) - PT(8,1,j)
         VEC(5,2,j) = PT(6,2,j) - PT(8,2,j)
                          VEC(6,1,j) = PT(6,1,j) - PT(9,1,j)
         VEC(6,2,j) = PT(6,2,j) - PT(9,2,j)
```

```
  300 Continue
c
c     Use the dot product between vectors (1) and (2) to get
c     angle of attack (AOA)
c
     Do 400 i=1, FRM
        DOT(1,i) = VEC(1,1,i)*VEC(2,1,i)+VEC(1,2,i)*VEC(2,2,i)
        MAG(1,i) = SQRT(VEC(1,1,i)**2+VEC(1,2,i)**2)
        MAG(2,i) = SQRT(VEC(2,1,i)**2+VEC(2,2,i)**2)
        AOA(i) = (PI/2) - ACOS(DOT(1,i)/(MAG(1,i)*MAG(2,i)))
        AOADEG(i) = (180/PI)*AOA(i)
  400 Continue
c
c     Use vectors (2) and (3) to find the vortex inclination
c     angle (B) and x/c (XC) position of vortex burst
c
     Do 500 i=1, FRM
        DOT(2,i) = VEC(2,1,i)*VEC(3,1,i)+VEC(2,2,i)*VEC(3,2,i)
        MAG(3,i) = SQRT(VEC(3,1,i)**2+VEC(3,2,i)**2)
        B(i) = ACOS(DOT(2,i)/(MAG(2,i)*MAG(3,i)))
    XC(i) = COS(B(i))*MAG(3,i)/(CFRAC*MAG(2,i))
           HC(i) = TAN(B(i))*XC(i)
           BDEG(i) = (180/PI)*B(i)
c
              If (PPF .eq. 9) then
        goto 425
      Endif
c    This section finds the same information described above --
c    for the dynamic stall vortex above the rectangular wing
c
        DOT(3,i) = VEC(2,1,i)*VEC(4,1,i)+VEC(2,2,i)*VEC(4,2,i)
        MAG(4,i) = SQRT(VEC(4,1,i)**2+VEC(4,2,i)**2)
           If (MAG(4,i).eq.0) then
               BV(i) = 0
               XCV(i) = 0
               HCV(i) = 0
               BVDEG(i) = 0
           else
               BV(i) = ACOS(DOT(3,i)/(MAG(2,i)*MAG(4,i)))
               XCV(i) = COS(BV(i))*MAG(4,i)/(CFRAC*MAG(2,i))
               HCV(i) = TAN(BV(i))*XCV(i)
               BVDEG(i) = (180/PI)*BV(i)
         endif
             Goto 450
c  Use points 7,8, and 9 to find the nondimensional spanwise
c  position of vortex breakdown
c
425 YS(i)=SQRT((PT(9,1,i)-PT(8,1,i))**2+(PT(9,2,i)-PT(8,2,i))
 &**2)/SQRT((PT(9,1,i)-PT(7,1,i))**2+(PT(9,2,i)-PT(7,2,i))**2)
c
c Generate time scale based on frames skipped and frame rate
c (Note: 60 Frames/Sec was used for all runs)
c
  450        j = i + 1
             TIME(1) = 0.0
```

```
            TIME(j) = TIME(i) + FSKIP/60.0
 500 Continue
       If (PPF .eq. 9) then
  Write(7,1000)
  Write(7,2000) (TIME(i),AOADEG(i),BDEG(i),XC(i),HC(i),YS(i),
    & i = 1,FRM)
       else
   Write(7,3000)
   Write(7,4000) (TIME(i),AOADEG(i),XC(i),XCV(i), i = 1,FRM)
endif
1000 Format('    Time        AOA       Beta       X/C        H/C
    &  Y/S')
2000 Format(6(2x,f9.2))
3000 Format('     Time        AOA     Sep (x/c)   Vortex(x/c)')
4000 Format(4(2x,f9.2))
   Close(4)
         Close(7)
     end
```

Appendix B

Remainder of Plotted Results

This Appendix contains the plotted results used to compare the wings but not necessarily referred to directly in the main body.

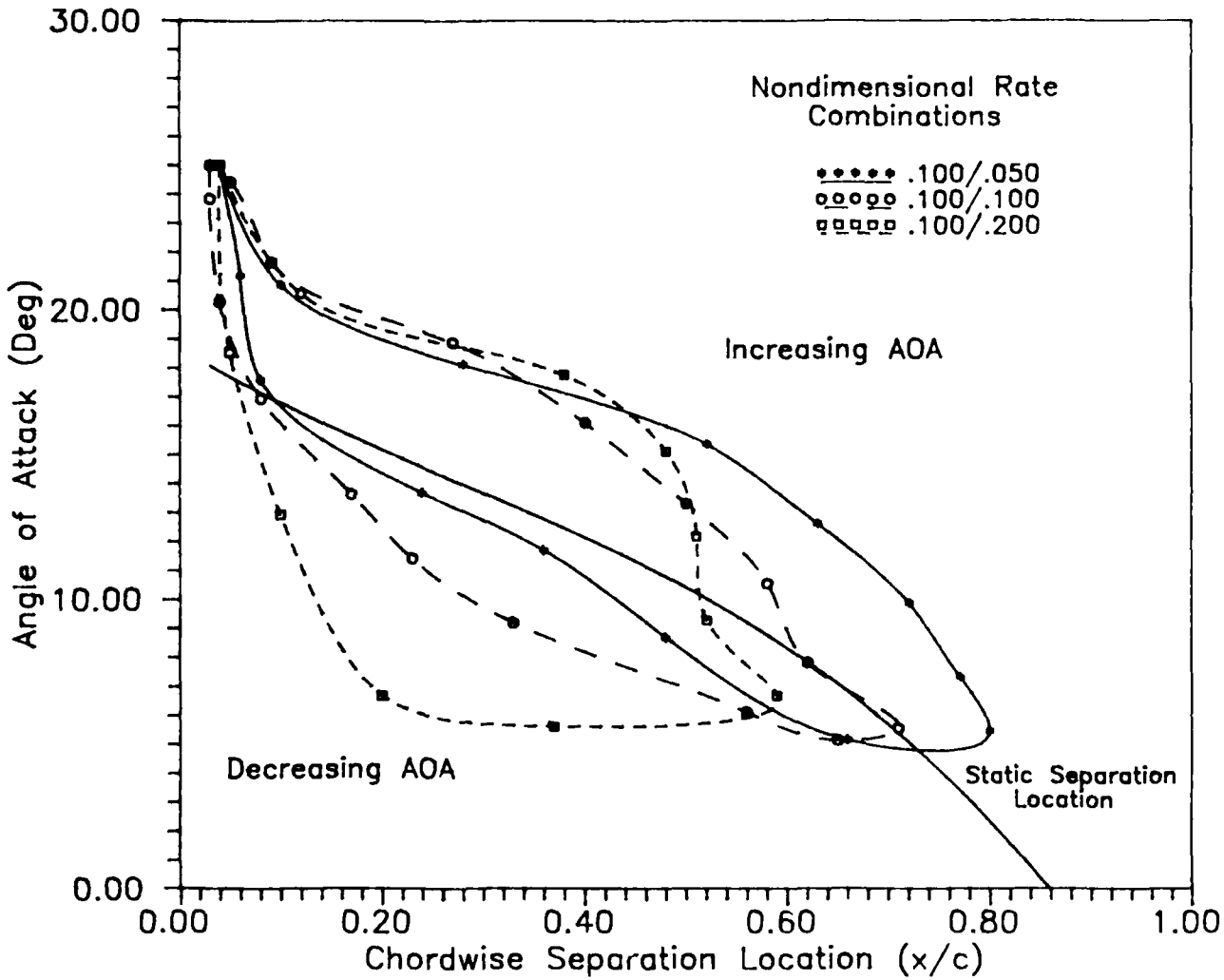

Figure 28. Chordwise Position of Flow Separation, Rectangular Wing, Mid-Span, $\dot{\alpha}_{ND}$ Up = 0.10, U = 0.60 in/sec

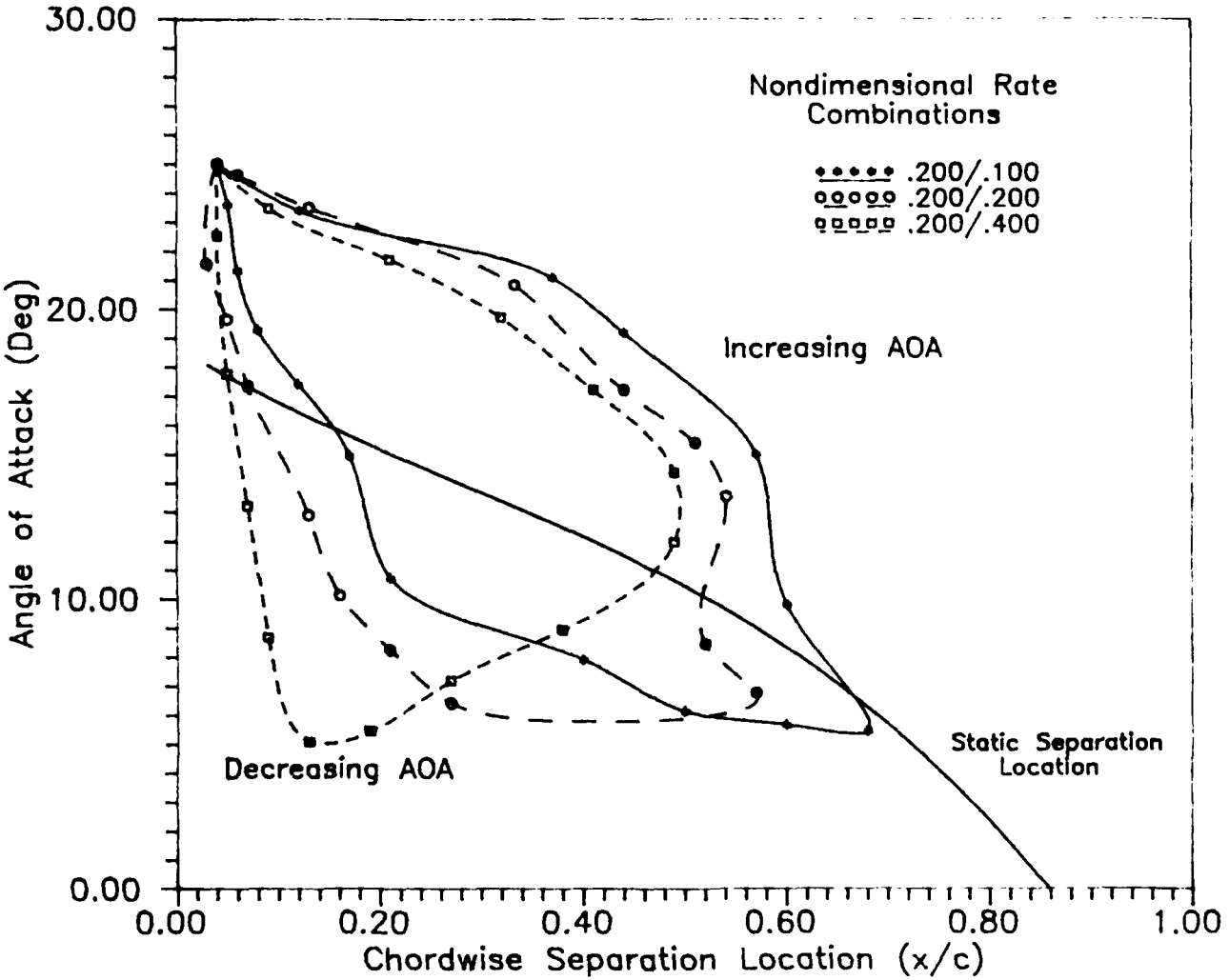

Figure 29. Chordwise Position of Flow Separation, Rectangular Wing, Mid-Span, $\dot{\alpha}_{ND}$ Up = 0.20, U = 0.60 in/sec

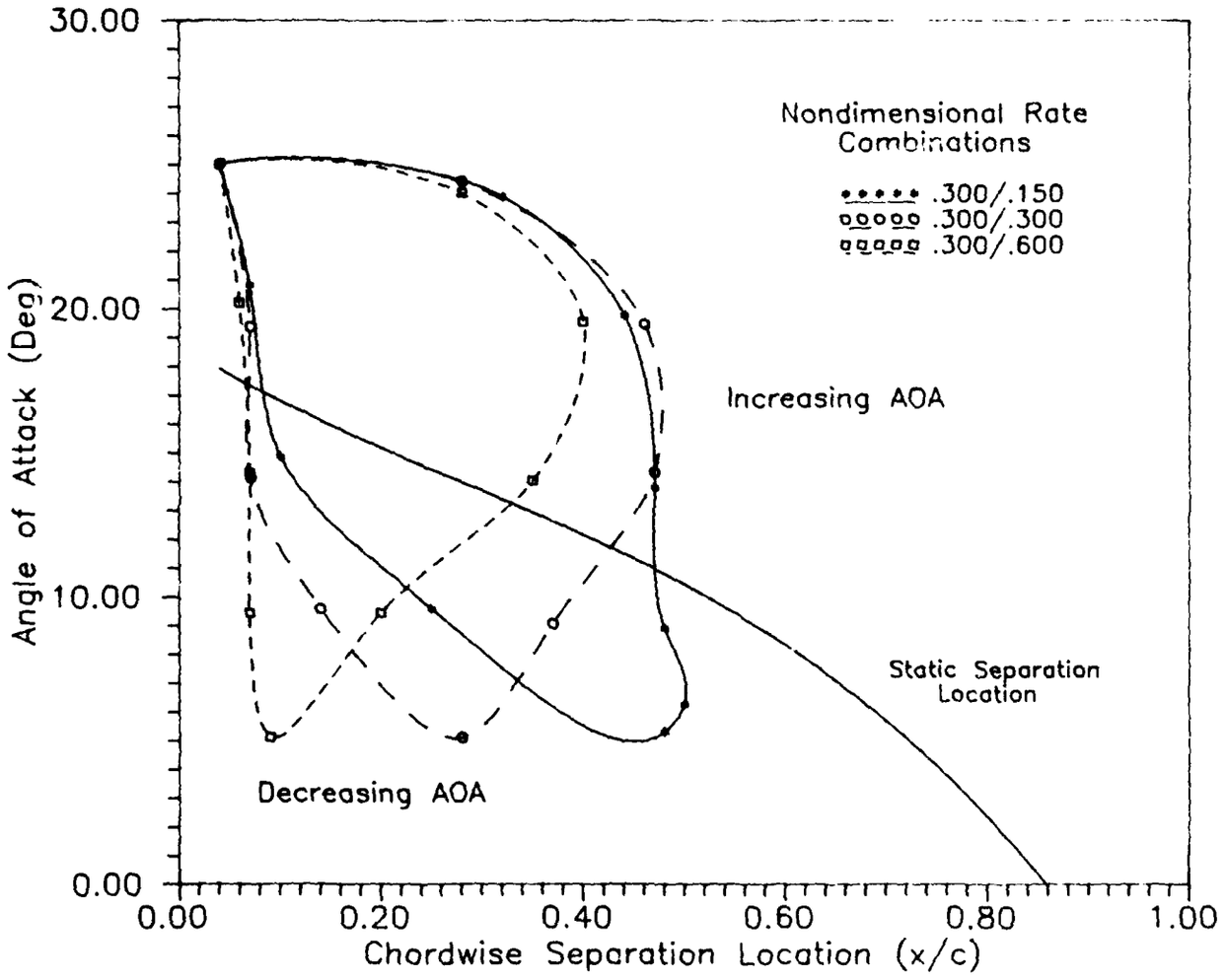

Figure 30. Chordwise Position of Flow Separation, Rectangular Wing, Mid-Span, $\dot{\alpha}_{ND}$ Up = 0.30, U = 0.60 in/sec

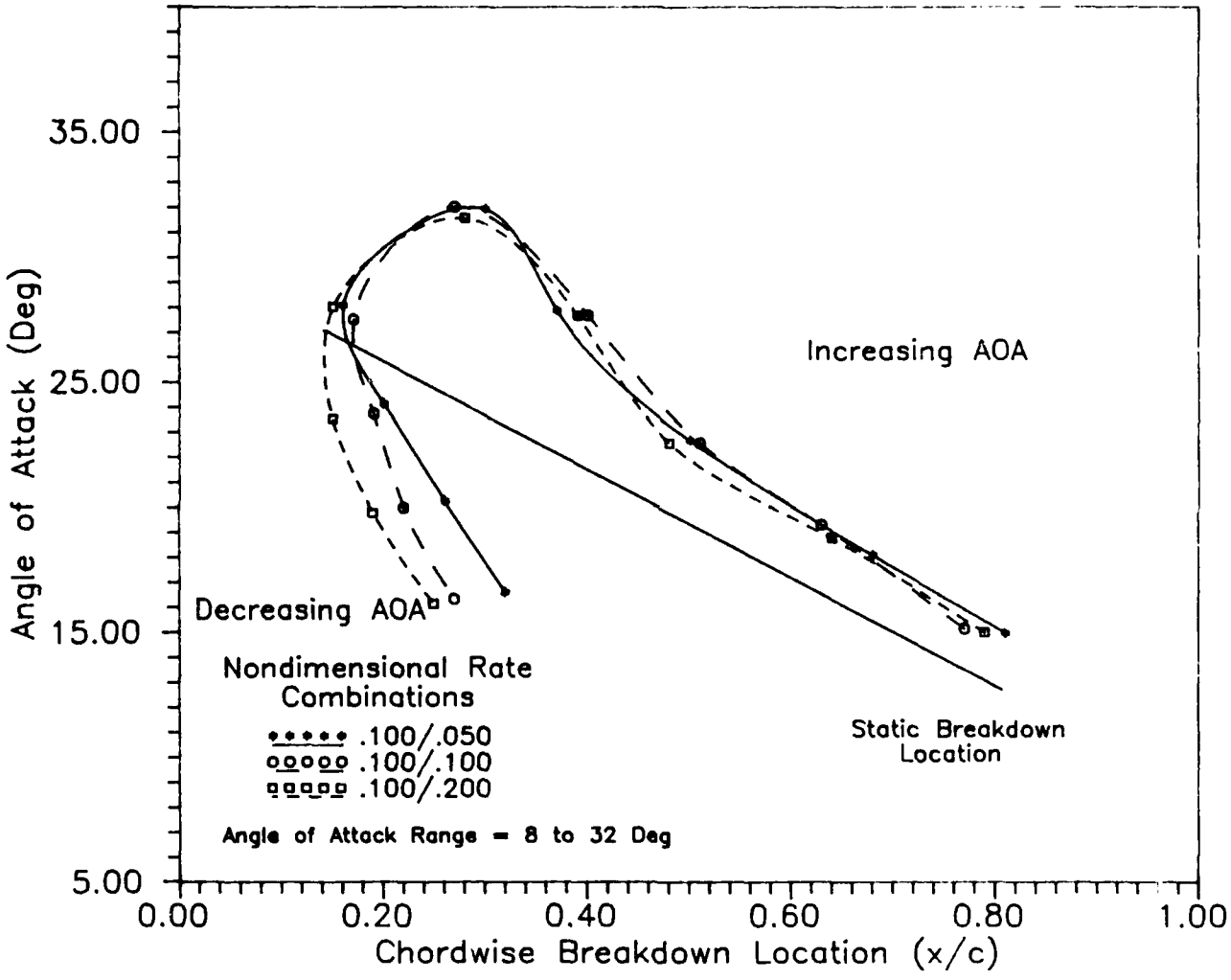

Figure 31. Chordwise Vortex Breakdown Location for the 45 Deg Sweep Flat Plate, $\dot{\alpha}_{ND}$ Up = 0.1, U = 1.8 in/sec

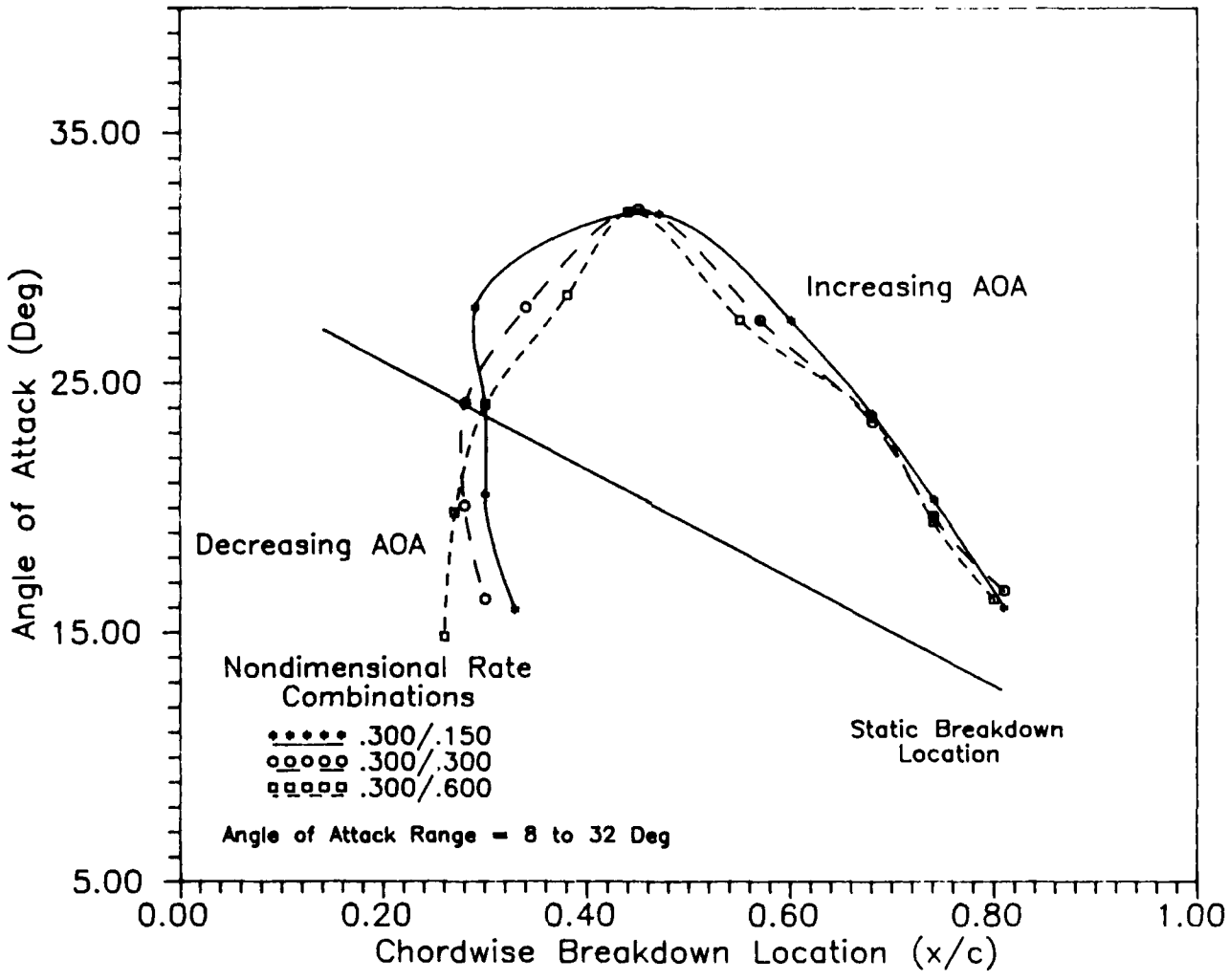

Figure 32. Chordwise Vortex Breakdown Location for the 45 Deg Sweep Flat Plate, $\dot{\alpha}_{ND}$ Up = 0.3, U = 1.8 in/sec

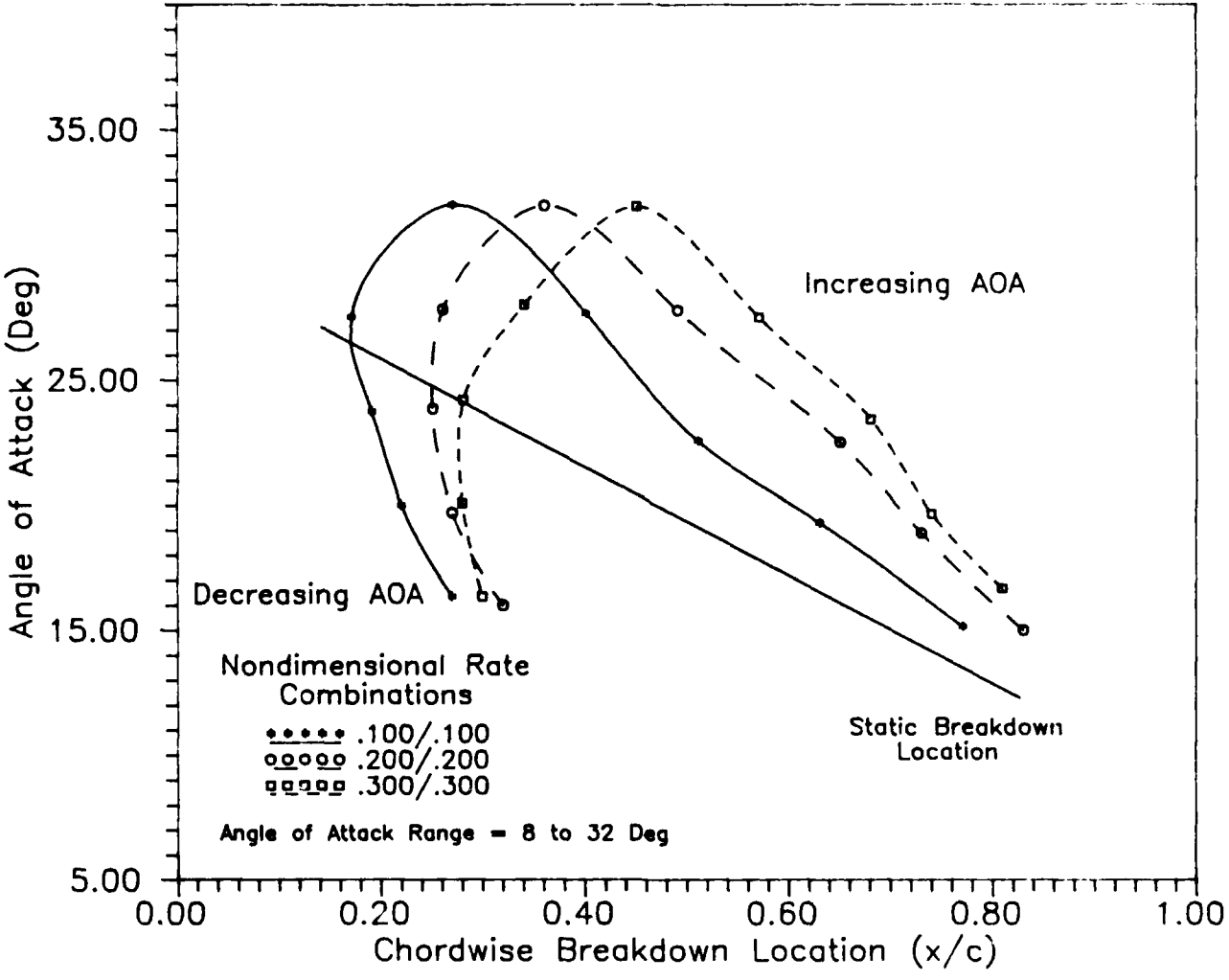

Figure 33. Chordwise Vortex Breakdown Location for the 45 Deg Sweep Flat Plate, $\dot{\alpha}_{ND}$ Up = 0.1, 0.2, and 0.3, U = 1.8 in/sec

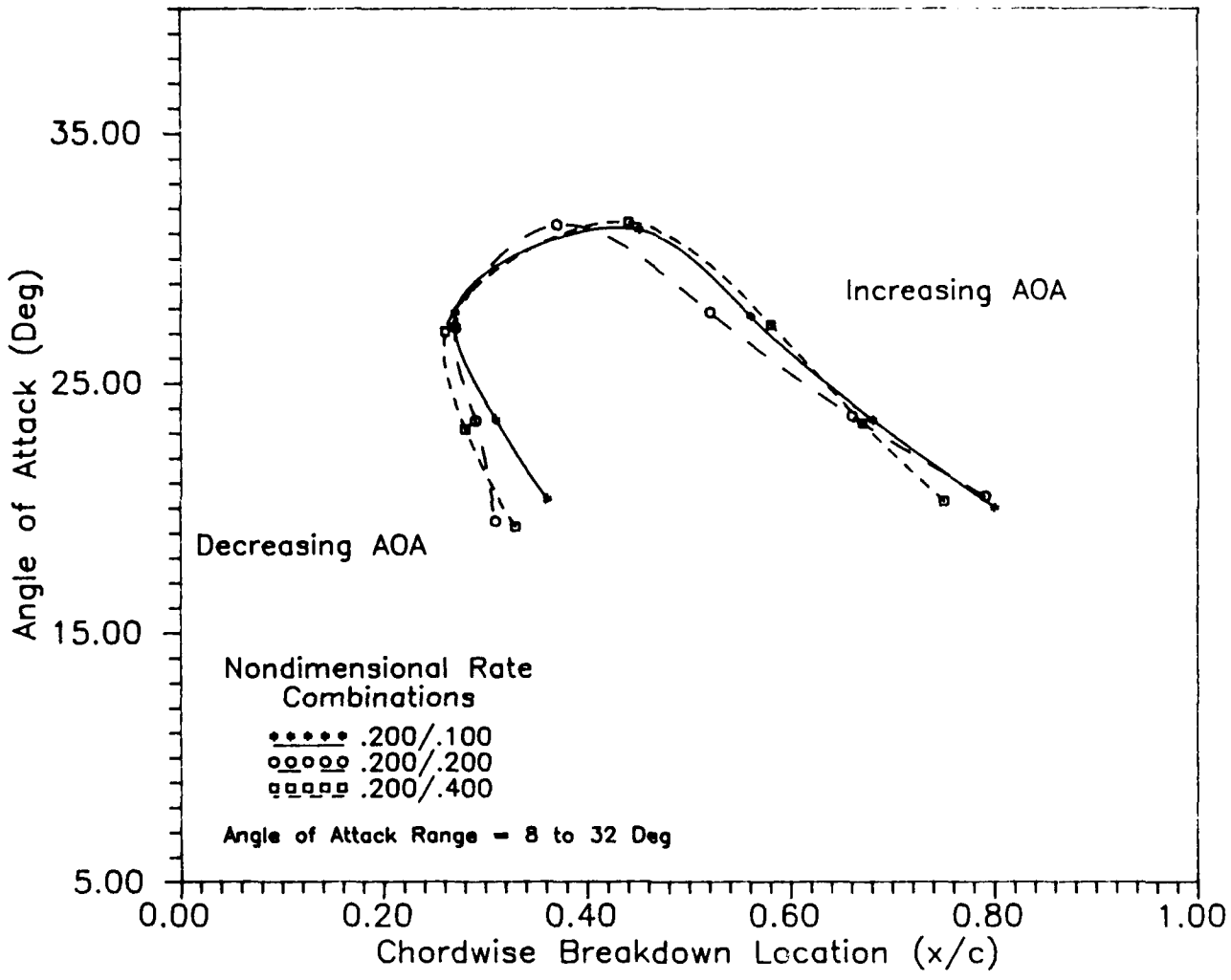

Figure 34. Chordwise Vortex Breakdown Location for the 45 Deg Sweep NACA 0012-34 $\dot{\alpha}_{ND}$ Up = 0.2, U = 1.8 in/sec

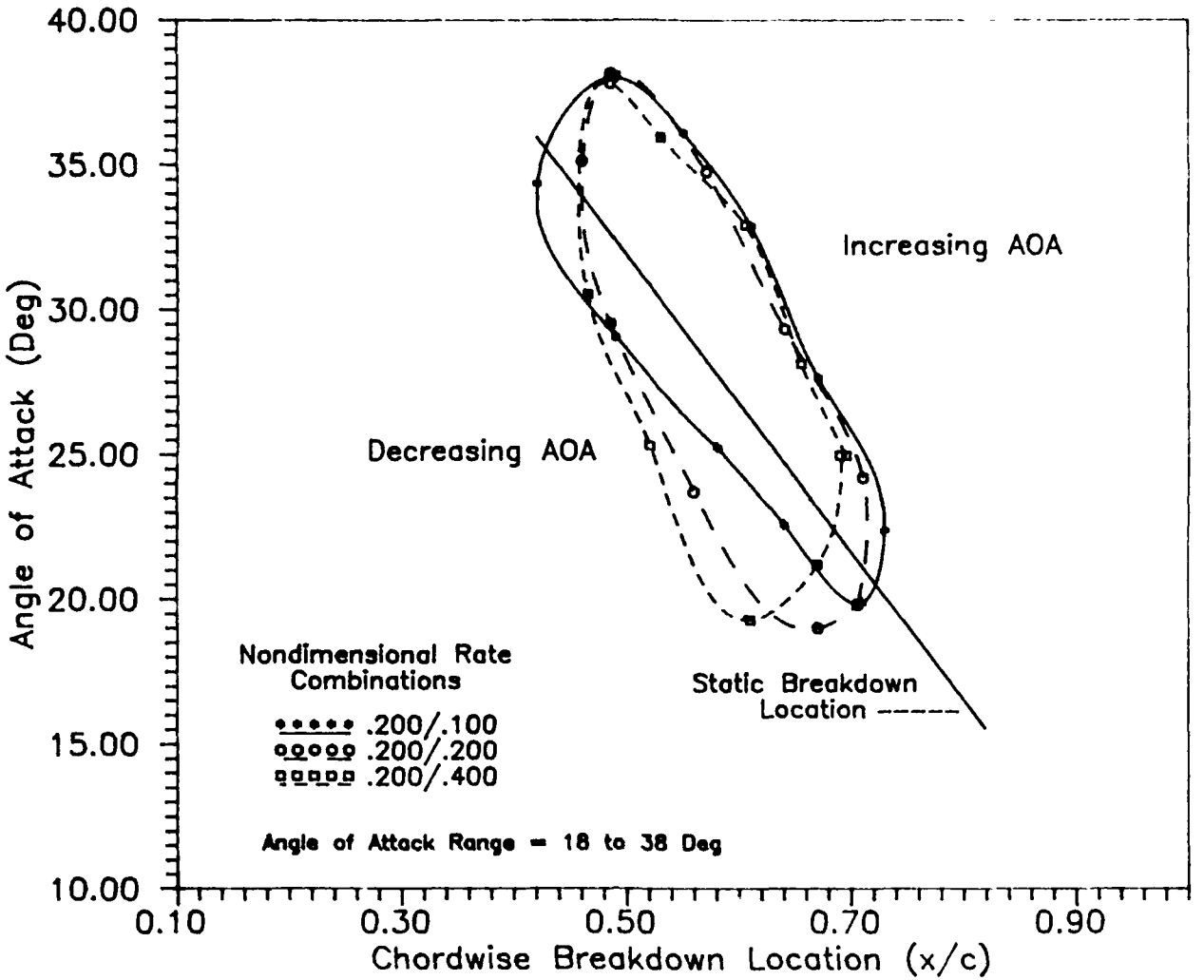

Figure 35. Chordwise Vortex Breakdown Location, 65 Deg Sweep NACA 0012–34, $\dot{\alpha}_{ND}$ Up = 0.2, U = 3.6 in/sec

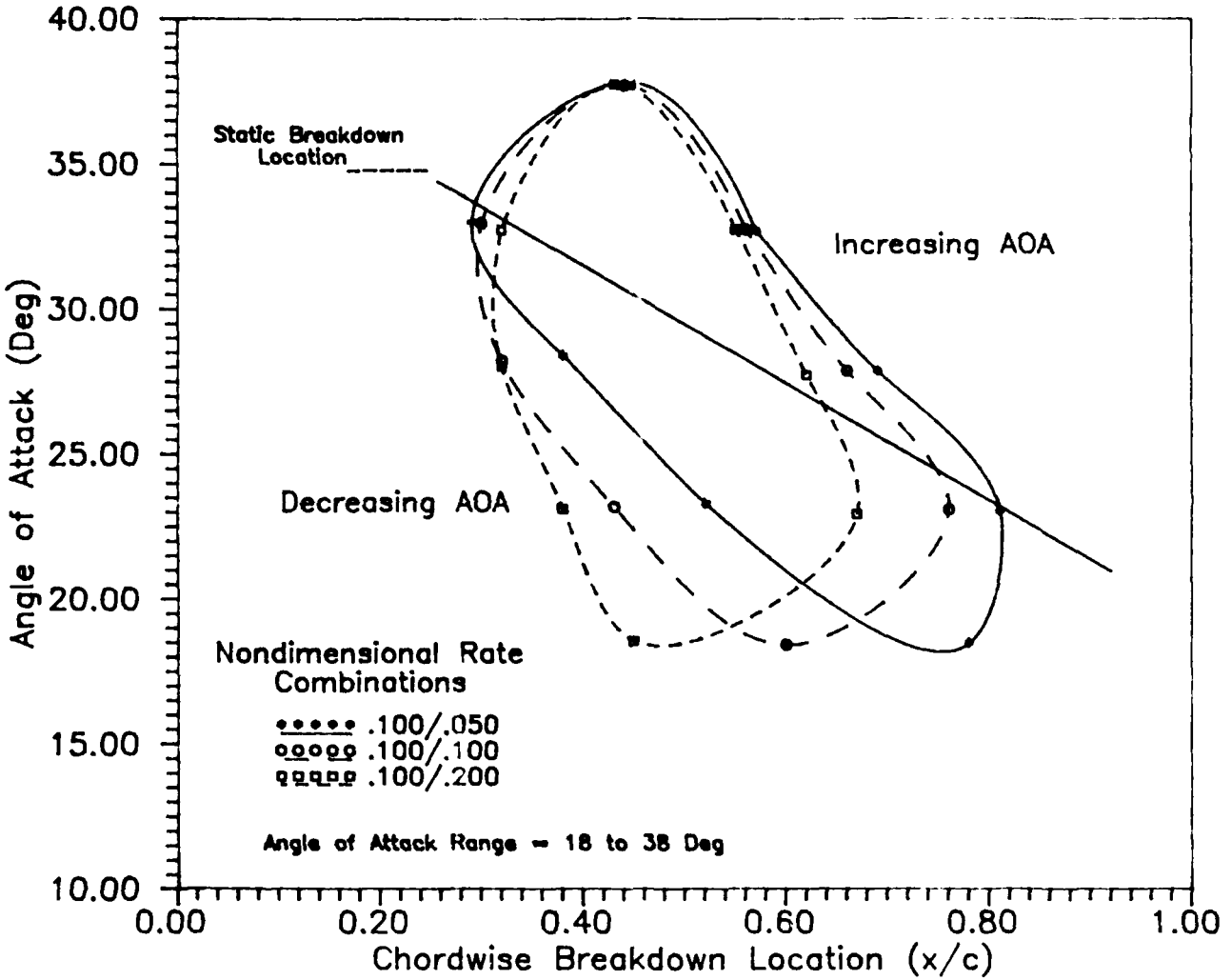

Figure 36. Chordwise Vortex Breakdown Location, 65 Deg Sweep Flat Plate, $\dot{\alpha}_{ND}$ Up = 0.1, U = 3.6 in/sec

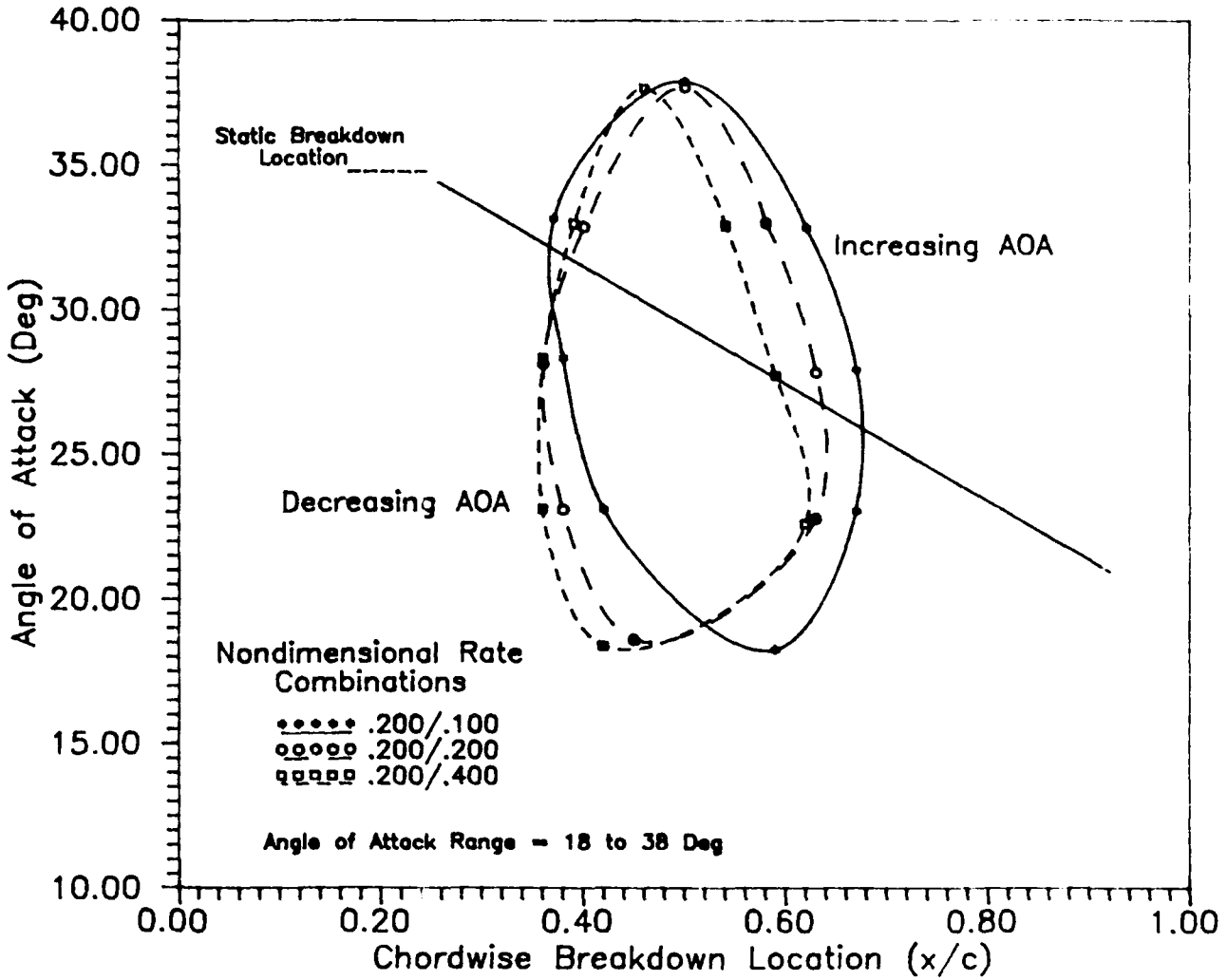

Figure 37. Chordwise Vortex Breakdown Location, 65 Deg Sweep Flat Plate, $\dot{\alpha}_{ND}$ = 0.2, U = 3.6 in/sec

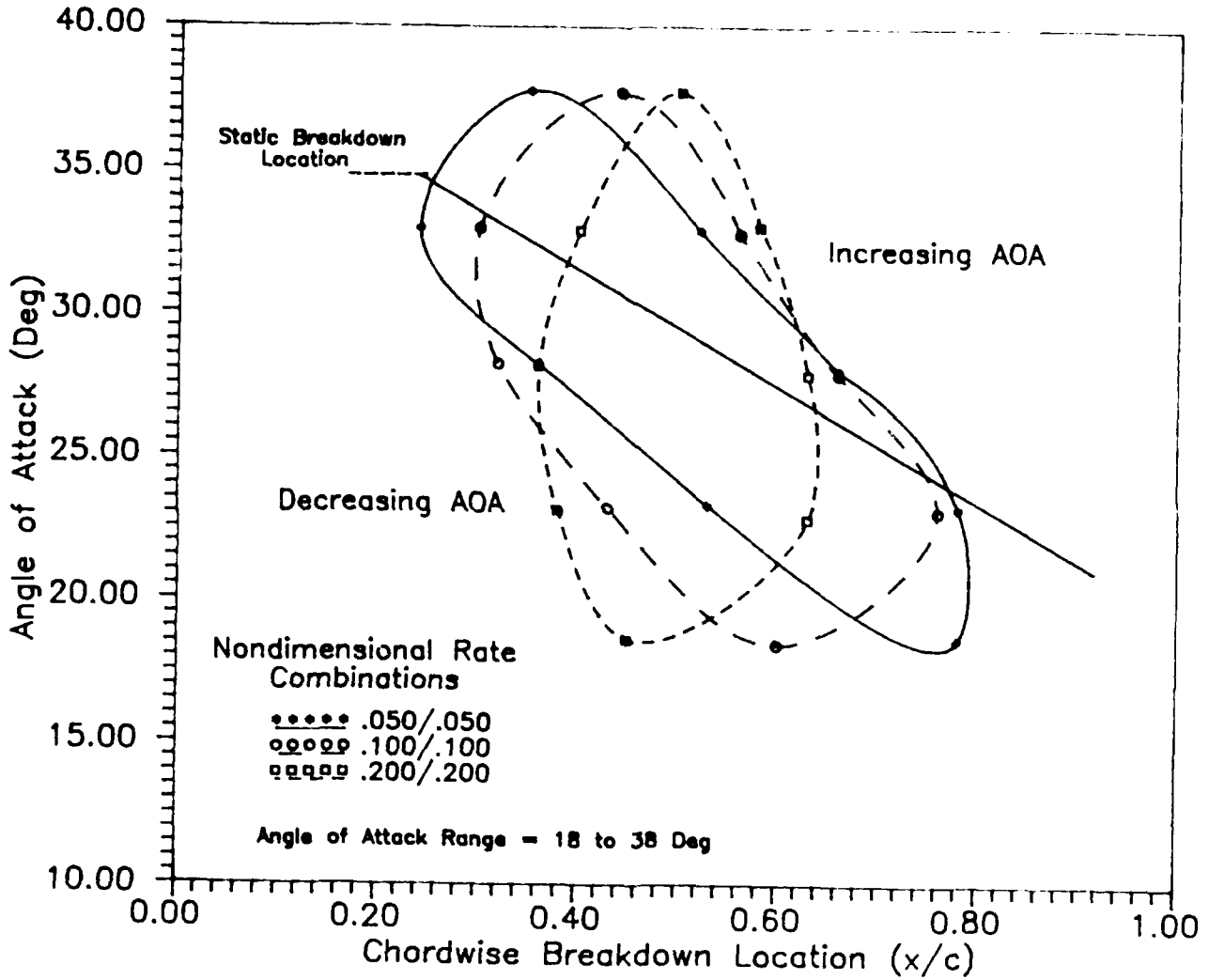

Figure 38. Chordwise Vortex Breakdown Location, 65 Deg Sweep Flat Plate, $\dot{\alpha}_{ND}$ = 0.05, 0.1, and 0.2; U = 3.6 in/sec

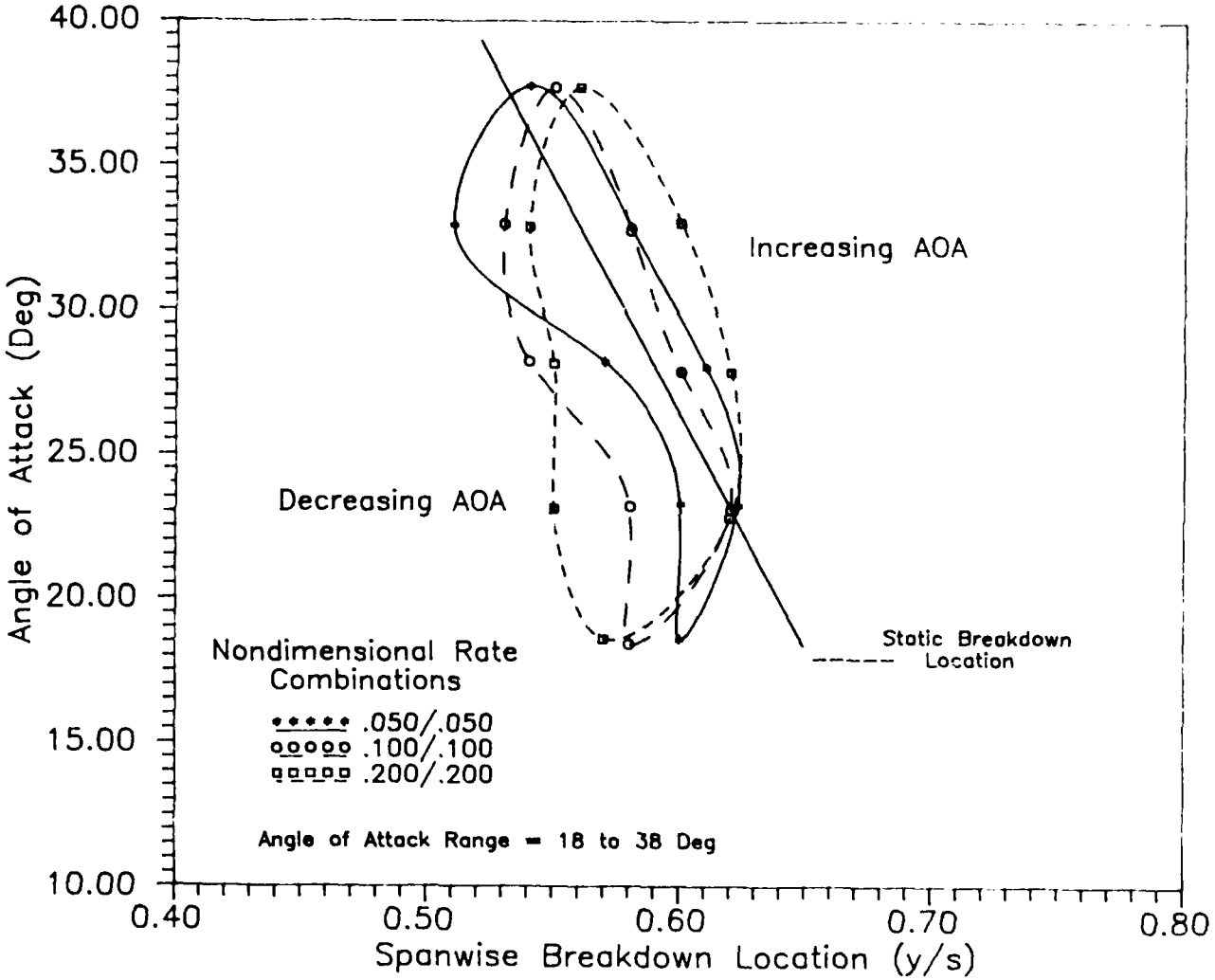

Figure 39. Spanwise Vortex Breakdown Location, 65 Deg Sweep Flat Plate, $\dot{\alpha}_{ND}$ = 0.05, 0.1, and 0.2; U = 3.6 in/sec

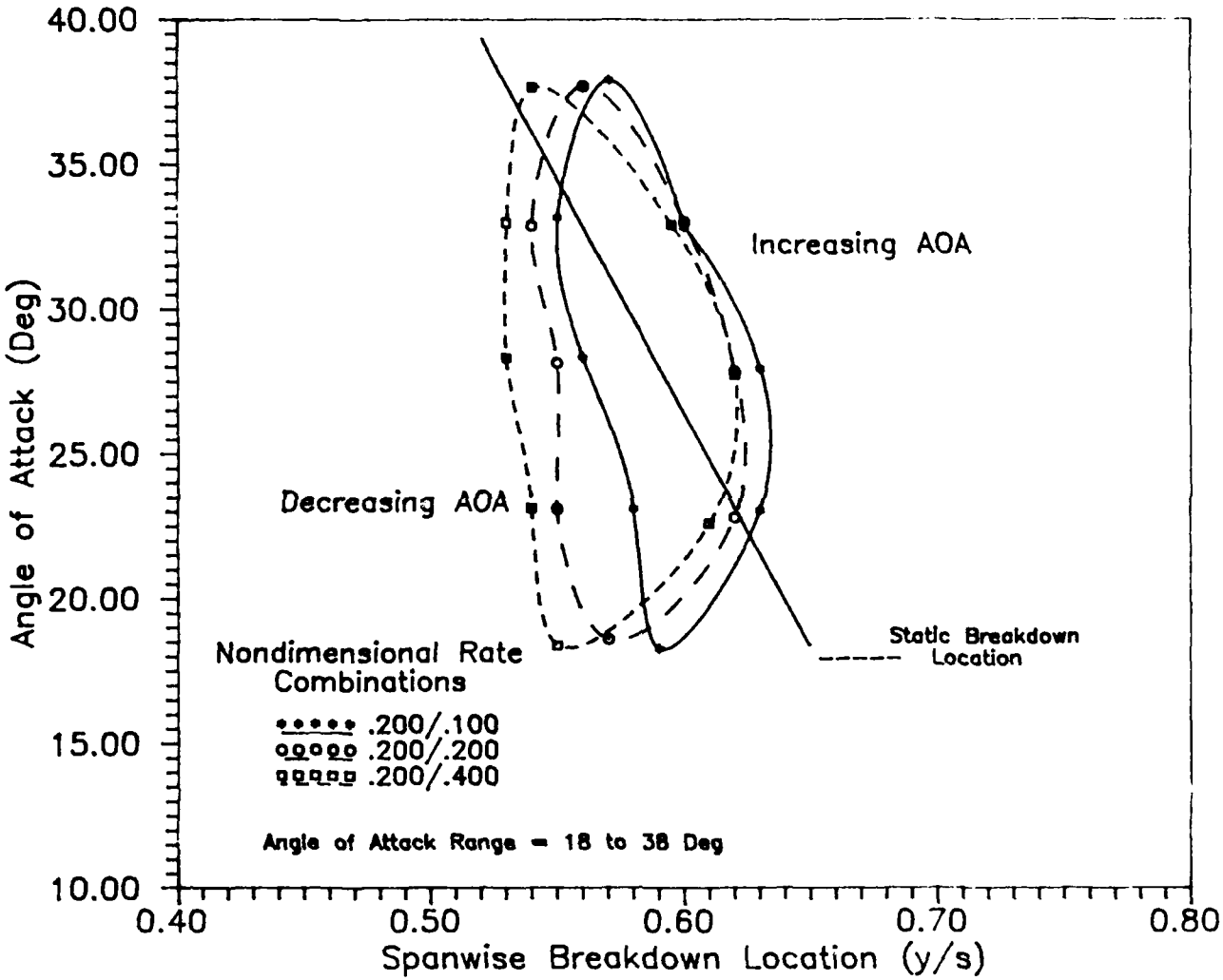

Figure 40. Spanwise Vortex Breakdown location, 65 Deg Sweep Flat Plate, $\dot{\alpha}_{ND}$ = 0.2, U = 3.6 in/sec

Appendix C

Calibration Information

Water Tunnel Flow Rate Calibration

The flow rate of the tunnel was calibrated by timing small dye elements in the flow using the Digital 5000 video camera. Although a more complete picture of the flow could have been obtained with a hot film anemometer or a laser velocimeter, neither was available for this study.

Calibration took place with the splitter plate and the rectangular (0° sweep) wing installed. Only a six-inch cubic area starting 8 inches upstream of the leading edge was actually tested. This area was considered representative of the flow the wings would see and was relatively easy to sweep with a dye rake installed at the top of the test section. Pulses of dye released from the rake were filmed crossing a grid marked on the splitter plate. After correcting for parallax error caused by the gap between the dye and the splitter plate the actual speed could be determined from the elapsed time on the tape.

Originally a single speed was going to be used for all the wings -- that was 0.2 ft/sec, however as the experiment progressed it became apparent that different wings required different speeds to produce the best flow visualization. Table VII is a summary of the results for the initial rate

of 0.20 feet/second (2.4 inches/second). Each point represents the average of a 10 sample ensemble. The mean speed was 2.36 in/sec, a 0.04 in/sec or about a 1.7 percent difference from the set speed. The maximum error was a .08 in/sec low reading in the center of the test cube which represents an approximate error of 3.4 percent. This showed that at 0.2 ft/sec the tunnel's flow meter provided an accurate measure of flow speed and also it provided a baseline speed to be used for the non-dimensional pitch rates.

TABLE VII

Tunnel Flow Calibration Summary (2.4 in/sec)

Grid Position (in)		Flow Speed (in/sec)
From Splitter Plate	From Center Line	
1	-3	2.37
1	0	2.35
1	3	2.43
4	-3	2.33
4	0	2.32
4	3	2.34
7	-3	2.33
7	0	2.35
7	3	2.39

Tables VIII and IX show a similar summary for flow rates of 0.05 ft/sec (0.6 in/sec) and 0.30 ft/sec (3.6 in/sec). Notice at 3.6 in/sec the error is about the same as at 2.4 in/sec -- about 3 percent. However, at 0.6 in/sec

the flow meter reads low by about 10 percent, although the magnitude of the difference remains fairly constant.

Table VIII

Tunnel Flow Calibration Summary (3.6 in/sec)

Grid Position (in)		Flow Speed (in/sec)
From Splitter Plate	From Center Line	
2	-3	3.54
2	0	3.55
2	3	3.54
5	-3	3.52
5	0	3.54
5	3	3.50
7	-3	3.40
7	0	3.47
7	3	3.45

Table IX

Tunnel Flow Rate Calibration Summary (0.6 in/sec)

Grid Position (in)		Flow Speed (in/sec)
From Splitter Plate	From Center Line	
2	-3	0.69
2	0	0.67
2	3	0.68
5	-3	0.65
5	0	0.66
5	3	0.65
7	-3	0.64
7	0	0.65
7	3	0.64

Model Motion Calibration

The pitching motion of the models was calibrated with the SP2000 high speed video system under tunnel flow conditions of 0.2 ft/sec (2.4 in/sec) using both the rectangular and 45 degree sweep wings. The time required to accelerate to a constant rate varied with pitch rate with typical values of 2 to 4 milliseconds based on the parameters used in the motion program (Appendix A). The formula from the Delta Tau motion card manual used to approximate this is shown below.

$$t = (84 \text{ sec})(i06/200000)(F/1000)(1/i08 \text{ or } i12) \quad (9)$$

Where

i06 = Rate Multiplier

F = Rate Set

i08 = Acceleration Control

i12 = Deceleration Control

Initial runs showed some backlash at the higher pitch rates as the wing reversed direction. This was remedied by increasing the feedback gain setting (i06). Higher gain resulted in a more robust response from the motor; however, increasing the gain too high caused a ratcheting motion at the lower pitch rates. The final setting shown in the

program (line 120) gave good results at both high and low rates. Also, some minor adjustments were required to the i24 parameter to get the desired rate. Figures 41 to 43 are plots for rates of 1, 10, and 20 degrees per second with similar results assumed for intermediate pitch rates.

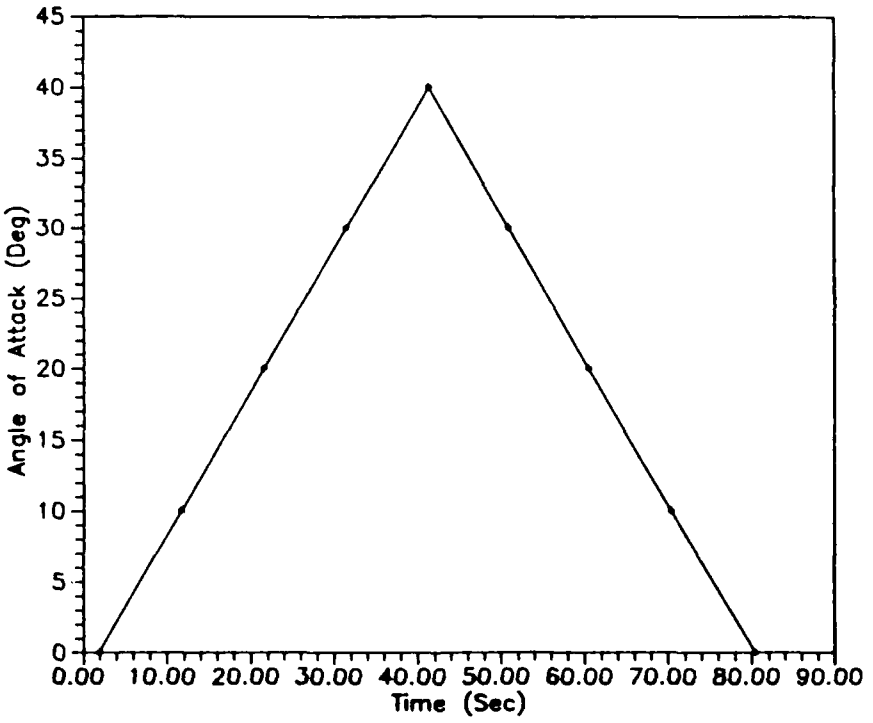

Figure 41. Saw-Tooth Motion Calibration, 1 Deg/Sec Up and Down, 45 Deg Sweep NACA 0012-34, U = 2.4 in/sec

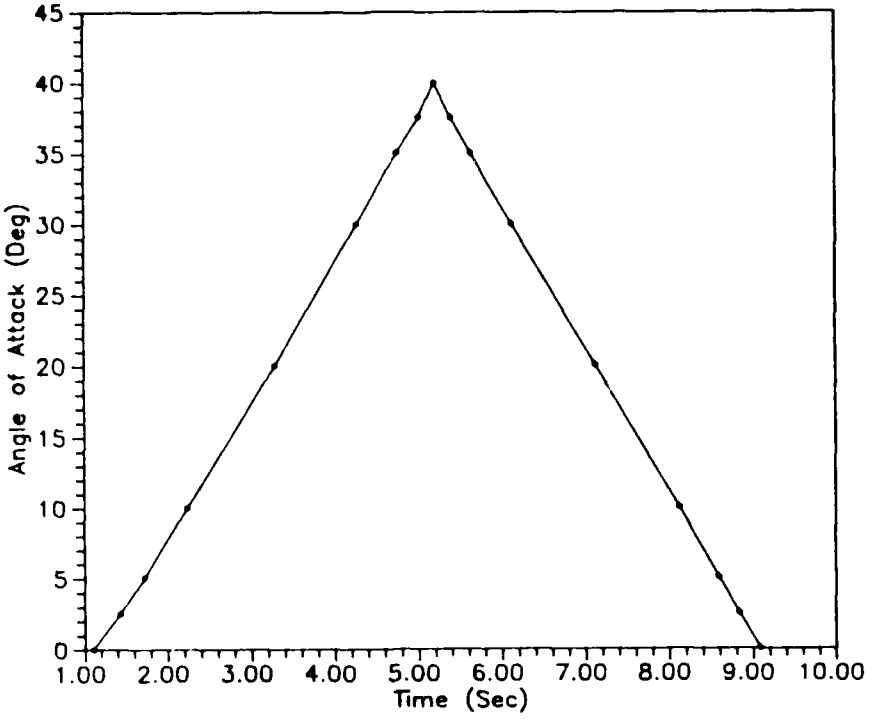

Figure 42. Saw-Tooth Motion Calibration, 10 Deg/Sec Up and Down, 45 Deg Sweep NACA 0012-34, U = 2.4 in/sec

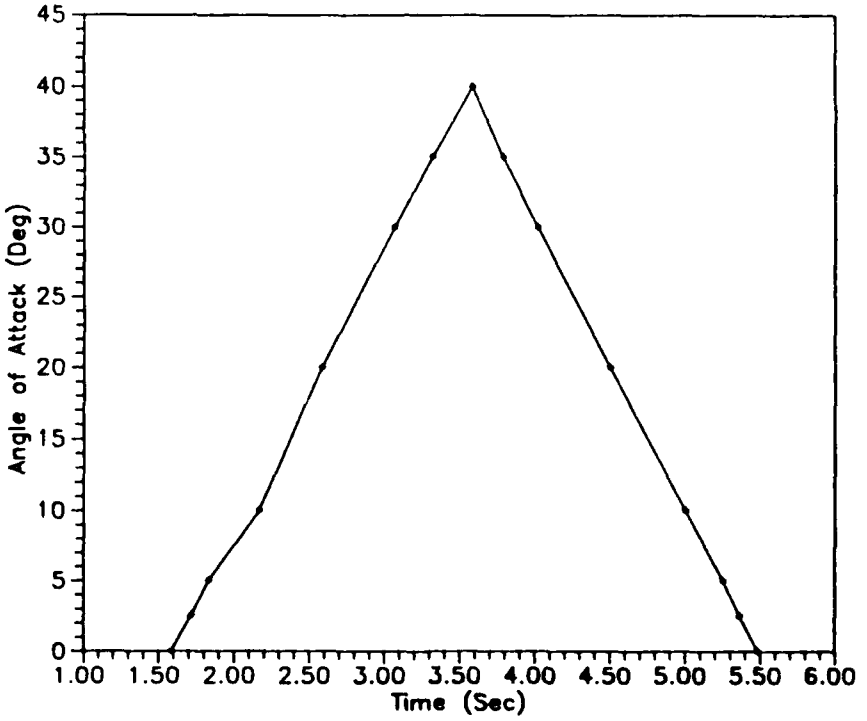

Figure 43. Saw-Tooth Motion Calibration, 20 Deg/Sec Up and Down, 45 Deg Sweep NACA 0012-34, U = 2.4 in/sec

Appendix D

Flow Visualization Lessons Learned

For this experiment use of the food color dye was considered most practical because the facility had an in-place dye injection system and most of the expertise of the lab's personnel was in this area. However no previous dynamic experiments had been performed in the tunnel, so much of the early part of the experiment involved trial-and-error tests to determine the best location, orientation and size of the dye ports.

The first wing examined was the rectangular wing--here the visualization goal was to track upper surface flow separation and vortex position. Previous experience had shown that placing the dye source on the lower surface and having the dye pulled to the upper surface by the pressure difference and circulation worked well, therefore the wing was designed with lower surface ports at 0.25, 0.50, 0.75, and 0.95 chord. The ports, 0.03 inches in diameter, were drilled parallel to the chord line, approximately 0.03 inches below the leading edge resulting in an elliptical opening when viewed perpendicular to the surface.

Initial runs with this configuration gave poor results because with the actual opening of the dye port flush with the surface much of the dye was forced away from the boundary layer and not drawn to the upper surface. In an

attempt to keep the dye near the lower surface, a small piece of stainless tubing (0.05 inches inner diameter) was attached so that the opening was just behind the leading edge and perpendicular to the lower surface. The larger diameter of the tube allowed for an equal mass flow rate at a slightly reduced pressure, avoiding a jet-like effect from the dye tube.

This worked--however there was a trade off on just how close to the leading edge the tube could be placed. At low angles of attack, if the tube was too far back the dye would not make it to the upper surface, but at high angles, if the tube was too far forward the dye would blow past the shear layer forming the vortex. For the flow rates of 0.6 to 1.8 in/sec used with the rectangular wing a spacing of about 0.1 inches from the leading edge worked well.

The dye flow from this setup was normally sufficient to judge separation on the upper surface. However, as the pitch rates were increased less dye was on the upper surface for a given angle of attack. An attempt was made to tap the wing's segmented dye manifold from both the upper and lower surface near the leading edge; however, this meant that the pressure being supplied to each port was equal. As a result, the dye would follow the path of least resistance and most of it would come out the top as angle of attack increased. One possible solution, which was not tried, would be to have multiple upper surface

ports along with the lower surface port--each fed from its own dye reservoir. The limiting factor here becomes the number of dye tubes that can be fit inside the model.

Armed with the experience from the rectangular wing the experiment moved on to the swept wings, the first of which was the 65 degree sweep wing (NACA 0012-34 profile) with ports located at 0.03, 0.25, 0.50, 0.75, and 0.91 of the trailing edge span.(This wing also included an upper surface port at approx. 0.6 chord and 0.4 span.) Unfortunately, this wing was built before the previous lessons learned could be passed on, so it also had ports drilled just below and perpendicular to the leading edge. The model was however still tested before making any modifications and in this case that configuration worked fine. Because of the angle between the port and the free stream flow the dye would move slightly downstream along the lower surface before coming around the leading edge to the upper surface. The problem experienced with this wing was getting dye into the core of the leading edge vortex to be able to clearly define the burst point.

Due to the shape of the wing the vortex appeared to start at a point slightly away from the apex. Therefore, dye from a port very close to the model's apex tended to miss the vortex and instead flowed directly downstream. In addition, dye from the ports further down the leading edge tended to get caught in the outer layers of the vortex

thereby masking the core. Placing the lead port at about 0.1 span (in this case about 0.4 inches from the splitter plate) worked the best and appeared to avoid any complicating effects from the splitter plate boundary layer.

Besides the thicker profiled (NACA 0012-34) wings a series of flat plate wings (sweep angles of 25, 45, and 65 degrees) were used. With these wings the dye tubes ran along the lower surface much like the additional tube used on the rectangular wing. This allowed much flexibility in their placement and in some cases two or three were grouped together near the apex. Unfortunately this part of the experiment was more of an afterthought--looking back, a lot of design problems could have been avoided by experimenting on the flat plates first.

When trying to track vortex breakdown, one technique that helped in some cases was the use of two different color dyes from the first two ports (for this experiment #1 - green and #2 - red). The colors, each relatively light, remained separated until breakdown at which they combined to form a darker, blackish color. This was especially helpful when taking black and white video because the red by itself hardly showed up at all.

At the end of the experiment some flow visualization work was done with a laser light sheet. Here the idea was to show a clear cross section of the vortex by exciting fluorescent dye with a narrow sheet of laser light.

However, because of the white background of the tunnel wall and the white color of the wings some of the light was reflected causing the entire vortex to be illuminated. To reduce reflections both the wall and the wings were painted flat black. The results were good--now the problem was how to photograph it. The best position to take pictures from, especially for highly swept wings, is behind the wing; but this tunnel is not presently setup to do that. Some photographs and video were taken--they show possibilities for the facility but no results for this experiment.

Vita

Captain Michael David [redacted] He graduated from Pilgrim High School in Warwick in 1974 and upon graduation received an appointment to the United States Air Force Academy. There he earned the degree of Bachelor of Science in Aeronautical Engineering. Following commencement in 1978, he completed Undergraduate Pilot Training at Columbus AFB where he served as a T-38 instructor pilot until 1983. In May of 1983 he was assigned to McGuire AFB where he was a C-141 pilot and flight examiner. In May of 1987, he entered the School of Engineering, Air Force Institute of Technology.

[redacted]

UNCLASSIFIED
SECURITY CLASSIFICATION OF THIS PAGE

REPORT DOCUMENTATION PAGE

Form Approved
OMB No. 0704-0188

1a. REPORT SECURITY CLASSIFICATION UNCLASSIFIED	1b. RESTRICTIVE MARKINGS
2a. SECURITY CLASSIFICATION AUTHORITY	3. DISTRIBUTION/AVAILABILITY OF REPORT Approved for public release; distribution unlimited
2b. DECLASSIFICATION/DOWNGRADING SCHEDULE	
4. PERFORMING ORGANIZATION REPORT NUMBER(S) AFIT/GAE/AA/88D-06	5. MONITORING ORGANIZATION REPORT NUMBER(S)
6a. NAME OF PERFORMING ORGANIZATION School of Engineering 6b. OFFICE SYMBOL (If applicable) AFIT/ENY	7a. NAME OF MONITORING ORGANIZATION
6c. ADDRESS (City, State, and ZIP Code) Air Force Institute of Technology Wright-Patterson AFB OH 45433	7b. ADDRESS (City, State, and ZIP Code)
8a. NAME OF FUNDING/SPONSORING ORGANIZATION 8b. OFFICE SYMBOL (If applicable)	9. PROCUREMENT INSTRUMENT IDENTIFICATION NUMBER
8c. ADDRESS (City, State, and ZIP Code)	10. SOURCE OF FUNDING NUMBERS PROGRAM ELEMENT NO. / PROJECT NO. / TASK NO / WORK UNIT ACCESSION NO.
11. TITLE (Include Security Classification) See Box 19	
12. PERSONAL AUTHOR(S) Michael David, B.S., Capt, USAF	
13a. TYPE OF REPORT MS Thesis 13b. TIME COVERED FROM _____ TO _____ 14. DATE OF REPORT (Year, Month, Day) 1988 December 15. PAGE COUNT 121	
16. SUPPLEMENTARY NOTATION	

17. COSATI CODES			18. SUBJECT TERMS (Continue on reverse if necessary and identify by block number)
FIELD	GROUP	SUB-GROUP	
01	01		Water Tunnel, Dynamic Stall, Pitching Wing, Vortex Breakdown.

19. ABSTRACT (Continue on reverse if necessary and identify by block number)

Title: Water Tunnel Investigation of the Vortex Dynamics of Periodically Pitched Wings

Thesis Advisor: Lanson Hudson, Maj, USAF

12 Jan 1989

20. DISTRIBUTION/AVAILABILITY OF ABSTRACT ☐ UNCLASSIFIED/UNLIMITED ☒ SAME AS RPT ☐ DTIC USERS	21. ABSTRACT SECURITY CLASSIFICATION
22a. NAME OF RESPONSIBLE INDIVIDUAL Paul King, Lt Col, USAF	22b. TELEPHONE (Include Area Code) (513) 255-2998 22c. OFFICE SYMBOL AFIT/ENY

DD Form 1473, JUN 86 *Previous editions are obsolete.* SECURITY CLASSIFICATION OF THIS PAGE

The vortex structure above semi-span wings was investigated in the Flight Dynamics Lab's 24-inch water tunnel to determine the effects of periodic pitching using a saw-tooth motion. Each of the six wings was pitched about the mid-chord at nondimensional upstroke rates ($c\dot{\alpha}/U$) ranging from 0.05 to 0.30 and downstroke rates from 0.025 to 0.600 at tunnel flow rates of 0.6 to 3.6 in/sec. Visualization of the vortices obtained through dye injection from the models was recorded using both high speed and three-quarter-inch standard speed video systems. Digitized data from the high speed system provided trend data which showed the saw-tooth motion caused a hysteresis effect on the vortex breakdown location for the swept wings where during the upstroke the vortex would burst further aft than during the downstroke. In addition, comparison of two 65-degree sweep wings with different cross sections (flat plate and NACA 0012-34) showed a smaller hysteresis effect for the thicker wing. For the rectangular wing, increasing downstroke rates resulted in higher dynamic stall vortex convection rates. Information was also gathered on the oscillation of static breakdown location and the effects on vortex breakdown of tunnel flow velocity.